EFFECT OF ELECTROSTATIC FIELDS ON MATERIAL BONDING AND ITS APPLICATION TO MANUFACTURING PROCESSES

by

QAMAR M. KHAN

DEPARTMENT OF MECHANICAL ENGINEERING

INDIAN INSTITUTE OF TECHNOLOGY, KANPUR

MARCH, 1983

DEDICATED

TO

MY MATERNAL UNCLE

MR. AHSAN M. KHAN

WHOSE

DEVOTION AND EFFORTS

ARE RESPONSIBLE

FOR

MY HIGHER EDUCATION

CERTIFICATE

This is to certify that the present work ''EFFECT OF ELECTROSTATIC FIELDS ON MATERIAL BONDING AND ITS APPLICATION TO MANUFACTURING PROCESSES'' has been carried out under our supervision and has not been submitted elsewhere for the award of a degree.

A. Ghosh
Professor
Department of Mechanical Engineering
I.I.T., Kanpur (India)

A. Mookerjee
Asstt.Professor
Department of Physics
I.I.T., Kanpur (India)

30.1.1984

ACKNOWLEDGEMENTS

I feel a deep sense of gratitude to Dr. A. Ghosh for suggesting the problem and constantly encouraging and inspiring me to work on this totally new problem which proved to be quite discouraging and frustrating in the beginning. I am greatly indebted to Dr. A. Mookerjee for his guidance in the theoretical analysis of the problem.

I am grateful to Dr. G.K. Mehta of Physics Department for supplying aluminised mylar and macrofol films and to India Foils Ltd., Calcutta for supplying Al-foils. Further, I am thankful to all those faculty members of I.I.T., Kanpur with whom I had many fruitful discussions from time to time.

The help and assistance rendered by Messers R.M. Jha, J. Singh and B.P. Bhartiya of Manufacturing Science Laboratory and Mr. B.K. Jain of Material Testing Laboratory (ACMS) in carrying out the experimental investigations is greatly appreciated and acknowledged. My colleagues Messers V.Raghuram and E.V. Nair helped me in conducting the experiments and I am grateful to them. Mr. J.P. Gupta deserves thanks for cutting the stencils.

In the last, I wish to acknowledge the indirect help and contribution made by my family members and friends to this work.

QAMAR M. KHAN

TABLE OF CONTENTS

SYNOPSIS

"EFFECT OF ELECTROSTATIC FIELDS ON MATERIAL BONDING AND ITS APPLICATION TO MANUFACTURING PROCESSES"

A Thesis Submitted
in Partial Fulfilment of the Requirements
for the Degree of
DOCTOR OF PHILOSOPHY

by

QAMAR M. KHAN

to the

DEPARTMENT OF MECHANICAL ENGINEERING
INDIAN INSTITUTE OF TECHNOLOGY, KANPUR

MARCH 1983

Most of the manufacturing processes for solid materials are accomplished by either plastic deformation or fracture of work materials in a controlled manner. Higher productivity and improved machinability can be achieved by reducing the resistance to deformation or fracture of work materials. In the past it has been attempted by heating the work material but such technique lead to undesirable permanent changes in the material properties. The present work is a beginning of the search to find out the feasibility of developing methods to reduce the material's resistance to deformation or fracture without causing any permanent change in the work material.

On a microscopic scale, the mechanical properties of a solid material, in general, are determined by the strength of the interatomic bonds and the defects in its crystal structure (mainly dislocations). Intuitively it is felt that the application of a suitable electrostatic field might affect both the strength of bonds and the dislocations dynamics leading to a reduction in the resistance to deformation and fracture of a material.

The present work is concerned with the study of the effect of an applied electrostatic field on the bond strength and some mechanical properties of a few solid materials. The study is concluded with the investigation of the effect of a field on ultrasonic machining of glass. Broadly, the work is divided into three sections.

The first section deals with the experimental investigations of the effect of an electrostatic field on tensile rupture strength of two types of materials, conductors and dielectrics. For this purpose, tensile rupture tests are performed on thin specimens of Al-foil, aluminised mylar and macrofol (both polymers), with and without a field. The field is produced by using an arrangement similar to a parallel plate capacitor which is connected across a high voltage d.c. supply. The dielectric specimen is tested by placing it between the plates of the capacitor. The Al-foil specimen, on the other hand, acts during the test as a plate of the capacitor connected to a high potential d.c. supply. It is found that the

effect of electrostatic field on tensile rupture strength of Al-foils is insignificant but it is quite significant in case of dielectric specimens. The rupture strengths of mylar and macrofol specimens are reduced by about 10-15 percent in the presence of a field depending on the intensity of the applied field. The effect increases with the intensity of the field. However, in the present work very high intensity fields could not be used because of other limitations.

Apart from these rupture tests, a few tests are performed on the wear characteristics of macrofol specimens in rubbing contact with a rotating mild steel disc, both with and without a field. However, the results do not show any conclusive evidence of the effect of field on the rate of wear of the macrofol specimens.

The second section deals with the theoretical study of the effect of an electrostatic field on bond strengths of the simplest molecules and cohesive or binding energies of simple mathematical models of solids, both dielectric and metallic. In the case of the simplest molecule, i.e. a hydrogen-ion like molecule, the bonding is covalent. The basis of covalent bonding is the redistribution of the atomic charge density due to the outermost electrons to produce the overlap charge which is a measure of the strength of binding. Using LCAO (linear combination of atomic orbitals) approach, the problem is dealt at microscopic level by finding the effect of an external electrostatic field on the bond strength of the

simplest molecule - a hydrogen molecular-ion (H_2^+). The presence of an external field distorts the individual atomic orbitals of the binding electrons. This distortion and its effect on the overlap charge is calculated. It is shown that the overlap charge always decreases in the presence of a field for all interatomic separations, clearly indicating a reduction in bond strength.

The same idea is, then, extended to covalently bonded solids. Since atoms are bonded two by two in these solids, it is argued that the above conclusions also hold for simple models of such solids. Considering a one-dimensional linear chain model of a covalently bonded solid, its binding energy is calculated. The effect of an external electrostatic field, (simulated by a chain of charges kept at a distance from the molecular chain) on the binding energy of the linear chain is analysed. It shows that the bond strength is reduced in the presence of a field.

Lastly, the effect of an external electrostatic charge distribution on the binding forces in a linear, one-dimensional metallic chain is studied. The screened electron-ion and ion-ion potentials are calculated taking into account the dielectric constant of the electron gas. The binding energy of the linear chain without and in the presence of a chain of charges is calculated and it is found that the effect of the presence of charges on the binding energy is insignificant.

The last section deals with the study of the effect of an applied electrostatic field on ultrasonic machining of glass. Cylindrical cavities are machined in glass specimens (approx. 1.3 mm thick) both without and with an electrostatic field. It is found that the time required for a depth of cut as small as 0.015" is reduced by about 10-20% in the presence of a field and the effect varies with the intensity of the applied field. Also, the tool penetration rate increases with the penetration of the tool into the workpiece. The experiments are repeated a large number of times and using the analysis of variance technique, the observed data are analysed to show that the change in the rate of machining in the two cases is not due to chance but due to the presence of the field.

CHAPTER 1

INTRODUCTION

1.1 Introduction

The basic objective of all conventional and unconventional machining processes is the removal of excess material from the workpiece in a controlled manner. The process of machining, like many other technological processes involves platic deformation and/or fracture failure of materials. Due to the everincreasing demand for improved machinability and higher productivity, there has been continuous effort by the research workers to ease the removal of material. The problem has become more acute with the development of high strength and temperature-resistant materials which are being used in space, nuclear and other modern technologies. Quite often such new materials possess extremely low machinability and pose critical problems in their machining. Moreover, difficulties in machining are encountered often due to extreme dimensional tolerances, complicated and miniaturised geometry of workpiece. As a result, a host of new technological processes have been developed during the past few decades under the common heading ''New Technology.''

To obtain higher productivity with improved machinability, one of the possibilities is the reduction of the resistance to deformation of work-materials. Therefore, an

extensive research has been conducted in the field of hot machining [1-3]. The introduction of such techniques in conventional machining operations is advantageous to some extent. However, their application is limited due to the fact that heating of work-material is generally accompanied by certain permanent changes in material properties. Apart from this, such heating of work-material may not be feasible in many cases where an unconventional method, for example, ultrasonic machining has to be used. Moreover, application of such heating techniques may not be desirable when work-dimensions are very small.

Most of the unconventional machining processes are characteristically very slow. The overall production time of components which require the application of such slow processes, depends mainly on the time consumed by these processes. Therefore, a significant reduction in machining time can be achieved by accelerating these slow processes. Though, research efforts are directed at developing and improving new technological processes, not much attention has been paid to improve the productivity by controlling the properties of work-materials. The present work is a beginning of the search to find out the feasibility of developing methods to reduce the resistance to deformation or fracture of work-materials without causing any permanent damage to them.

Since the bonding in a solid arises from attractive interactions between atoms which cause a decrease in the aggregate free energy of valence electrons, it is intuitively felt that the application of a suitable electrostatic field might cause a decrease in the bonding forces. If so, the strength or the resistance to deformation and fracture of the solid should decrease as it depends on the strength of the bonds. Further, the strength of a solid also depends on the defects present in its crystal structure and their dynamic characteristics. Therefore, some change in the strength of a solid is also possible due to a change in the defect dynamics caused by an external electrostatic field.

1.2 Review of Previous Work

The effect of steady, external magnetic fields on the mechanical properties of ferromagnetic materials has been investigated in the past [4-7]. It has been reported that certain types of dislocation mobilities are very sensitively dependent on the presence of an external magnetic field. These discloation mobilities control mainly the rate processes and therefore, the rates of wear, creep etc. are significantly enhanced. However, the phenomenon is not of much use for application in machining operations as the strength of work materials during direct plastic deformation remains unaffected.

The effects of high current density pulses on plastic deformation and creep of metal single crystals and polycrystals have also been reported [8-11]. This phenomenon, commonly described as ''electroplastic effect,'' leads to a reduction in flow stress. The effect has been usefully applied to wire drawing and rolling of very hard and tough materials like titanium, tungsten, molybdenum and their alloys etc. [12-13, 42].

The effects of electric fields on heat transfer and combustion [14], surface tension [15], bubble deformation [16] and liquid jets [17] etc. have been investigated. It is reported that the presence of an electric field promotes combustion of liquid fuels, enhances vaporization of a liquid and improves the rate of heat transfer [14], etc. Further, the electrostatic fields have been commercially exploited in the form of electrostatic precipitation and separation, electrostatic imaging, electrostatic coating, electrography and non-impact printing etc. [18]. Though studies on the effect of electrostatic fields in the above areas have been conducted, the author has yet to come across any work concerning the influence of an electrostatic field on the bond strengths and mechanical properties of solid materials. Therefor,, it is logical to assume that no or very little work has been done with the aim to improve the productivity of conventional and unconventional machining operations by applying electrostatic fields.

1.3 Objective and Scope of Present Work

The present work is aimed at conducting theoretical and experimental investigations on the effect of an electrostatic field on interatomic bonding forces and mechanical strength of solid materials. Furthermore, some investigations are carried out to explore the feasibility of practical application of this effect in the machining of solid materials.

Theoretical analysis is to be conducted to find out the effect of an electrostatic field on bond strengths of metals and dielectric materials. It is to be noted that theoretical analysis for actual polycrystalline or amorphous materials is too complicated to be taken up in this work. However, enough indications regarding the effect of electrostatic fields on solids can be obtained by studying diatomic molecules and linear atomic chains.

The experimental work is proposed to be divided into mainly two groups. The objective of the first group of experiments is to find out the effect, if any, of an electrostatic field on some selected mechanical properties of a few materials. For the purpose of investigations, the tensile rupture strength of a material is found to be a suitable mechanical property as it is directly related to the strength of interatomic bonds. To achieve enough intensity of electrostatic field with a voltage source of limited capacity, specimens to be tested are taken in the form of very thin sheets and foils etc.

The objective of the other group of experiments is to apply this principle to a suitable machining operation and investigate the possibility of any resulting improvement. It has already been mentioned that there exist a few processes which are characteristically very slow and ultrasonic machining operation is one of them. Inspite of its inherent low material removal rate, the process is fairly useful in machining electrically non-conducting materials with low machinability. Therefore, it is felt that if the application of an electrostatic field shows some improvement in the productivity of such operations, future intensive research work might lead to a successful development of the electrostatically enhanced ultrasonic machining operations. Therefore a few pilot tests are to be conducted to investigate the effect of an electrostatic field on ultrasonic machining of glass

The theoretical study is ab-initio and based on very simple models. The idea is not of an exact, exhaustive study of a real material but the beginning of an understanding of what the effects of such a field may be, as deduced from very simple but non-trivial models. The scope of the experiments to be conducted is also quite limited. The hardware development necessary for carrying out sophisticated and extensive experimental work of this nature is quite elaborate and has not been attempted because of the limited availability of time. Moreover, since necessary precautionary arrangements cannot be developed and fabricated within the short period of

time available, experiments using very high voltages are ruled out. This restriction obviously limits the magnitude of any effect due to the presence of an electrostatic field. It is possibly because of this reason that some of the experimental observations do not show any effect at all, making it difficult to draw any definite conclusions. Thus, the present work is more or less a feasibility study which lays the foundation for further research in this area. From the point of view of application to manufacturing processes, the idea appears to be quite promising.

CHAPTER 2

INTER-ATOMIC BONDS AND MECHANICAL PROPERTIES

Any study of the behaviour of engineering materials must necessarily begin with an understanding of how the material is constituted from its fundamental units - the atoms. To begin with, one should know how the atoms are bonded to one another and what is the nature and origin of these bonds. Only then, it would be possible to understand the microscopic structure of engineering materials and their mechanical behaviour like deformation and fracture under the action of external influences.

2.1 Binding Energy

The origin of bonding lies in the fact that a system of neutral atoms can rearrange their outer-most electrons among themselves so as to lower their aggregate free energy. In order to see what happens when two atoms are brought together in close proximity, let at first two atoms in their ground states, infinitely far apart be considered. The potential energy of interaction at the beginning, therefore, is zero, since potential energy is inversely proportional to some power of the distance of separation. Assuming that the atoms consist of moving electrical charges, either they will attract or repel mutually as they approach each other. The

potential energy due to the attraction is negative, since the atoms do the work of attraction. The repulsive energy is positive because external work must be done to bring two such atoms together and it is also inversely proportional to some power of the distance of separation of these atoms. The total potential energy is then the sum of two such terms,

$$U = -\frac{\alpha}{r^n} + \frac{\beta}{r^m} \qquad (2.1)$$

where α and β are the proportionality constants for attraction and repulsion, respectively. Figure 2.1(a) shows a plot of Eq. (2.1). The dashed lines show the repulsive and attractive terms and the solid curve the total potential energy.

The forces of interaction can be derived directly from Eq.(2.1) as the force is the derivative of potential energy. Thus,

$$F = -\frac{dU}{dr} = -\frac{n\alpha}{r^{n+1}} + \frac{m\beta}{r^{m+1}} \qquad (2.2)$$

The form of Eq. (2.2) is similar to that of Eq. (2.1) and so is the resultant plot of force as a function of separation shown in Fig. 2.1(b).

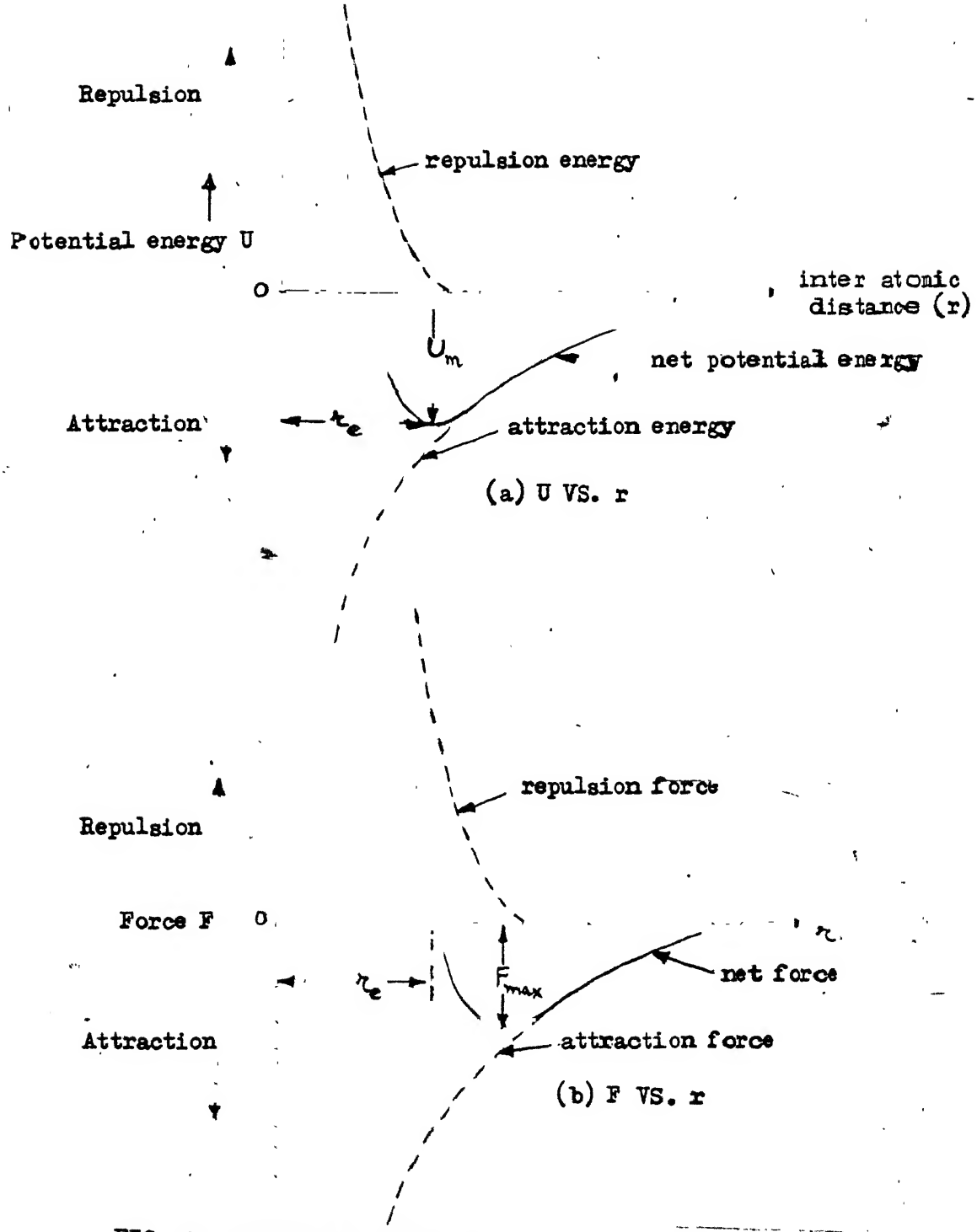

FIG. 2.1 POTENTIAL ENERGY (U) AND INTER-ATOMIC FORCE (F) VS. INTER-ATOMIC SEPARATION DISTANCE (r)

At large distances, the two atoms are attracted by weak electrostatic forces. As they approach each other, the attractive forces increase, and become appreciable when the atoms are separated by only a few atomic diameters. These forces are essentially due to the attraction between opposite charges of these two atoms. Simultaneously, the repulsive forces between the like charges of the nuclei, however, start to assert themselves although somewhat more slowly. At some separation, called the equilibrium separation, r_e, the forces of attraction are equal to the forces of repulsion, and the potential energy is at a minimum. As the atoms try to move closer than this equilibrium separation, the repulsive forces increase more rapidly than the attractive forces and a great deal of work must be done to accomplish such a movement, as can be seen from the rapid increase in the potential energy. The equilibrium separation, r_e, and the corresponding minimum potential energy, U_m, represent the bond length and bond energy, respectively.

2.2 Atomic Bonds

The atoms in a solid are held together by chemical bonds arising from net attractive interaction between two atoms. The bonds can be divided into three general types :

(i) ionic or electrostatic bonds

(ii) covalent bonds, and

(iii) metallic bonds.

2.2.1 Ionic Bond

The ionic bond arises from electrostatic attraction between the oppositely charged ions. These ions result from transfer of one or more electrons from an electropositive atom to an electronegative atom, so that positive and negative ions are formed. When atoms of two different elements react chemically to form a compound, the atoms tend to attain the electronic configuration of an inert gas, i.e. eight electrons in their outer shell. Thus atoms of metallic elements that have only upto three valency electrons in their outer shell will lose their electrons and become positive ions or cations, whereas electronegative elements tend to acquire additional electrons to complete their octet and become negative ions, or anions. The binding energy for an ionic pair, say for Na^+Cl^-, can be estimated from Eq. (2.1). For ionic bonds, n=1 and since both ions have the same electric charge (equal to the charge of an electron, $e_1 = e_2 = e$), the attractive energy term is written as the Coulomb electrostatic attraction in the following form :

$$U_{attr.} = -\frac{e_1 e_2}{r} = -\frac{e^2}{r} \qquad (2.3)$$

The exponent m in the repulsive energy term, β/r^m, is called the Born exponent and can be estimated for specific electronic configurations of the ions. Thus, the net interaction energy of the ion pair (NaCl) is given by

$$U = -\frac{e^2}{r} + \frac{\beta}{r^m} \qquad (2.4)$$

Considering the formation of ionic bonds in case of neutral atoms (e.g. of sodium and chlorine), the net energy necessary for the formation of the corresponding ions Na^+ and Cl^- is equal to the difference between the ionization energy of the sodium atom I_{Na} and the electron affinity of the chlorine atom, EA_{Cl}. The resulting binding energy between the two ions is given by

$$U = -\frac{e^2}{r} + \frac{\beta}{r^m} + (I_{Na} - EA_{Cl})$$

$$= -\frac{e^2}{r} + \frac{\beta}{r^m} + \Delta E \qquad (2.5)$$

Since the electrostatic attraction between the oppositely charged ions acts in all directions, the ionic bond is non-directional. Thus the ions are free to take up any relative positions that are convenient and as many negative ions can be attracted by a positive ion as geometric configuration and the need for preserving electrical neutrality in the solid permit. This accounts for the fact that ionic bonds result in the formation of a three-dimensional giant aggregate in which all units are joined by strong ionic bonds, forming the solid. However, for determining the cohesive

energy of the ionic solid, it is necessary to consider the effect of the other neighbouring ions in the crystal in addition to the electrostatic attraction between the two ions with opposite charges. In order to account for many interactions between ions in ionic crystals, a constant, M, called the Madelung Constant is introduced in the coulombic attraction term, so that the Eq. (2.4) takes the following modified form :

$$U = -\frac{Me^2}{r} + \frac{\beta}{r^m} \qquad (2.5)$$

The Madelung constant depends on the type of the structure of the ionic solid, the charge of the ions, and their relative sizes which, in turn, control their geometric arrangement in the solid.

2.2.2 Covalent Bond

Covalent bonding is basically a two-atom bonding, where outermost loosely bound electrons are shared between similar atoms, thus, lowering the total energy. The electrons participating in the bond are contributed by both atoms as, for example, in a hydrogen molecule (H_2)[1].

$$H. + {}^{*}H = H.{}^{*}H$$

[1] The symbols . and * indicate electrons.

A covalent bond forms when the half-filled atomic orbitals of two atoms overlap and the outermost valence electrons can be shared by these atoms. When the two electrons have oppositely directed spins, this sharing leads to an increased density of the electron cloud between the atoms holding them together. When the spins are parallel, however, the atoms repel each other and no bonding takes place.

The covalent bond lies in the direction in which the orbitals are concentrated in order to achieve the maximum overlap.

2.2.3. Metallic Bond

The valency or conduction electrons in a metal lie much further out from the core of the atom than those in non-metals. Being subjected to the attraction of the positive charges of neighbouring nuclei, the valency electrons pass easily to regions remote from their parent atoms. Consequently, the valency electrons in metals are never permanently associated with any particular atom but flow freely in a random manner and form a "free-electron gas". The typical metallic bond is a many-body effect and can be regarded as an assemblage of positive ion cores immersed in a ''gas'' of free-electrons. The bonding results from the indirect attractive interaction between ion-cores via this

valency electron cloud. The free mobility of the electron ''gas'' accounts for the high electrical and thermal conductivities of metals, as well as for their lustre. Furthermore, the metallic bond is non-specific and non-directional. This leads to highly coordinated close-packed structures, accounting for the unique plastic properties of metals and for their ability to form alloys.

In general, the fewer valency electrons an atom has and the more loosely they are held, the more metallic is the bonding.

In addition, there are weaker secondary bonds originating from dipole-interactions. There is, however, a competition between these various bondings resulting, often, in a compromise for greater stability. This is known as resonating bonding.

2.2.4 Packing of atoms in Solids

The local arrangement of atoms in a solid is usually regular and predictable even though the long range structure may be either regular (crystalline as in metals) or irregular (amorphous as in glasses and many polymers). The arrangement depends partly on whether the bonding is directional or non-directional. If the bonding is directional, the local atomic arrangement is determined by the bond angles. If the bonding is non-directional, the arrangement depends on the relative

sizes of the atoms. In metals, the bond is non-directional and, therefore, each atom tries to surround itself by as many other atoms as possible. This results in close-packed structures like f.c.c., h.c.p or b.c.c.

2.3 Bonding and Mechanical Behavior

In general, the physical and mechanical properties of solid materials are related to their crystal structures and the strength of inter-atomic bonds. For example, the behavior of metals having high mechanical strength properties (e.g. Cr, Ni) is attributable to the very strong inter-atomic bonds which can be broken and formed only by the expenditure of substantial amounts of energy. Consequently hard and strong metals are characterized by a high modulus of elasticity, high yield and fracture stresses. Their physical properties are also affected by the strong atomic bonds, therefore, they have high melting, boiling and recrystallization temperatures and high surface energies. However, soft metals (e.g. Pb, In) have weak atomic bonds and, therefore, exhibit low strength and have low melting and boiling points.

The mechanical properties of a material determine its mechanical behavior. In the study of mechanical behavior of materials, the processes of deformation and fracture are of fundamental importance and are discussed briefly in the following pages.

2.3.1 Deformation

Most of the solid materials change in shape, volume or both under the influence of applied stresses. The applied stresses are transmitted through a solid by way of interatomic forces or internal stresses, which, as a natural result of bonding, arise concurrently with inter-particle-distance-changes or bond-angle-changes. Thus, stress induced change in shape or volume of a solid is simply a macroscopic manifestation of changes in bond-lengths or in bond angles between atoms, ions or molecules in the solid. The deformation is called elastic if the change is completely recovered on the removal of stresses. On the other hand, permanent deformation is due to flow, a process of shear in which particles in a substance change neighbors without any volume change. Interatomic and intermolecular forces and structure play an important role in both elastic and permanent deformations, although the former are much less significant in flow than they are in elastic behavior.

The permanent deformation may take place due to either plastic flow, as in case of crystalline solids, or viscous flow as in case of non-crystalline substances. Plastic flow involves the sliding of atomic planes relative to one another in a crystallographically organised fashion. It has been established from numerous studies of crystal plasticity in mineral crystals that crystal structure tends

to be preserved during a plastic change of shape [19]. This fact is consistent with energy minimization principle since crystalline form is the minimum energy state for an aggregate of atoms. The fact that plastic flow does not destroy the crystal structure severely limits the number of ways in which the deformation can occur. Actually there are only two modes of deformation that completely conserve a crystal's structure and these are translation and twin-gliding [19].

Translation-gliding or slip is the most important mechanism of plastic deformation and causes the plane of atoms to glide over one another as shown in Fig. 2.2(a) by the motion of dislocations. Thus, one part of the crystal slides or translates over the rest. Such translations always restore the pattern, but out of the large number of geometrically possible translations in a given structure, only those that have a kinetically favorable mechanism actually take place when a stress is applied. That is why slip occurs over specific crystallographic planes in definite crystallographic directions. Usually slip occurs most easily on the most densely packed planes in a close-packed direction for a given crystal structure. The number of slip systems in a crystal is the number of possible combinations of slip planes and slip directions.

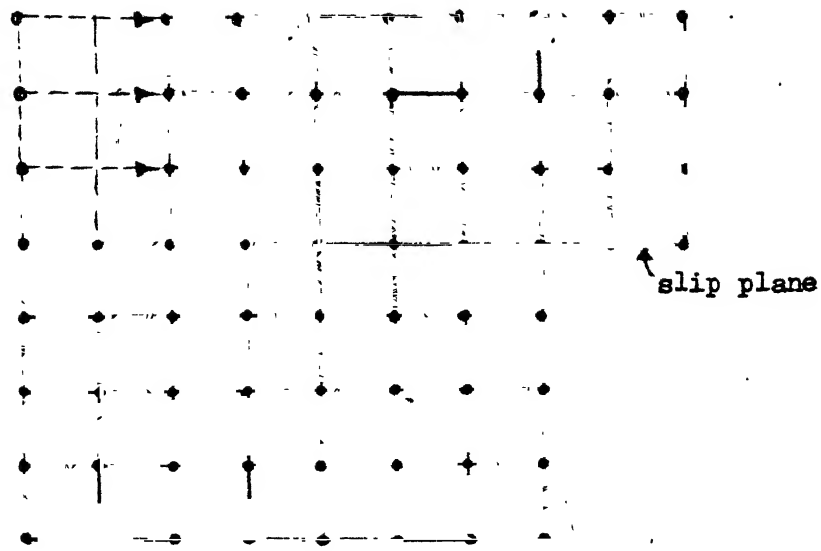

(a) Slip

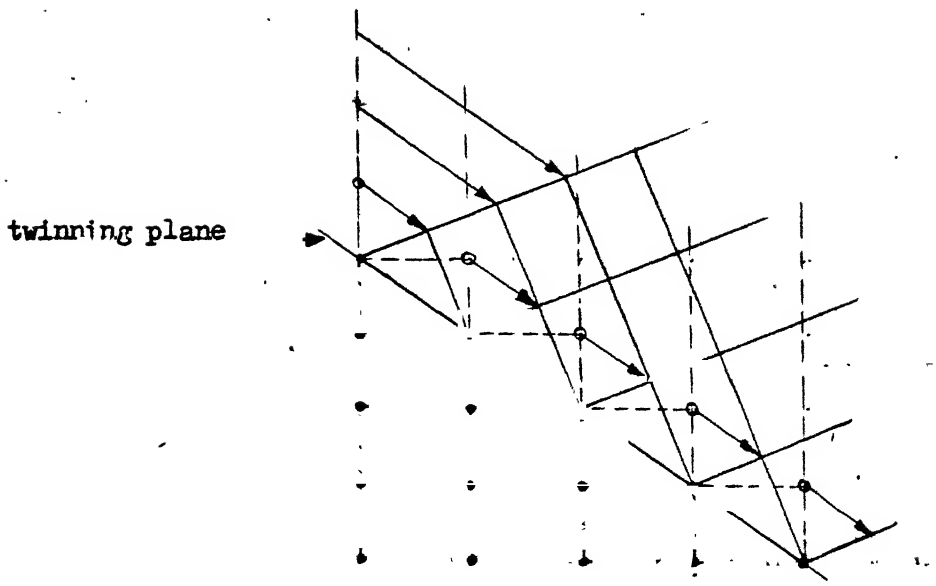

(b) Twinning

FIG. 2.2 SLIP AND TWINNING

The large number of slip systems (≥ 12) for most metals is responsible for the extensive plastic flow or ductility of metals. The ease with which dislocations in metals move readily at small applied stress levels arises due to the fact that atomic bonds are not broken in this process. However, the inherent resistance to motion of dislocations originates from the unfavorable atomic configurations and bond stretching concurrent with any motion. Accordingly, the critical resolved shear stress, required to initiate slip in a single crystal, depends directly on the type of crystal structure and the nature of chemical bonds.

In contrast to metals, ionic and covalent engineering solids are normally brittle at room temperature. This is not due to inherently greater bond strengths or due to a lack of dislocations; rather, these materials have fewer active slip systems which can not accomodate significant plastic flow.

The second mechanism of plastic deformation, which is important in some materials, is deformation twinning. Twinning is the process in which the atoms in a part of a crystal, subjected to stresses, rearrange themselves so that one part of the crystal becomes a mirror image of the other part as shown in Fig. 2.2(b). Every plane of atoms shifts in the same direction by an amount proportional to its distance from the twinning plane. Twinning, usually

its distance from the twining plane. Twinning, usually requires a higher shear stress than slip, and it is relatively insignificant in many plastic deformations. However, whenever the possible slip systems are considerably limited, as in the case of metals having h.c.p. structure, twinning becomes an important mode of deformation. It frequently occurs in b.c.c. and h.c.p. structures.

2.3.2 Fracture

Fracture is separation of a body, caused by applied forces, into two or more parts resulting in the creation of new surfaces. There are many mechanisms leading to fracture, depending on the nature of the material, the nature of the applied stress, temperature conditions, strain-rates, and other environmental factors. But, usually, fracture is characterized as either brittle or ductile and can be considered to consist of two phases - crack initiation and crack propagation. A ductile fracture is characterized by appreciable plastic deformation prior to and during the slow propagation of a crack which is formed as a result of formation and coalescence of voids. Ductile fracture occurs when the stress applied to a specimen exceeds the strength of inter-atomic forces holding its atoms together. Brittle fracture is characterized by a rapid rate of crack propagation, with no gross deformation and very little micro-deformation. It occurs if the component of stress normal

to the slip plane exceeds the bonding strength before the critical resolved shear stress is reached.

(a) Mechanism of ductile fracture

A ductile fracture under tensile stress, in general, involves three successive events. First, the specimen necks, cavities form in the necked region, and join together. Second, a cavity eventually becomes large enough to spread fairly rapidly in the transverse direction. Finally this crack spreads to the surface following a direction inclined at about 45° to the tensile axis. The result is the familiar ''cup and cone'' fracture of moderately ductile metals.

It has been reported [20] that during tensile loading, the shear deformation creates flaws which the tensile stress helps to open; that is, the tensile stress exerts a directing influence on the shear deformation, causing the cavities to enlarge and, thus, producing a crack. When a crack is present in a material, the stress close to the crack, σ_{local}, is greater than the average tensile stress, σ, applied to the material. Mathematically, local stress ahead of a sharp, central crack of length 2a, in an elastic material is given by [21]

$$\sigma_{local} = \sigma\left(1 + \sqrt{\frac{a}{2r}}\right) \qquad (2.6)$$

where, r is radius vector measured from crack tip along crack-axis as shown in Fig. 2.3. The closer one approaches to the tip of the crack (r decreasing), the higher the local stress becomes, until at some distance, r_y, from the tip of the crack, the stress reaches the yield stress, σ_y, of the material, and plastic flow occurs.

The distance r_y can be calculated by setting $\sigma_{local} = \sigma_y$ in Eq.(2.6). Assuming that $r_y \ll a$,

$$r_y = \frac{\sigma^2 a}{2\sigma_y^2} = \frac{K^2}{2\pi\sigma_y^2} \qquad (2.7)$$

where, $K = \sigma\sqrt{\pi a}$. K is called the stress intensity factor and represents the loading condition. The crack propagates when $K = K_c$ (the critical value of K which is a property of the material) and then the width of the plastic zone is given by

$$r_y = \frac{K_c^2}{2\pi\sigma_y^2} \qquad (2.8)$$

It is clear that the size of the plastic zone shrinks rapidly as σ_y increases, i.e., cracks in soft ductile metals have a large plastic zone and cracks in hard ceramics have a small zone, or none at all.

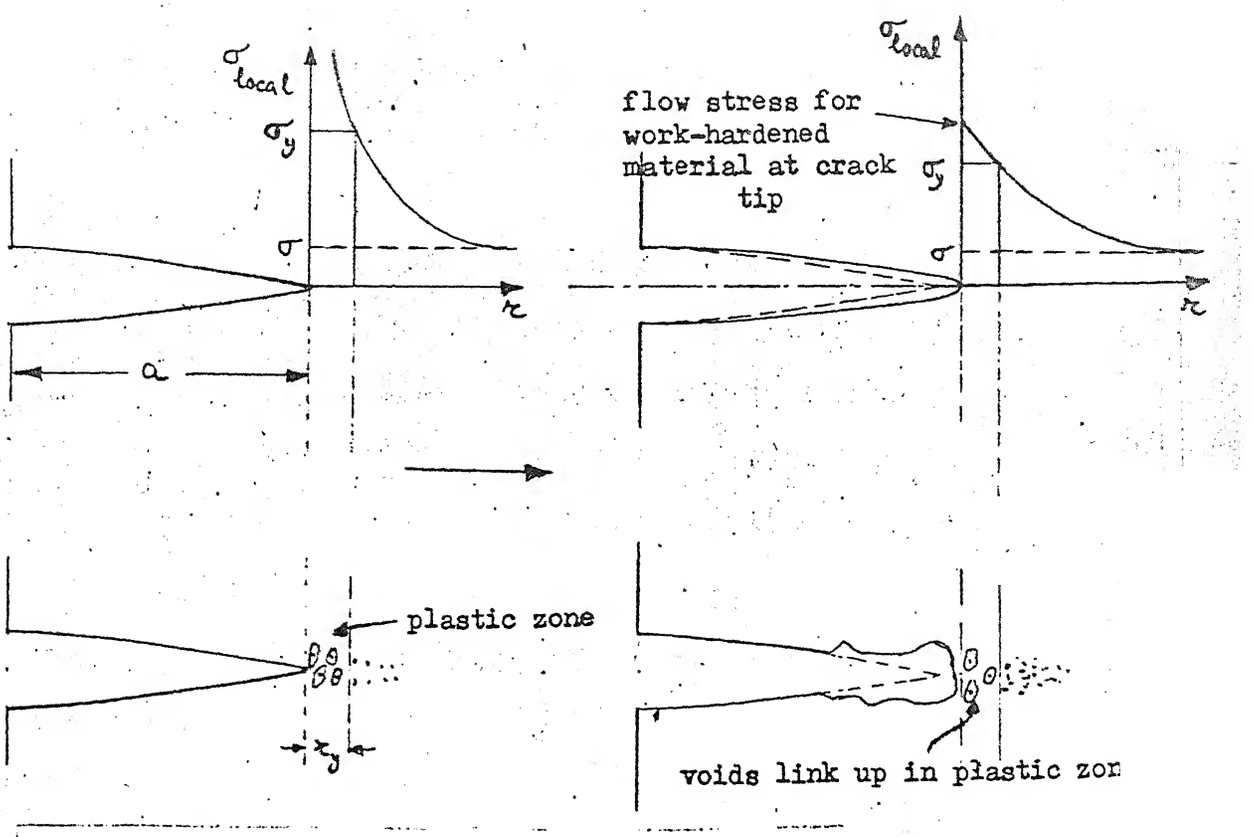

FIG. 2.3 CRACK PROPAGATION BY DUCTILE TEARING

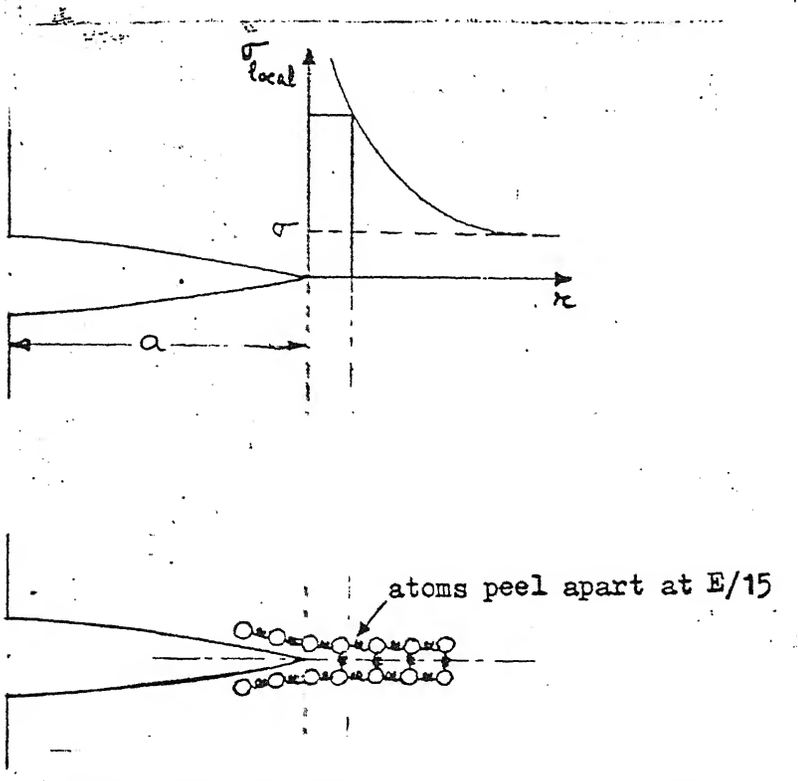

FIG. 2.4 CRACK PROPAGATION BY BRITTLE CLEAVAGE

Most metals, even when nominally pure, contain tiny inclusions (or particles) of chemical compounds formed by reaction between the metal and impurity atoms. Within the plastic zone, plastic flow takes place around these inclusions, leading to elongated cavities, as shown in Fig. 2.3. As plastic flow progresses, these cavities link up, and the crack advances by means of this ductile tearing. The plastic flow at the crack tip naturally turns initially a sharp crack into a blunt crack, decreasing σ_{local}. The decrease (in σ_{local}) is such that σ_{local} is still sufficient to keep the plastic deformation of the work-hardened material in the region near the crack tip, going [21].

An important aspect of crack growth by ductile tearing is that it consumes a lot of energy in plastic flow; the bigger the plastic zone, the more energy is absorbed. This is the reason for ductile metals being so tough.

(b) Mechanism of brittle fracture

The characteristic feature of brittle fracture is that little or no plastic deformation takes place during the spread of a crack. This is evident from the fracture surfaces of a ceramic or glass which, on examination, are found to be featureless, flat surfaces. When a brittle material containing a crack is subjected to a tensile loading, the local stress ahead of the crack tip, given by Eq. (2.6) can approach

very high values near to the crack tip provided that blunting of sharp crack tip does not occur. In amorphous materials like ceramics and glasses which have very high yield strengths, very little plastic deformation takes place at crack tips and, thus, the chances of crack blunting are very small. Even allowing for a small degree of crack blunting, the local stress at the crack tip is still in excess of the ideal strength and is, thus, large enough to literally break apart the local inter-atomic bonds as shown in Fig. 2.4; the crack then spreads between a pair of atomic planes giving rise to an atomically flat surface by cleavage [21]. The energy required to simply break the inter-atomic bonds is much less than that absorbed in ductile tearing of a tough material, and this is why materials like ceramics and glasses are so brittle. However, these materials possess a critical normal fracture stress several order of magnitude less than the theoretical cohesive material strength, suggesting that the existence of dislocations also plays a part in the failure of these materials.

Dislocation movement is greatly hampered in brittle materials by their types of inter-atomic bonding. The metallic bonds permit the ion-cores to arrange themselves in various close-packed arrays, but as their structures change, the partially covalent natures of these bonds increase. They become relatively restricted in space, requiring much larger forces to disrupt them than the non-oriented bonds do.

The dislocations which are present, even in completely covalent materials such as diamond, are, therefore, severely constrained in their mobility. The application of external stress fields to such covalently bonded materials tends to produce microcracks, rather than induce slip in their structures. When a sufficient number of these microcracks develop, or when they exceed a certain critical size, they will propagate through the crystal, causing brittle cleavage along the cleavage plane.

2.3.3 Other Aspects of Mechanical Behavior

In addition to deformation and fracture, there are other phenomena which are important in the study of mechanical behavior of solids. The phenomena of friction, wear and fatigue are well known and have been studied extensively. They are discussed here very briefly.

(a) Friction

Frictional behavior is attributed to the possible adhesion between plastically deforming asperities at the interfacial contact under the application of normal loads; followed by shearing of the cold-welded junctions when tangential motion is exerted. On the basis of experimental evidence, it has been reported that friction depends on the strength of inter-atomic bonds and displays a periodic variation relative to the atomic number in a manner analogous to that of other properties [22].

(b) Wear

Wear occurs as a natural consequence when two surfaces with a relative motion interact with each other. It can be defined as ''the debris of material produced as a result of repeated disturbances of the frictional bonds''. Wear may occur due to adhesion, abrasion, diffusion, and corrosion etc. It depends on the strength of inter-atomic bonds as strong and hard materials wear less in comparison to weak and soft ones.

(c) Fatigue

Fatigue is a manifestation of a cumulative process leading to progressive fracture under cyclic loading. The stress level required to cause fatigue failure is much less than that required for static failure. The mechanism of fatigue is based on the initiation and propagation of a crack. The fatigue failure of ductile metals is considered as a consequence of slip in certain local regions of a crystal, where the limiting lattice strains are exceeded resulting in rupture of atomic bonds and thus, causing discontinuities in the lattice.

2.3.4 Strength

A solid is characterized by its resistance to deformation that is its strength. The ''strength'' of a solid represents the following three characteristics :

(i) Its resilience, or elasticity, when subjected to transient forces;

(ii) Its resistance to flow i.e. the resistance to a permanent change in shape under the action of a sustained force ;

(iii) Its resistance to fracture or crack propagation.

Thus, strength depends on the collective response of a solid to applied stresses, in other words, it depends on the behavior of aggregates of particles (elasticity), surfaces composed of particles (fracture), or lines of particles (flow via dislocation) and not simply the behavior of single particles [19].

The large variation in the resistance to plastic deformation of solids is a consequence of the dislocation mechanism of the flow process. The resistance to plastic flow depends on

(i) the strength of chemical bonds that exist between adjacent atoms in the structure,

(ii) the atomic pattern or crystal structure, because the ease with which dislocations move through a crystal is sensitive to the periodicity of the pattern, and

(iii) the impurities present.

Crystals that are not pure are, usually, much more resistant to deformation than those that are pure. This results from disturbance of the periodic crystal structure by the impurities and from local bonds that arise between impurities and their neighbors.

CHAPTER 3

EFFECT OF AN EXTERNAL ELECTROSTATIC FIELD ON MECHANICAL PROPERTIES - EXPERIMENTAL INVESTIGATIONS

3.1 Interaction of an Applied Field with a Material

A material placed in an electric field, as between the plates of a capacitor, interacts with the field through the displacement of charged particles within the material. If the material is a conductor, some of the free electrons simply move to the side nearest the positive electrode until they completely counteract the applied field. Thus no field is left within the material. The shift occurs almost instantaneously, bringing about equilibrium.

If the material is a dielectric, it polarizes under the influence of a field. The polarization, like elasticity, owes its origin to the existence and stability of atomic and molecular forces. It varies linearly with the applied field for most dielectric materials and is caused by the following factors :

(a) The displacements of electric charges with respect to each other which induce dipoles in the material. The displacements are reversible.

(b) Interaction between the applied field and the permanent dipoles present in the material. An electric field acts to align a permanent electric dipole in the direction of the field.

The displacements of electric charges or dipoles activate restoring forces which either do work, releasing electrical energy or resist the displacements causing the external forces to do work on the system and, thereby, storing electrical energy. It should be noted that the forces that come into play due to an applied electric field are weak compared to the atomic forces. They are in fact so weak that the displacements produced by these forces are quite small compared to the radius of the molecule.

Depending on the origin of the restoring forces acting on the charges, the polarization can be divided into electronic, ionic and orientation components. Electronic polarization arises because the center of the electronic charge cloud around a nucleus is displaced under the action of an applied electric field, creating a small induced dipole as shown in Fig. 3.1(a). Ionic polarization occurs in ionic materials because an applied field acts to displace cations in the direction of the field and anions in a direction opposite to the field, giving rise to a net dipole moment per cation - anion pair as shown in Fig. 3.1(b). Both the electronic and ionic polarizations essentially proceed in an instantaneous,

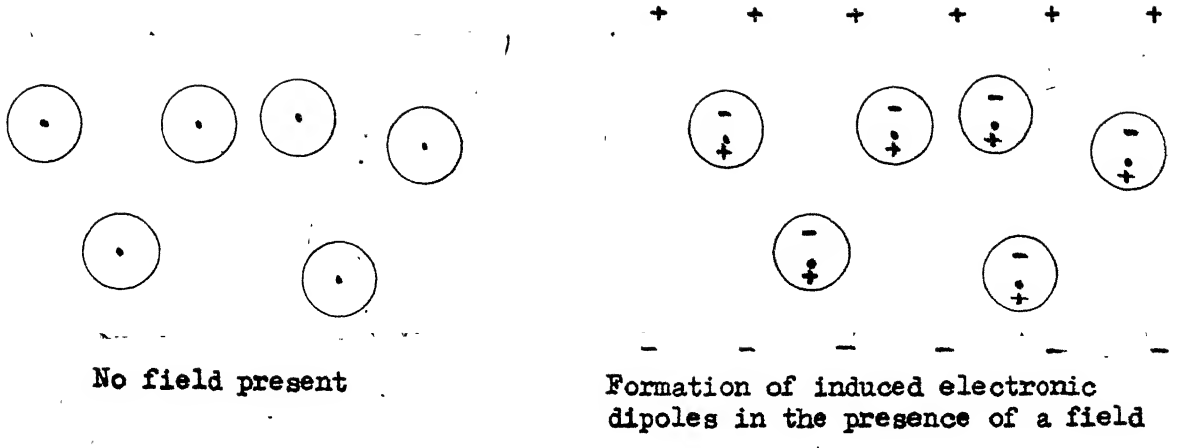

No field present

Formation of induced electronic dipoles in the presence of a field

(a) Electronic Polarization

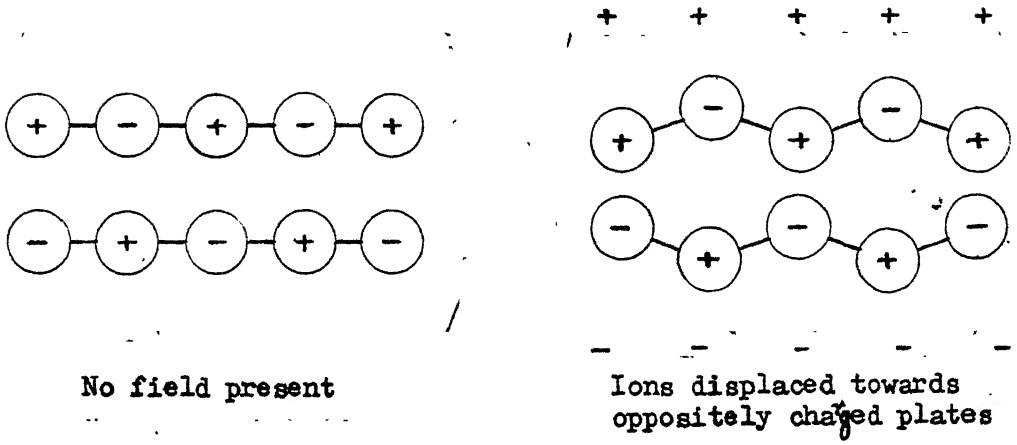

No field present

Ions displaced towards oppositely charged plates

(b) Ionic Polarization

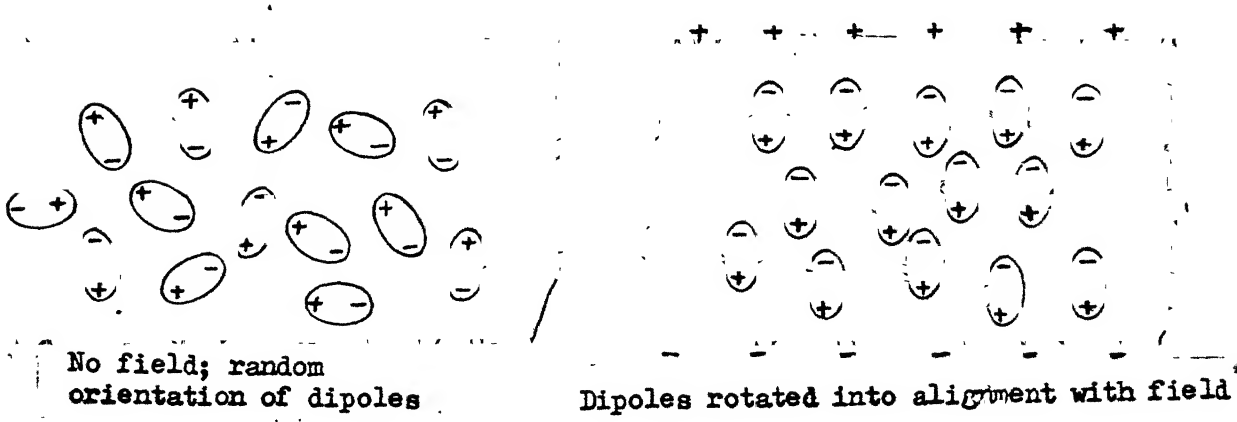

No field; random orientation of dipoles

Dipoles rotated into alignment with field

(c) Dipole Polarization

FIG. 3.1 DIFFERENT TYPES OF POLARIZATIONS

fairly elastic manner, without dissipation of energy in the form of heat.

Orientation polarization occurs in substances composed of molecules that have permanent electric dipole moments, for example polar polymers and glass. These permanent dipoles tend to become aligned with an applied field as shown in Fig. 3.1(c), but the randomizing effect of thermal agitation (entropy effects) tend to neutralise this. However, permanent dipole moments are, in general, much larger than induced dipole moments and therefore have a greater polarizing effect when fully oriented. The orientation polarization builds up and decays slowly with the dissipation of energy in the form of heat [23].

Conductors of electricity do not exhibit a dielectric behaviour, because the displacement of charges in the conductor is not accompanied by any restoring forces.

The common origin of dielectric polarization and elastic deformation accounts for the weak interaction or coupling existing between these two properties which gives rise to the phenomena of electrostriction and piezoelectricity. Electrostriction is a deformation caused by the shift of electron clouds or nuclei in an electric field and is common to all dielectric solids. It is a one-sides effect, i.e., polarization deforms a dielectric solid, but, deformation of a dielectric material does not cause its polarization [24].

3.2 Field in a Parallel-Plate Capacitor

During the experimental study of the influence of an electrostatic field on some mechanical properties of a few materials, the field is produced by using an arrangement similar to a parallel plate capacitor shown in Fig. 3.2. When a voltage is impressed across the plates of the capacitor, one plate becomes charged positively and the other negatively. The field between the plates is uniform and directed from the positive to the negative plate and its intensity is given by

$$E = \frac{V}{l} \qquad (3.1)$$

where, V is the applied voltage across the plates, and

l is the distance separating the plates.

The space between the plates is filled with a dielectric material of thickness l. The magnitude of charge per unit area on either plate, called the electric displacement, D, is directly proportional to the field, i.e.,

$$D = \varepsilon E \qquad (3.2)$$

where, D is electric displacement in C/m^2

E is in V/m

ε is a constant, called permittivity of the dielectric material placed between the plates.

The electric displacement, D, can also be represented as the sum of two components as follows:

$$D = D_o + P \qquad (3.3)$$

where, D_o is electric displacement if the plates are separated by a vacuum, and

P is an electric displacement proportional to the polarization of dielectric material between the plates.

Thus,

$$D = \varepsilon E = D_o + P$$

$$= \varepsilon_o E + P \qquad (3.4)$$

where, ε_o is permittivity of vacuum ($= 8.854 \times 10^{-12}$ C/V.m.)

The relative permittivity or dielectric constant, ε_r, is a property of the dielectric material and is defined as

$$\varepsilon_r = \frac{\varepsilon}{\varepsilon_o} = \frac{D}{D_o} = 1 + \frac{P}{D_o}$$

and is always greater than unity.

It is clear from Eq. (3.1) that for a given applied voltage, the smaller the thickness of dielectric material introduced between the plates, the higher the electric field strength. The maximum field strength is determined by the dielectric strength. Thus, by using sufficiently small thicknesses of dielectric material between the plates of the capacitor, very high intensities of the electric field can be obtained.

3.3 Experimental Investigations

The objective of the experimental study, as explained earlier, is to find out the effect of an electrostatic field on some mechanical properties of a few materials. The mechanical property chosen for experimental investigations should be directly related to the strength of interatomic bonds. Since, the interatomic bonds are broken across the fracture surface during a tensile rupture, the tensile rupture strength is found suitable for the purpose of experimental investigations. The effect of field is investigated on both conductors and dielectrics. Further, a few simple tests are carried out to determine the effect of an electrostatic field on the wear of a dielectric material.

3.3.1 Tensile Rupture Test

When a specimen is subjected to a tensile loading, it ultimately breaks into two or more pieces. The force required to fracture the specimen depends mainly on the strength of inter-atomic bonds as the bonds are ruptured during fracture. It is, therefore, possible to determine qualitatively the effect of an electrostatic field on bond strengths by comparing the tensile rupture strengths measured without and in the presence of a field.

The tensile rupture tests are conducted on the following materials during the present investigations:

(i) Aluminium foil, 10 mm wide, 10 and 20 micron thick.

Such thin foils of aluminium are used to detect the effect, if any, of a surface charge distribution on its strength.

(ii) Aluminised mylar, 10 mm wide and 20 micron thick.

Mylar is polyethylene terephthalate, also known as melinex or terylene. It is a polyester material. Its dielectric constant is approximately 3.0 and has a dielectric strength of about 200 V/micron.

One of its surface is coated with aluminium to make that surface conducting giving rise to the name aluminised mylar.

(iii) Macrofol film, 10 mm wide and 20 micron thick.

It is a film of a polymer known as polycarbonate.

(a) Experimental Procedure

The tensile rupture tests are performed on an Instron Machine (Model TT-CM-L). The machine can be operated at various cross-head speeds to obtain different rates of straining. A load cell of 0-50 Kg. range is used during the tests to measure the tensile load on the test specimen which is held in insulated grips of the machine. A trace of the load versus cross-head displacement is recorded on the chart moving at a constant speed during the tests. To test the specimens of conductor and dielectric materials in the presence of an external electric field, the arrangements for producing the field are made as follows :

(i) Arrangement for specimens of Al-foil

In case of Al-foil test specimens, the electric charges are distributed over their surfaces by using an arrangement similar to a parallel plate capacitor as shown in Fig. 3.3. The test specimen acts as one of the plates of the capacitor and is connected to either terminal of a high potential d.c. supply (Cenco made).

The actual arrangement used during the tests is shown in Fig. 3.4 and the materials required for it are given

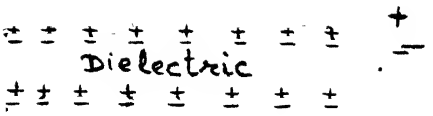

FIG. 3.2 A PARALLEL PLATE CAPACITOR

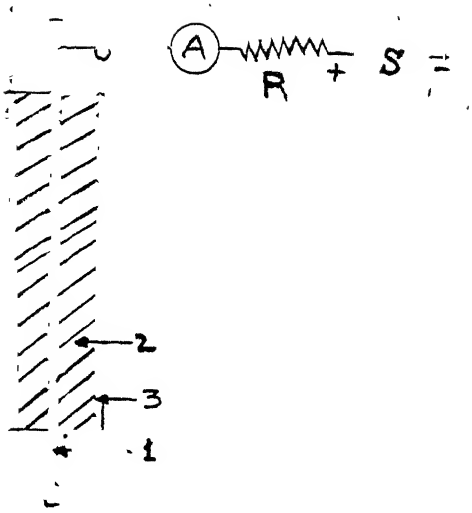

FIG. 3.3 DIAGRAM ILLUSTRATING THE APPLICATION OF ELECTRO-STATIC FIELD DURING TENSILE TESTING

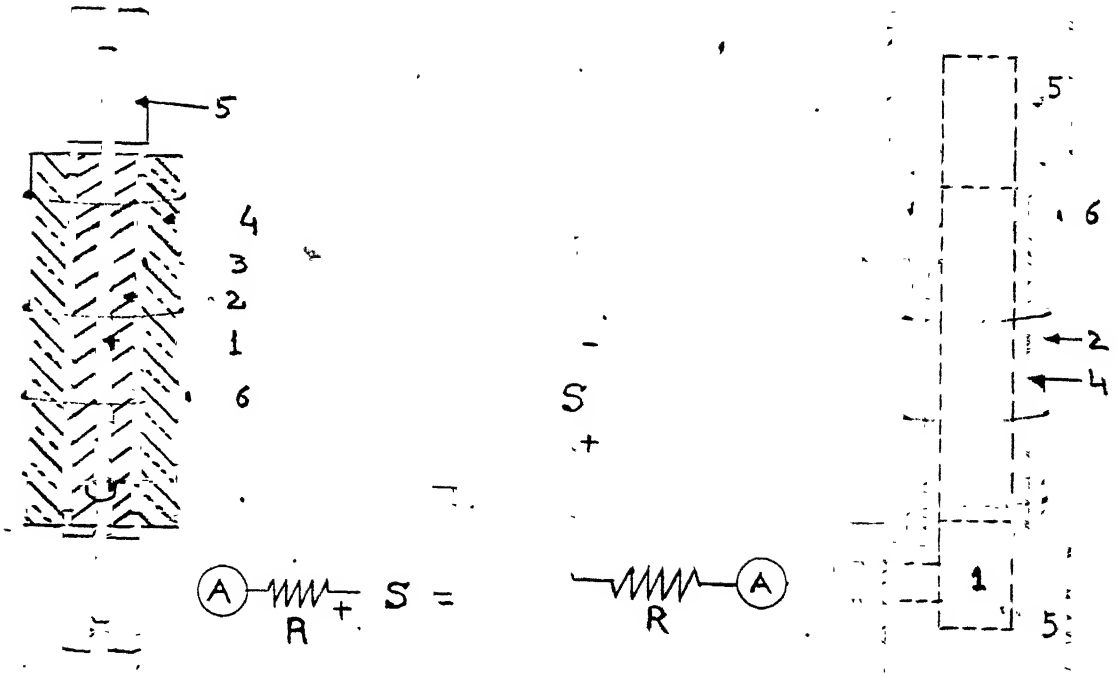

(a) Side view (b) Front view

FIG. 3.4 ARRANGEMENT FOR APPLYING FIELD TO ALUMINIUM-FOIL TEST SPECIMENS

1- Test specimen (conductor) 2- PVC sheet
3- Capacitor plates (Al-foil) 4- Perspex sheet
5- Insulated grips 6- Rubber bands
A-Microammeter S-High potential D.C. supply
R-Resistance (0.3 megaohms)

in Table 3.1. The Al-foil strip with a side projection (for making electrical connections) is pasted on the perspex piece by an adhesive and then the piece of PVC sheet is pasted over this Al-foil strip to cover it. Two pieces of perspex are prepared like this and allowed to set and dry for some time. The specimen to be tested is cut from a sheet of Al-foil and arranged between the two perspex pieces symmetrically as shown in Fig. 3.4(a). Rubber bands are put around this assembly to hold it which is now mounted on the Instron Machine by gripping the projecting ends of the test specimen in insulated grips. Whether the field is applied or not, all the specimens are tested in the same fashion so that, as far as possible, the tests are performed under identical conditions.

To distribute an electrostatic charge (positive in this case) on the surface of the test specimen, the specimen is connected to the positive terminal of the high potential d.c. supply. The connection is made through a 0.3 mega-ohms resistance and an ammeter (0-100 μA range). The other terminal of the supply is connected to the outer plates of the capacitor as shown in Fig. 3.4(a). The d.c. supply is connected through a 115 V transformer to the 230 V mains.

The charge per unit area, D, on Al-foil test specimens is approximately given by

Table 3.1 : Materials required for tensile rupture tests.

Material	Size	Numbers
1. Perspex sheet	58 mm x 18 mm x 3.25 mm	2
2. Al-foil strips with side projections	54 mm x 16 mm x 0.04 mm	2
3. P.V.C. sheet	60 mm x 22 mm x 0.125 mm	2
4. Al-foil test specimens	80 mm x 10 mm x 0.01 mm	50
	80 mm x 10 mm x 0.02 mm	40
5. Macrofol test specimens	80 mm x 10 mm x 0.02 mm	100
6. Aluminised mylar specimens	80 mm x 10 mm x 0.02 mm	80

$$D = \varepsilon E = \varepsilon_o \varepsilon_r \frac{V}{l} \quad C/m^2$$

with

$\varepsilon_o = 8.854 \times 10^{-12}$ C/V.m. for vacuum

$\varepsilon_r \simeq 3.5$ for PVC sheet at low frequencies

$l = 0.125 \times 10^{-3}$ m (= the thickness of PVC sheet)

D comes out to be approximately $2.45 \times 10^{-7} V$ C/m^2

Therefore, with V = 1000 volts, $D \simeq 2.45 \times 10^{-4}$ C/m^2.

(ii) Arrangement for specimens of aluminised mylar

The tensile rupture tests on aluminised mylar specimens are conducted by arranging them as shown in Fig. 3.5(b) where one of the PVC sheets is removed and the conducting surface of mylar specimen is placed in contact with the Al-foil fixed to the perspex piece.

(iii) Arrangement for specimens of macrofol film

The macrofol test specimens are placed between the plates of a parallel plate capacitor according to three different schemes as follows :

I. The test specimen is placed symmetrically as before but now the plates of the capacitor are connected to different terminals of the d.c. supply as shown in Fig. 3.5(a). In this case, the thickness of the dielectric material separating the plates of the capacitor, l, is given by

l = thickness of two PVC sheets+thickness of macrofol specimen

$= 2(0.125) + 0.02 = 0.27$ mm

Therefore, electric field strength, $E = \frac{V_{mm}}{0.27}$

$= 3.7V$ volts/mm.

II. The test specimen is placed as in (a) above but one of the P.V.C. sheet piece is removed so that the test specimen is now, in an asymmetric position with respect to the parallel plates of the capacitor. The plates of the capacitor are connected to the supply as shown in Fig. 3.5(b). The electric field strength, in this case, is given by

$$E = \frac{V}{0(0.125 + 0.02)} = 6.9V \text{ volts/mm.}$$

III. In this arrangement, the second PVC sheet is also removed so that the test specimen is now, directly

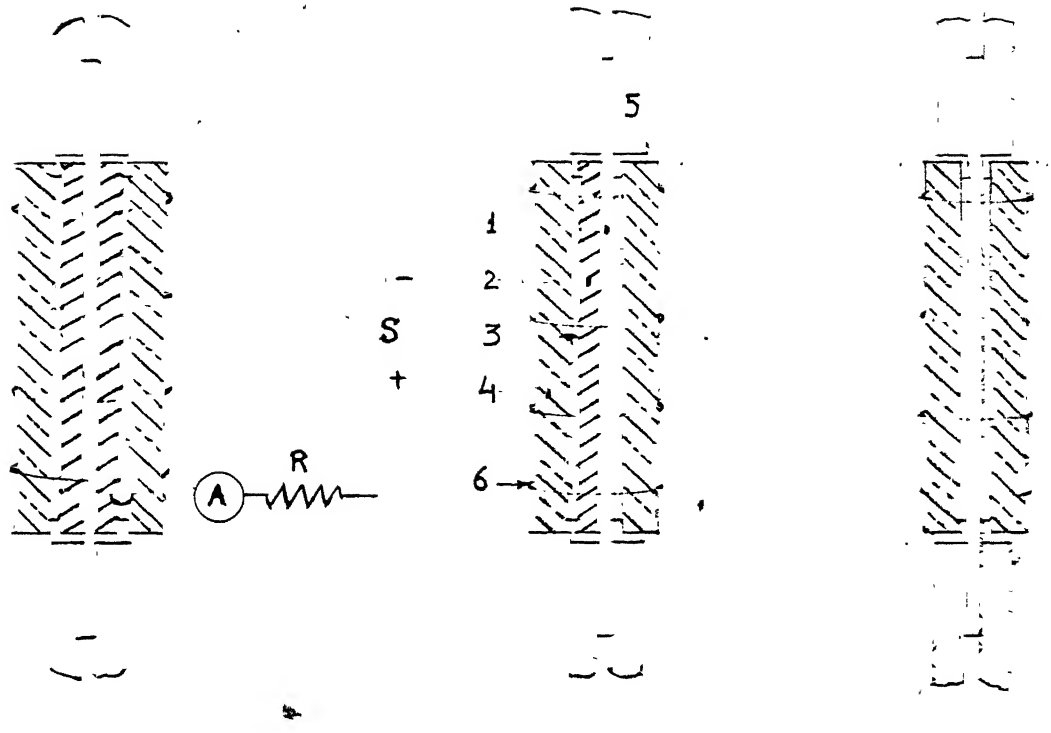

I-Symmetric II-Asymmetric III-Symmetric

FIG. 3.5 ARRANGEMENT FOR APPLYING FIELD TO MACROFOL TEST SPECIMENS

1 - Test specimen
2 - PVC Sheet
3 - Capacitor plates (Al-foil)
4 - Perspex sheet
5 - Insulated grips
6 - Rubber bands
A - Microammeter
S - High potential D.C. supply
R - Resistence (0.3 megaohms)

placed between the plates of the capacitor as shown in Fig. 3.5(c).

The electric field strength, in this case, is given by

$$E = \frac{V}{0.02} = 50\ V \text{ volts/mm.}$$

This arrangement is not very suitable for conducting tensile rupture tests with a field because, on loading the specimens, it is found, sometimes, that sparking occurs across the narrow gap ($\simeq 0.02$ mm) between the capacitor plates which are connected to a high voltage supply. The sparking may cause the deposition of electric charges on the surface of dielectric specimen which distorts the electric field in the material, making the field non-uniform. Therefore, the observations in this case may not give a true indication of the effect of field on rupture strength.

(b) Results and Discussions

After mounting the test specimen in the grips of the Instron machine, a suitable cross-head speed is selected for loading the specimen. The chart on which load-displacement curve is to be recorded is switched on. If the specimen is to be tested in the presence of a field, the d.c. supply is also switched on. As the machine is started, the specimen is loaded gradually at a constant rate. Simultaneously, the load-displacement curve is recorded on the chart. The machine

is stopped after the specimen fractures and the load at fracture (in number of divisions of chart) is read from the chart. The observations are shown in Tables 3.2 to 3.4. The results shown in Table 3.2 indicate the effect of electrostatic charge accumulation on the rupture strengths of Al-foils. Results are given for both positive and negative charge distributions and they clearly indicate that there is no significant effect of external charges on rupture strength of the foils. Most probably the effect of the charge distribution is nullified by the conduction electron clouds.

Table 3.3 shows the rupture strengths of aluminised mylar specimens without and in the presence of an electrostatic field. To get a qualitative idea about the effect of an electrostatic field, experiments are conducted with only one intensity of the field. In spite of some scatter in the rupture load, it is quite clear that rupture strength decreases in the presence of the field. The frequency distributions of rupture strengths are calculated and shown in Table 3.5. The distributions are plotted in Fig. 3.6(a). The shift in the frequency distribution curve is an indication of the effect of electrostatic field on the rupture strengths of mylar specimens.

More elaborate experiments are conducted on macrofol film specimens. Not only that the different schemes of applying the field are used but, also, the experiments are

conducted with varying intensities of the field. The results are shown in Table 3.4. The columns I and III of the table show the results for symmetric configurations (corresponding to Fig. 3.5(I) and (III)) whereas the column II shows the results for asymmetric case (corresponding to Fig. 3.5(II)). It is clear from the results shown in the table that the rupture strength decreases in the presence of a field. The decrease in rupture strength varies from 6.5 to 14 percent depending on the intensity of the field applied. Comparing the results of columns (3), (4) and (5) of the table, it is seen that the drop in rupture strength increases with the intensity of the field. Further, when the drop in rupture strength in symmetric case (col. (2)) is compared with that of asymmetric situation (col.(4)), it is found that the decrease in rupture strength is more in asymmetric case although the field intensities are approximately the same in the two cases. The same fact is revealed when results of columns (2) and (5) are compared where the intensity of field in column (5) is approximately half of that in column (2) but the drop in rupture strength is approximately the same. On the basis of these observations, it is concluded that an applied field has a stronger effect when the (dielectric) test specimen is arranged asymmetrically between the plates of the capacitor.

Table 3.2 : Results of tensile rupture tests on specimens of Al-foil.

Instron machine cross-head speed = 0.5 mm/min.
Gage length of test specimens = 62.0 mm.
Width of test specimens = 10.0 mm

	Thickness of test specimen = 10 micron			Thickness of test specimen = 20 micron	
	5 divisions of chart = 1.0 Kg			2 divisions of chart = 1.0 Kg	
D.C. Volts	0.0	-4.0 KV	+4.0 KV	0.0	+4.0 KV
S.No.	Rupture load read from the load - elongation curve in terms of no. of divisions of chart.				
	(1)	(2)	(3)	(4)	(5)
1	9.1	8.20	7.85	7.15	7.30
2	9.1	9.00	8.18	7.00	7.30
3	8.77	8.38	9.05	7.16	7.20
4	8.98	9.13	9.20	7.22	7.30
5	8.90	9.07	8.80	7.32	7.32
6	8.93	8.32	9.30	7.13	7.15
7	8.99	8.57	8.42	7.38	7.12
8	8.90	8.90	9.00	7.13	7.18
9	8.80	8.86	8.50	7.20	7.16
10	8.65	9.10	8.90	7.20	7.10
Average rupture strength	8.912	8.753	8.72	71.89	72.13
Percent change in rupture strength	-	-1.78	-2.15	-	+0.334

Table 3.3 : Results of tensile rupture tests on specimens of aluminised mylar.

Instron machine cross-head speed = 2 cms/min.
Gage length of specimens = 42.0 mm
Width of test specimens = 10.0 mm
Thickness of test specimens = 20.0 micron

5 division of chart = 1.0 Kg

D.C. Volts	0.0 V	+ 4.0 KV
S.No.	Rupture load read from the load - elongation curve in no. of divisions of chart	
	(1)	(2)
1	8.94	7.87
2	8.65	8.78
3	8.50	7.80
4	9.25	8.95
5	9.20	9.00
6	9.00	7.30
7	8.58	7.15
8	8.40	7.38
9	8.48	7.50
10	10.10	9.90
11	7.94	7.00
12	8.90	9.05
13	9.20	7.20
14	9.00	9.73
15	11.25	7.78
16	7.60	8.15
17	10.70	9.20
Average rupture strength	9.04	8.22
Percent decrease in rupture strength	-	9.07

Table 3.4 : Results of tensile rupture tests on specimens of macrofol film.

Instron machine cross-head speed = 2.0 cm/mm
Width of test specimens = 10 mm
Thickness of test specimens = 20 micron
Gage length of specimens = 61 mm

	Arrangement I (symmetric)			Arrangement II (asymmetric)		Arrangement III (symmetric)
Field in KV/mm	0.0	18.5	34.5	20.7	10.35	75.0
D.C.Volts	0.0 V	5.0 KV	5.0 KV	3.0 KV	1.5 KV	1.5 KV
S.No.	Rupture load read from the load-elongation curve in terms of no.of divisions of chart, 2 divisions of chart = 1.0 Kg					
	(1)	(2)	(3)	(4)	(5)	(6)
1	5.40	4.90	3.70	4.94	5.25	4.12
2	4.60	5.35	3.70	3.55	4.75	4.70
3	4.76	4.70	4.07	4.24	4.73	4.87
4	5.34	4.80	4.20	5.62	5.15	4.80
5	5.35	4.47	3.40	4.88	4.50	4.03
6	5.02	4.35	4.55	4.95	4.33	4.73
7	5.17	5.40	4.47	4.00	4.80	4.45
8	4.64	4.52	4.70	3.92	4.30	4.30
9	4.24	3.67	4.71	3.18	4.30	4.14
10	5.00	4.39	4.20	5.20	4.10	4.58
11	3.30	4.29	2.75	4.64	3.30	5.05
12	5.94	4.45	5.44	5.70	3.45	4.45
13	5.08	4.39	5.15	2.72	6.25	3.60
Total	63.84	59.68	55.04	57.54	59.21	57.82
Average rupture strength	4.911	4.591	4.234	4.426	4.555	4.447
Percent decrease in rupture strength	-	6.51	13.80	9.87	7.25	9.43

Table 3.5 : Frequency distributions of rupture strengths of aluminised mylar specimens.

D.C. Volts	0.0 V		4.0 KV	
Load-range (no. of div. of chart)	No. of obs. (n)	rel. freq. (f)	(n)	(f)
7.01 - 7.50	0	0.0	6	0.353
7.51 - 8.00	2	0.117	3	0.176
8.01 - 8.50	3	0.176	1	0.059
8.51 - 9.00	6	0.353	3	0.176
9.01 - 9.50	3	0.176	2	0.117
9.51 - 10.0	0	0.0	2	0.117
10.01- 10.5	1	0.059	0	0.0
10.51- 11.0	1	0.059	0	0.0
11.01- 11.5	1	0.059	0	0.0

The frequency distributions of rupture loads are calculated and shown in Table 3.6. A few of these distributions are plotted in Fig. 3.6(b). The shift in the frequency distribution curves towards the left, when a field is present indicates a reduction in strength due to the effect of field.

(c) Analysis of Variance of test data

The analysis of variance is an arithmatic device for partitioning the total variation exhibited by sample observations according to the various sources of variation that are present, thus permitting hypothesis tests regarding the respective variation sources. The most simple analysis-of-variance model is a completely randomized, one variable design in which attention is on a comparison of the effects of treatments T_j. Letting x_{ij} designate the ith observed effect of the jth treatment, $\bar{x}_{.j}$ the sample mean of the jth treatment effect, and $\bar{x}_{..}$ the mean of all observations x_{ij}, the total variation as measured by the total sum of squares (SS) can be partitioned as follows :

$$\sum_j \sum_i (x_{ij} - \bar{x}_{..})^2 = \sum_j \sum_i (\bar{x}_{.j} - \bar{x}_{..})^2 + \sum_j \sum_i (x_{ij} - \bar{x}_{.j})^2$$

The first term on the right hand side of the above equation is called the sum of squares between treatments and measures ''explained error'' (i.e. that part of the total variation

Table 3.6 : Frequency distributions of rupture strengths of macrofol specimens.

	Arrangement I				Arrangement II						Arrangement III	
D.C.Volts	0.0 V		5.0 KV		5.0 KV		3.0 KV		1.5 KV		1.5 KV	
Load range (No. of div. of chart)	No. of obs. (n)	Rel. freq. (f)	(n)	(f)	(n)	(f)	(n)	(f)	(n)	(f)	(n)	(f)
2.51 - 3.0	0	0.0	0	0.0	1	0.077	1	0.077	0	0.0	0	0.0
3.01 - 3.5	1	0.077	0	0.0	1	0.077	1	0.077	2	0.154	0	0.0
3.51 - 4.0	0	0.0	1	0.077	2	0.154	3	0.231	0	0.0	1	0.077
4.01 - 4.5	1	0.077	6	0.462	4	0.308	1	0.077	5	0.385	6	0.462
4.51 - 5.0	4	0.308	4	0.308	3	0.231	4	0.308	3	0.231	5	0.385
5.01 - 5.5	6	0.462	2	0.154	2	0.154	1	0.077	2	0.154	1	0.077
5.51 - 6.0	1	0.077	0	0.0	0	0.0	2	0.154	0	0.0	0	0.0
6.01 - 6.5	0	0.0	0	0.0	0	0.0	0	0.0	1	0.077	0	0.0

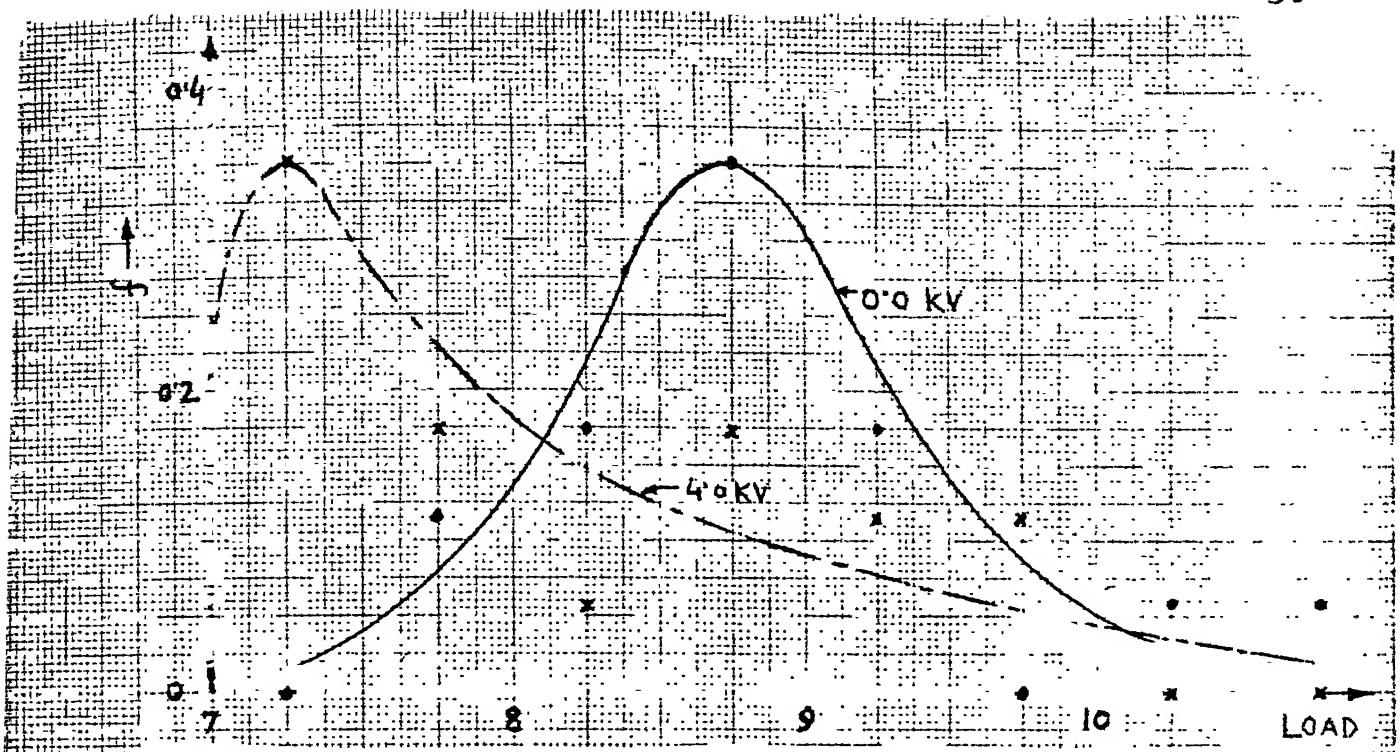

(a) Relative frequency (f) VS. rupture load for aluminised mylar specimens

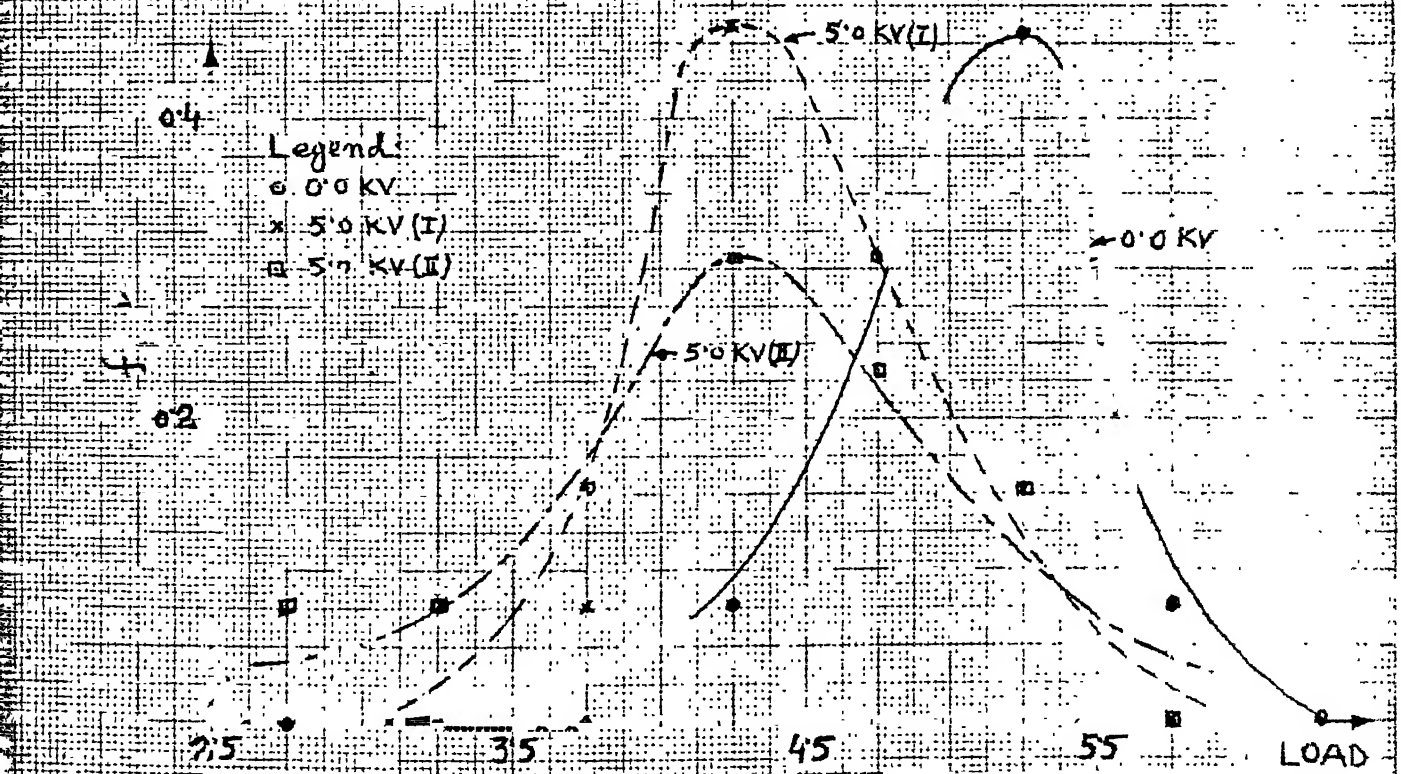

(b) Relative frequency (f) VS. rupture load for macrofol specimens

FIG. 3.6 FREQUENCY DISTRIBUTION CURVES

due to differences between treatment effects). The second term is called the sum of squares within treatments or error SS and represents the SS due to unexplained variation.

The results shown in Tables 3.3 and 3.4 are analysed statistically by applying the analysis of variance test to them. The analysis will show whether the variation in the rupture strengths exhibited by the observations is due to chance alone or because of the presence of an electrostatic field (i.e. the treatment).

From the data of column (1) of Table 3.3, we have

$$X_1 = \sum x_i = 8.94 + 8.65 + \ldots + 10.70 = 153.69$$

$$X_2 = \sum x_i^2 = 8.94^2 + 8.65^2 + \ldots + 10.70^2 = 1403.0015$$

Similarly, from column (2) of the same table, we have

$$Y_1 = \sum y_i = 7.87 + 8.78 + \ldots + 9.20 = 139.74$$

$$Y_2 = \sum y_i^2 = 7.87^2 + 8.78^2 + \ldots + 9.20^2 = 1163.1110$$

Now,

$$X_1 + Y_1 = 293.43$$

$$X_2 + Y_2 = 2566.1125$$

Total number of observations, N = 34

$$\text{Total SS} = X_2 + Y_2 - \frac{(X_1 + Y_1)^2}{N} = 33.7253$$

$$\text{Between treatments SS} = \frac{X_1^2 + Y_1^2}{17} - \frac{(X_1+Y_1)^2}{N} = 5.7236$$

$$\text{Within treatment SS} = 33.7253 - 5.7236 = 28.0017$$

The summary analysis of variance table is shown in Table 3.7. The null hypothesis to be tested is

H_o : average rupture strength of mylar specimens without field

= average rupture strength of mylar specimens with field

and the test is at an $\alpha = 0.025$ significance level.

The mean square (MS) represent two independent, chi-square distributed, unbiased estimates of the observations variance σ_x^2 when H_o is true. Their ratio is F-distributed with 1 and 32 degrees of freedom (d.f.). If H_o is true, by chance alone this F-ratio is expected to exceed

$F_{0.025,1,32} = 5.53$ only 2.5% of the time. Since,

$$F_{cal} = \frac{5.7236}{0.8750} = 6.54 > 5.53,$$

the hypothesis H_o is rejected. The conclusion is that the effect of field on rupture strength exists.

Similarly, the analysis-of-variance test is applied to the data of columns (1) and (3) of Table 3.4. The results of

Table 3.7

A summary analysis of variance table

Sources of variation	For the data of col.(1) and (2) of Table 3.3 d.f.	SS	MS	For the data of col.(1) and (3) of Table 3.4 d.f.	SS	MS
Between rupture tests with and without field	1	5.7236	5.7236	1	2.9785	2.9785
Within rupture tests with or without field	32	28.0017	0.8750	24	11.4188	0.4758
Total	33	33.7253		25	14.3973	

the analysis-of-variance are shown in Table 3.7. Using the same H_o and α as before, since

$$F_{cal} = \frac{2.9785}{0.4758} = 6.26 > F_{0.025,1,24} = 5.72 ,$$

H_o is rejected and the conclusion is that the field affects the rupture strength of macrofol film.

3.3.2 Wear Test

The objective of wear tests is to find out whether the electrostatic field affects the rate of wear of a dielectric material or not. The test specimens are subjected to wear in repetitive rubbing contact with a metallic surface. For this purpose, a simple experimental set-up is designed and fabricated in the laboratory.

In the present investigation, specimens of macrofol film are rubbed against a mild steel disc, both, in the presence of and without a field. The size of wear scars produced in a specified interval of time is measured in both the cases. Any significant difference in the average size of wear scars in the two cases is an indication of the fact that the field does affect the process of wear.

(a) Experimental Details

The set-up used for testing the specimens is shown in Fig. 3.7. A circular disc of mild steel, about 22 cms. in diameter and 1.25 cms. thick, is grounded to a fine surface finish on a surface grinder. The grounded surface is then cleaned with kerosene oil. The disc is mounted on a shaft which is gripped in a small drilling chuck after wrapping a PVC sheet around it to insulate it from the chuck. The chuck is, then, mounted in the spindle of a vertical drilling machine so that the disc can be rotated at a constant speed. The rotating disc makes contact with a steel ball which is held in a ball-holder as shown in the figure. The ball-holder is made of perspex and consists of a cylindrical bolt and a cap fitting the bolt. A tapered hole in the center of the cap accomodates a steel ball such that the ball projects partly outside the cap as shown in Fig. 3.8. The bolt, when tightened into the cap, presses the ball into its seat. The ball-holder is fixed at one end of a long arm (made of Al pipe) which is supported in a specially designed bearing such that the arm can be rotated in both horizontal and vertical planes. A flat disc with internal threads is provided on the other end of the arm to be used as a movable counter-weight. The provision of a counter-weight makes it possible to carry out rubbing action between the test specimen and M.S. disc under a very light load. The wear tests are performed by moving

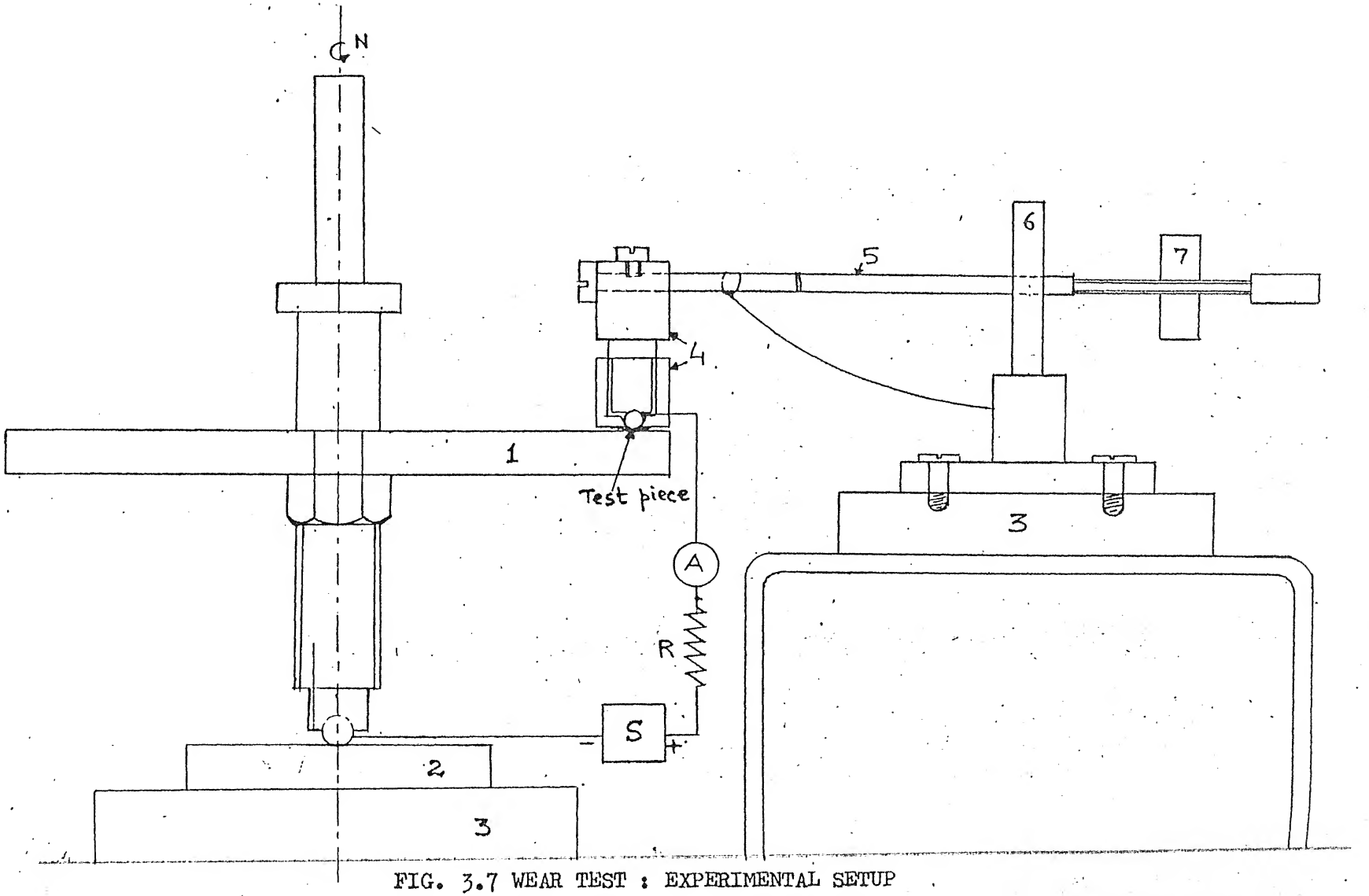

FIG. 3.7 WEAR TEST : EXPERIMENTAL SETUP

1 - Mild steel disc
2 - Metallic plate
3 - Perspex sheet
4 - Ball holder
5 - Arm
6.- Bearing
7 - Threaded counter-weight

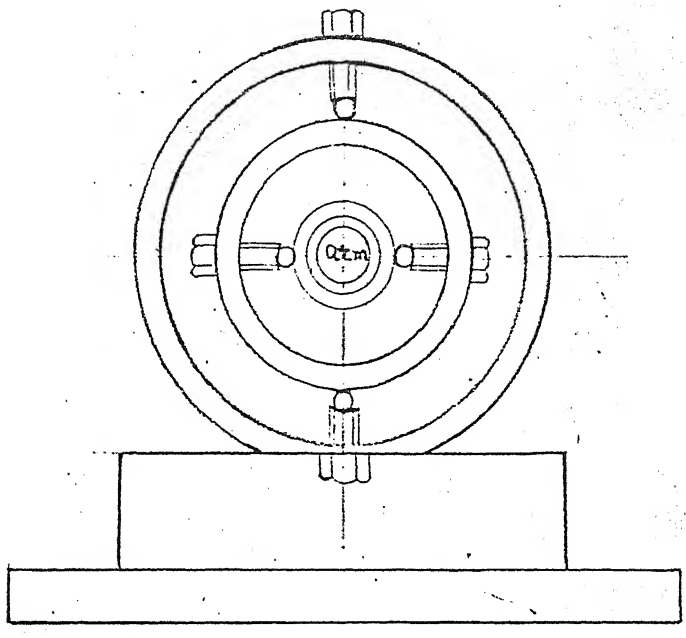

Bearing

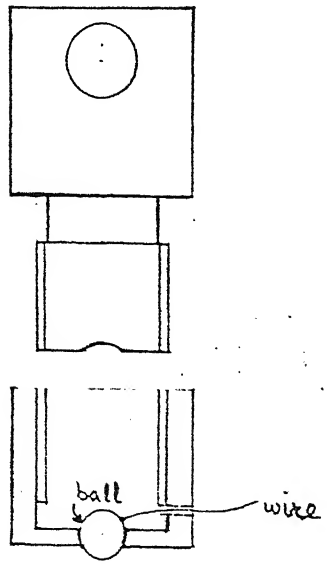

Ball holder

FIG. 3.8 BALL HOLDER AND BEARING

the counter-weight to a position farthest from the point at which the arm is supported so that the lightest contact load between the ball and disc is obtained. The contact load is determined by weighing the ball-holder along with the arm in a physical balance.

The specimens to be tested are cut from a 10 mm wide tape of macrofol in lengths of approximately 10 mm. Tests are performed on specimens of 20 and 40 micron thicknesses. For subjecting a specimen to rubbing-action in contact with the rotating disc, the specimen is placed over the projected portion of the ball, slightly stretched and fixed to the external surface of the cap by adhesive tapes. The arm is now positioned in a radial direction with respect to the disc and the ball is made to contract the disc near its outer edge.

For conducting the tests in the presence of a field, the disc and the ball are connected across a high potential d.c. supply (0-5 KV) as shown in Fig. 3.7. When doing tests without field, a low voltage supply (5 V) is connected in the circuit so that any ball-to-disc contact resulting from the wear of test specimen is indicated by the flow of a current in the circuit.

During the tests, the disc is rotated at a constant speed of 40 r.p.m. to give a rubbing speed of 41 cms. per second. The rubbing occurs under a normal load of approximately 23 gms. The specimens are rubbed, both in the presence

of and without field. For each interval of rubbing time, a set of five specimens is tested at each intensity of applied field. The tested specimens are collected for observation in a projector.

The wear scars on the test specimens are projected on the screen of the projector after a magnification of hundred times. The scars are found to be nearly circular in shape and their diameters are measured in two perpendicular directions. The measured diameters are shown in Table 3.7. The average sizes of the scars under various test conditions are shown in Table 3.8.

(b) Results and Discussions

Table 3.8 shows the growth in the size of the wear scar mark with time, both in the presence of and without the electrostatic field. Tests under identical conditions are repeated five times without and the same number of times with a strong electrostatic field. Results are shown for two different thicknesses of the polymer film. Average values are given in Table 3.9. It is found that in case of 20 micron thick film, the wear scar growth curve in the presence of field is lower than that without field as shown in Fig. 3.9 though the effect is very small. In the case of 40 micron thick specimens, the effect is not perceptible. Therefore, it is concluded that the electrostatic field does not have any significant effect on the wear rate of macrofol film.

Table 3.8: The values of diameter of wear scar measured in mms.

Thickness of test-specimen = 20 micron

Voltage applied	5.0 V					3000 V		
Duration of rubbing contact in seconds	30	60	90	120	180	30	60	90
Dia. of a scar in Y-direction	0.533	0.606	0.840	0.680	0.707	0.593	0.566	0.571
X-direction	0.490	0.652	0.812	0.593	0.677	0.537	0.562	0.567
	0.654	0.611	0.633	0.652	0.696	0.533	0.635	0.630
	0.569	0.588	0.604	0.626	0.681	0.511	0.623	0.606
	0.540	0.649	0.630	0.702	0.781	0.566	0.583	0.618
	0.529	0.670	0.582	0.666	0.740	0.542	0.575	0.591
	0.524	0.580	0.612	0.642	0.728	0.552	0.583	0.638
	0.480	0.558	0.573	0.629	0.711	0.555	0.585	0.601
	0.607	0.639	0.632	0.636	0.725	0.538	0.608	0.618
	0.549	0.601	0.592	0.609	0.701	0.516	0.588	0.603
Average diameter of the scar in mms.	0.5475	0.6154	0.6510	0.6435	0.7147	0.5443	0.5908	0.6043

Thickness of test-specimen = 40 micron

Voltage applied	5.0 V			4000 V		
Duration of rubbing contact in seconds	60	120	240	60	120	240
Dia. of a scar in —Y-direction	0.650	0.575	0.702	0.532	0.610	0.648
X-direction	0.649	0.604	0.690	0.623	0.622	0.650
	0.483	0.564	0.647	0.544	0.571	0.622
	0.509	0.570	0.640	0.570	0.594	0.641
	0.627	0.547	0.677	0.524	0.564	0.662
	0.641	0.561	0.651	0.551	0.599	0.674
	0.548	0.537	0.652	0.657	0.619	0.622
	0.556	0.548	0.640	0.660	0.639	0.608
	0.552	0.609	0.557	0.530	0.580	0.636
	0.581	0.640	0.566	0.554	0.615	0.609

Table 3.9 : Average diameter of wear scar under different test conditions.

Contact load 23.2 gms.

Thickness of test specimen	Voltage applied / duration of rubbing contact in seconds	5 V	3000 V
	30.0	0.5475	0.5443
	60.0	0.6154	0.5908
20 micron	90.0	0.6510	0.6043
	120.0	0.6435	-
	180.0	0.7147	-
	Voltage applied / duration of rubbing contact in second	5 V	4000 V
	60.0	0.5796	0.5745
40 micron	120.0	0.5755	0.6013
	240.0	0.6422	0.6372

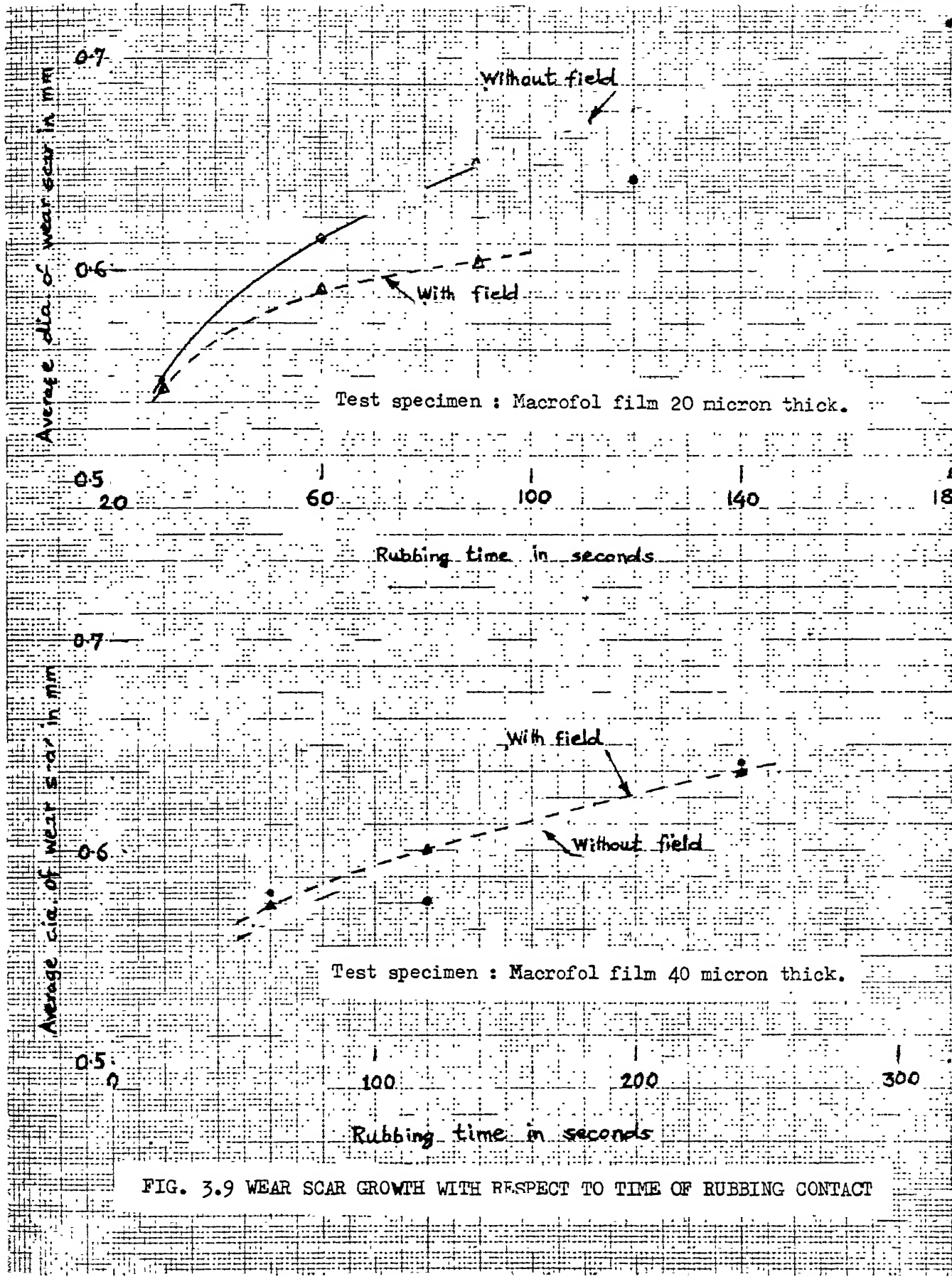

FIG. 3.9 WEAR SCAR GROWTH WITH RESPECT TO TIME OF RUBBING CONTACT

CHAPTER 4

EFFECT OF ELECTROSTATIC FIELD ON THE BINDING ENERGY OF SOLIDS

4.1 Introduction

The present chapter deals with the analysis of the effect of an applied electrostatic field on the binding energy (a measure of the strength of the binding) of a few microscopic systems. As pointed out earlier, the lowering of valence electron energies is responsible for the interatomic bonds between two or more atoms. Therefore, a knowledge of electron distributions and energies which are determined by electron wave functions is essential for an understanding of the nature of bonding. When an atom is placed in an electric field, the field interacts with the atom and distorts its electron charge distribution. The Stark effect [25] - the effect of an external electric field on the energy levels of a hydrogen atom, is an example of this. Therefore, it is logical to think of the effect of an external electric field on the strength of the binding in a molecule or a solid. Considering the simplest molecule, i.e. a hydrogen molecular ion (H_2^+), which is covalently bonded, the existence of the overlap charge between the nuclei is known to be responsible for the attraction between the atoms [26] since the magnitude of overlap charge is intimately tied up with the magnitude of the interatomic force or the strength of the binding, the

effect of an external electric field on the overlap charge in a H_2^+ ion is studied first. It is found that the overlap charge always decreases due to the presence of a field. The decrease in overlap charge is an indication of the weakening of the bond.

The same logic is then extended to covalently bonded solids in which the atoms are bonded two by two. Taking a simple one dimensional model of a dielectric solid, the effect of an external electric field (produced by a chain of charges) on its binding energy is studied. Finally, the effect of an external electric field on the binding energy of a linear one-dimensional model of a metallic solid is studied. Since the basic idea is of only a preliminary study, therefore, very simple and mathematically tractable models are employed. The models may not be applicable to realistic solids but have sufficient structure to qualitatively reflect their behaviour. In this sense they are not trivial and indicate the trend of the effect of an external electric field on the binding energy of solids. A rigorous analysis based on a more realistic model is difficult, time consuming and beyond the scope of interest of the author.

4.2 Binding in a Hydrogen Molecular Ion, H_2^+

The basis of covalent bonding is the redistribution of the charge density due to the outermost electrons of an atom, to produce the overlap charge. The overlap charge can

be calculated exactly only in the case of simplest molecules like the hydrogen like molecular ion (H_2^+) and the hydrogen like molecule (H_2). The H_2^+-ion consists of a single electron moving in the field of two protons held at fixed positions separated by a distance, R as shown in Fig. 4.1. Using LCAO (linear combination of atomic orbitals) approximation, the ground state wave function, ψ, for the molecular orbital can be written in terms of atomic orbitals as [26]

$$\psi(r) = \left(N \frac{\alpha^3}{\pi}\right)^{\frac{1}{2}} \left(e^{-\alpha r_a} + e^{-\alpha r_b}\right) \qquad (4.1)$$

where r_a and r_b are the distances of the electron from the nuclei at A and B respectively.

α is a variable parameter and a function of R to be chosen by variation method.

N is the normalisation constant.

The square of the wave function, ψ, gives the charge density, which if integrated over all space gives the normalisation integral as

$$N \frac{\alpha^3}{\pi} \int \left(e^{-2\alpha r_a} + e^{-2\alpha r_b} + 2\, e^{-\alpha(r_a + r_b)}\right) dv = 1 \qquad (4.2)$$

where the first and the second terms inside the integral sign represent the spherically symmetric atomic charge

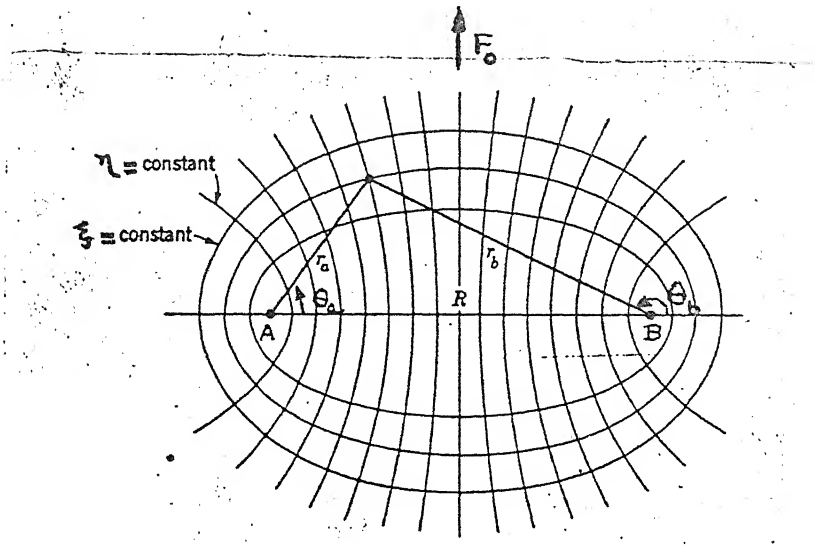

FIG. 4.1 SPHEROIDAL COORDINATES FOR THE TWO-CENTRE PROBLEM.

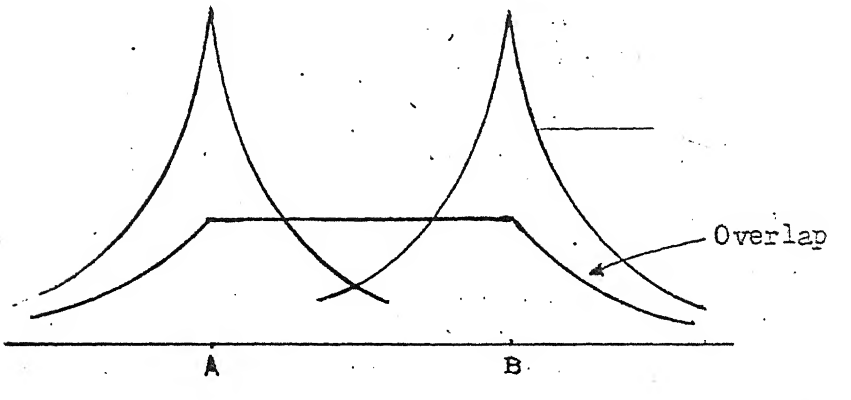

FIG. 4.2 DENSITY OF SPHERICAL CHARGE DISTRIBUTIONS AND OF OVERLAP CHARGE ALONG INTERNUCLEAR AXIS, FOR H_2^+ , R=2.

distributions around the nuclei A and B while the third term represents the overlap charge. The overlap charge is proportional to the overlap integral, S, defined as

$$S = \frac{\alpha^3}{\pi} \int e^{-\alpha(r_a+r_b)} \, dv \qquad (4.3)$$

Substitution of Eq. (4.3) in Eq. (4.2) gives

$$N = \frac{1}{2(1+S)}$$

The Eq. (4.2) shows that the fraction 1/(1+S) of the total charge is still in the atomic configuration and the fraction S/(1+S) of the originally atomic charge is redistributed in the form of overlap charge. The contours of constant overlap charge density are the confocal ellipsoids, r_a+r_b = constant, with the nuclei A and B as the foci. Hence the overlap charge distribution is of a spheroidal form, with maximum density along the line joining the two nuclei and falling off as the distance from the line increases as shown in Fig. 4.2. The overlap charge is zero for very large inter-atomic distances, R, and builds up as the nuclei approach each other. The build up of overlap charge leads to an attractive interaction between the atoms. At the same time, as R decreases, the electrons (or its wave functions) are squeezed into a restricted volume increasing the kinetic energy of the electrons which leads to a repulsive inter-atomic force. At the

equilibrium interatomic separation, R_o, the two opposing forces balance each other. Thus the magnitude of the overlap charge is intimately tied up with the magnitude of the interatomic force. Therefore, to find out the effect of an external electric field on the binding energy of a simple molecule like H_2^+-ion, it is sufficient to consider the effect of presence of the field on the overlap integral S.

For evaluating integral S in the presence of an external field, it is necessary to know the distortion or perturbation in the wave function of an electron (moving in the field of a hydrogenic atom) due to the field.

The unperturbed wave function for an electron moving in the field of a hydrogenic atom is

$$\varphi_o(\vec{r}) = \left(\frac{Z^3}{\pi a_o^3}\right)^{\frac{1}{2}} e^{-Z\frac{r}{a_o}} \qquad (4.4)$$

where $a_o = \frac{\hbar^2}{me^2}$ is the Bohr radius ($\simeq 0.5\ A^o$)

Z atomic number of hydrogenic atom

m is the reduced mass of the electron

$\hbar = \frac{h}{2\pi}$ where h is Planck's constant.

Fortunately, an exact, closed form expression for the first order correction $\delta\emptyset\ (\vec{r}, t)$ is known for a static electric field [25, 27]. It is given by

$$\delta\phi(\vec{r}) = -\left(\frac{Z^3}{\pi a_o^3}\right)^{\frac{1}{2}} \left(\frac{eF_o a_o}{2Z\hbar\omega_c}\right) e^{-\frac{Zr}{a_o}} \left[\frac{Zr}{a_o} + \tfrac{1}{2}\left(\frac{Zr}{a_o}\right)^2\right]\cos\theta$$

$$= -\left(\frac{Z^3}{\pi a_o^3}\right)^{\frac{1}{2}} \lambda\, e^{-\frac{Zr}{a_o}} \left[\frac{Zr}{a_o} + \tfrac{1}{2}\left(\frac{Zr}{a_o}\right)^2\right]\cos\theta \qquad (4.5)$$

where, $\hbar\omega_c = \frac{Z^2 e^2}{2\, a_o}$ is the ionisation energy,

F_o is the strength of the static field,

$-e$ is the electron charge,

$$\lambda = \frac{e\, F_o\, a_o}{2\, Z\, \hbar\omega_c}$$

Therefore,

$$\varphi(\vec{r}) = N\left[\varphi_o(\vec{r}) - \left(\frac{Z^3}{\pi a_o^3}\right)^{\frac{1}{2}} \lambda\, e^{-\frac{Zr}{a_o}} \left\{\frac{Zr}{a_o} + \tfrac{1}{2}\left(\frac{Zr}{a_o}\right)^2\right\}\cos\theta\right]$$

$$= N(\varphi_o + \delta\varphi) \qquad (4.6)$$

where N is the normalisation constant.

Using the atomic coordinates as shown in Fig. 4.1 and substituting Z = 1 in Eq. (4.6), the perturbed wave function for a hydrogen atom is given by

$$\varphi(\vec{r}) = N(\pi a_o^3)^{-\frac{1}{2}}\, e^{-r/a_o} \left(1 - \lambda\left\{\frac{r}{a_o} + \frac{1}{2}\left(\frac{r}{a_o}\right)^2\right\}\cos\theta\right) \qquad (4.7)$$

The normalising condition gives

$$\int \varphi^2(r) \, dv = 1$$

or

$$\frac{N^2}{\pi a_o^3} \int_0^\infty dr \int_0^\pi d\theta \int_0^{2\pi} e^{-\frac{2r}{a_o}} \left(1 - \lambda \left(\frac{r}{a_o}\right) + \frac{1}{2}\left(\frac{r}{a_o}\right)^2\right\} \cos\theta)^2 \, r^2 \sin\theta \, d\phi = 1$$

Simplifying, we get

$$N^2 \left(1 + \frac{43}{8} \lambda^2\right) = 1$$

or

$$N = \frac{1}{\sqrt{(1+5.375\,\lambda^2)}} = \frac{1}{\sqrt{(1 + \lambda'^2)}} \qquad (4.8)$$

where $\lambda'^2 = 5.375\,\lambda^2$.

Now, the overlap charge in the case of a hydrogen molecular ion (H_2^+) is calculated by using the spheroidal coordinates (ξ, η, φ) where

$$\left.\begin{aligned} \xi &= \frac{r_a + r_b}{R} \quad \text{and } \xi \text{ varies from 1 to } \infty \\ \eta &= \frac{r_a - r_b}{R} \quad \text{and } \eta \text{ varies from } -1 \text{ to } 1 \end{aligned}\right\} \qquad (4.9)$$

and φ is the angle of rotation about the axis joining the nuclei. Further,

$$\int f(\xi,\eta,\varphi)\, dv = \frac{R^3}{8} \int_0^{2\pi} d\varphi \int_{-1}^{1} d\eta \int_1^{\infty} f(\xi,\eta,\varphi)(\xi^2-\eta^2)\, d\xi \tag{4.10}$$

For the unperturbed hydrogen molecular ion, the overlap charge between the centers is calculated by using Eq. (4.3) and is given as

$$S_o = \frac{\alpha'^3}{\pi} \int e^{-\alpha'(r_a+r_b)}\, dv \qquad \text{where } \alpha' = \frac{\alpha}{a_o}$$

After substitutions,

$$S_o = \frac{\alpha'^3}{\pi} \int_1^{\infty} e^{-\alpha' R\xi}\, d\xi\, \frac{R^3}{8} \cdot 2\pi \int_{-1}^{1} (\xi^2-\eta^2)\, d\eta$$

$$= e^{-\alpha' R}\left[1+\alpha' R+\frac{1}{3}(\alpha' R)^2\right] \tag{4.11}$$

using the general formula

$$\int_x^{\infty} x^n e^{(-ax)}\, dx = \frac{n!}{a^{n+1}} e^{(-ax)}\left[1+ax+\frac{1}{2!}(ax)^2+\ldots+\frac{1}{n!}(ax)^n\right]$$

Similarly, the overlap charge between the centers in the presence of external field is calculated by using the perturbed wave functions

$$\varphi(r_a) = \left(\frac{\alpha'^3}{(1+\lambda'^2)\pi}\right)^{\frac{1}{2}} e^{-\alpha' r_a} \left[1 - \frac{\lambda r_a}{a_o}\cos\theta_a - \frac{\lambda}{2}\left(\frac{r_a}{a_o}\right)^2 \cos\theta_a\right] \tag{4.12a}$$

and $$\varphi(r_b) = \left(\frac{\alpha'^3}{(1+\lambda'^2)\pi}\right)^{\frac{1}{2}} e^{-\alpha' r_b} \left[1 - \frac{\lambda r_b}{a_o}\cos\theta_b - \frac{\lambda}{2}\left(\frac{r_b}{a_o}\right)^2 \cos\theta_b\right] \tag{4.12b}$$

The overlap charge is given by

$$S = \int \varphi(r_a)\, \varphi(r_b)\, dv \tag{4.13}$$

Now, from Fig. 4.1, it is clear that

$$\text{Cos}\,\theta_a = \frac{R^2 + r_a^2 - r_b^2}{2 R r_a}$$

$$\text{Cos}\,\theta_b = \frac{r_a^2 - (R^2 + r_b^2)}{2 R r_b}$$

Therefore

$$r_a r_b \cos\theta_a \cos\theta_b = \frac{r_a^4 + r_b^4 - R^4 - 2 r_a^2 r_b^2}{4 R^2}$$

$$= \frac{R^2}{4}\left(\xi^2 \eta^2 - 1\right) \tag{4.14}$$

on substitution from Eq. (4.9).

Similarly,

$$r_a \cos\theta_a + r_b \cos\theta_b = \frac{r_a^2 - r_b^2}{R} = R\xi\eta \tag{4.15}$$

$$r_a^2 \cos\theta_a + r_b^2 \cos\theta_b = \frac{1}{2R}[R^2(r_a - r_b) + r_a^3 - r_b^3 + r_a r_b (r_a - r_b)]$$

$$= \frac{R^2}{2}\eta(1 + \xi^2) \tag{4.16}$$

$$r_a^2 r_b^2 \cos\theta_a \cos\theta_b = \frac{R^4}{16}(\xi^4\eta^2 - \xi^2\eta^4 + \eta^2 - \xi^2) \tag{4.17}$$

Substituting Eqs. (4.12a,b) in Eq. (4.13) and making use of the relations given by Eqs. (4.14-4.17), we get after simplification

$$S = \frac{1}{(1+\lambda'^2)}[S_o + \lambda^2 e^{-\alpha' R}(\frac{43}{8} + \frac{43}{8}(\alpha' R) + \frac{67}{40}(\alpha' R)^2 - \frac{7}{60}(\alpha' R)^3$$

$$- \frac{29}{140}(\alpha' R)^4 - \frac{41}{840}(\alpha' R)^5 - \frac{1}{280}(\alpha' R)^6)] \tag{4.18}$$

Therefore,

$$S - S_o = \frac{\lambda^2 e^{-\alpha' R}[-\frac{7}{60}(\alpha' R)^2 - \frac{7}{60}(\alpha' R)^3 - \frac{29}{140}(\alpha' R)^4 - \frac{41}{840}(\alpha' R)^5 - \frac{1}{280}(\alpha' R)^6}{1 + \frac{43}{8}\lambda^2}$$

(4.19)

< 0 for all positive values of α'.

Thus fractional decrease in overlap charge $= \frac{S-S_o}{S_o} = \frac{\Delta S}{S_o}$

(4.20)

For H_2^+, the equilibrium internuclear distance $\alpha' R = 2$ Bohr unit. Therefore, for H_2^+ ion,

$$\Delta S = \frac{-6.5 \lambda^2 e^{-2}}{1 + 5.375\lambda^2}$$

and $$S_o = 4.33\, e^{-2}$$

Thus, for H_2^+-ion,

$$\frac{\Delta S}{S_o} = -\frac{6.5}{4.33} \cdot \left(\frac{\lambda^2}{1+5.375\,\lambda^2} \right)$$

where $\lambda = \frac{eF_o a_o}{2\hbar\omega_c}$ now.

For very large values of λ, $\left.\frac{\Delta S}{S_o}\right|_{max} = -\frac{6.5}{4.33}\frac{1}{5.375}$

$$\simeq -0.279.$$

Thus, the limiting maximum fractional reduction in overlap charge in H_2^+-ion is 0.279. Since $(S - S_o)$, given by Eq. (4.20) is negative for all admissible values of α', therefore, irrespective of at what equilibrium separation, R_o, the minimum of energy curve is reached, ΔS at R_o is always negative due to the presence of field. It may then be deduced

that the binding must be weaker in the presence of an external electric field and the energy curves are expected to look like that shown in Fig. 4.3.

4.3 A Linear Chain Model for a Dielectric Material

A simplified analysis of the effect of an external electrostatic field on the binding energy of a solid dielectric is presented here. It is known that dielectrics are polarized in the presence of an electric field. The objective of the present study is to investigate whether the polarization leads to a decrease in the binding energy and consequently a weakening of interatomic bonds or not. The analysis is restricted to a very simple model of the dielectric solid - a one-dimensional linear chain of atoms having one valence electron per atom.

The core potentials for the one-dimensional linear chain of atoms are considered to be δ-functions like as shown in Fig. 4.4, with the Hamiltonian

$$H = -\frac{\hbar^2}{2m}\frac{d^2}{dx^2} - \sum_n A\,\delta(x - x_n) \qquad (4.21)$$

where, $x_n = na$, $n = \pm 1, \pm 3, \ldots$ are the atomic positions with $2a$ the interatomic separation distance, and A the strength of the core potentials. The larger the A, the more tightly will the bonding electron be bound to the core and the looser

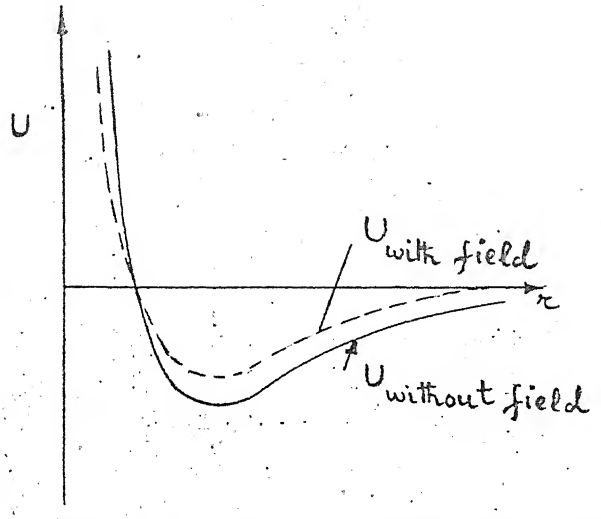

FIG. 4.3 POTENTIAL ENERGY (WITH AND WITHOUT FIELD) VS. INTERATOMIC DISTANCE.

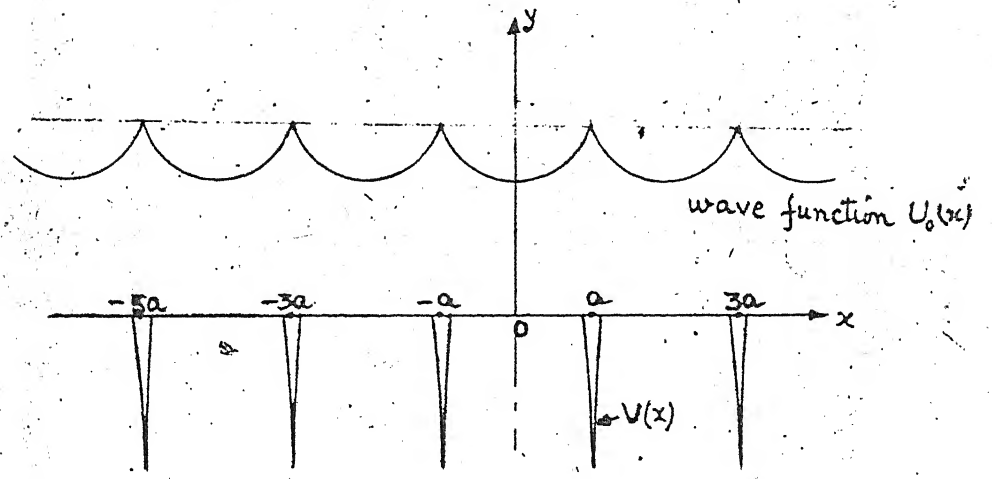

FIG. 4.4 POTENTIAL ENERGY AND WAVE FUNCTION OF AN ELECTRON IN A LINEAR CHAIN.

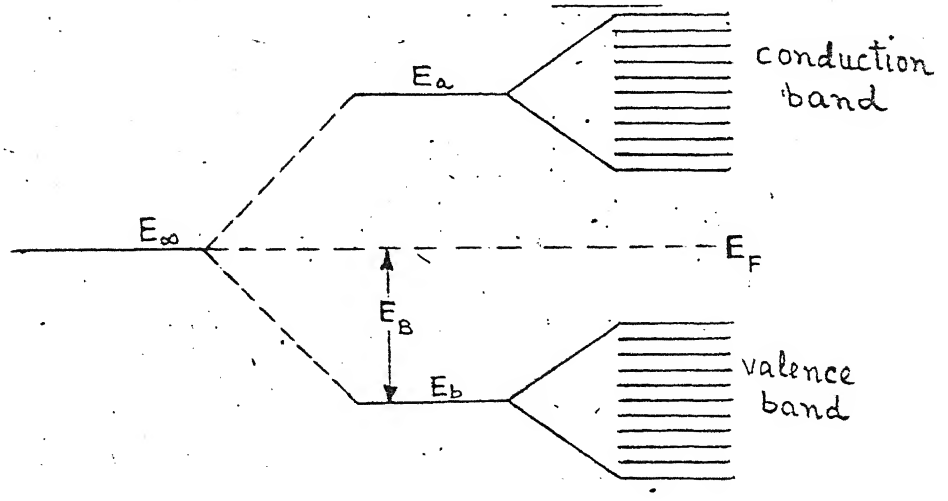

FIG. 4.5 ENERGY BANDS IN A DIELECTRIC MATERIAL.

the binding with nearest neighbour atoms. The binding energy is a function of 'a', being minimum at the equilibrium value of 'a' and vanishing as $a \to \infty$ where the system degenerates to a collection of unbound atoms.

Let at first the formation of energy bands in a solid be examined. In the unbound system of N-atoms, the outer electrons have an energy E_∞ which is N-fold degenerate. When two atoms bond together, the level E_∞ splits into the lower bonding level E_b and the higher antibonding level E_a. Within the solid, when all atoms bond together, these levels broaden into the bonding or valence band and the anti-bonding or conduction band as shown in Fig. 4.5. In a dielectric, these bands do not overlap and in the ground state, the former is fully occupied by the electrons while the latter is fully empty. The binding energy per atom is then,

$$E_B = \int_{-\infty}^{E_F} (E - E_\infty)\, n(E)\, dE \qquad (4.22)$$

where, $n(E)$ is the density of states per electron and E_F the Fermi energy. For a one-dimensional chain of dielectric material,

$$n(E) = \begin{cases} \sqrt{(4V_1^2 - E^2)} & (E_b - 2V_1) < E < (E_b + 2V_1) \\ -\sqrt{(4V_2^2 - E^2)} & (E_a - 2V_2) < E < (E_a + 2V_2) \end{cases} \qquad (4.23)$$

and $$E_F = (E_a - E_b)/2$$

where V_1 and V_2 are the effective overlap integrals of the tight binding model in the valence and conduction bands. Since the density of states is symmetric,

$$E_B = E_b - E_\infty = E_B^o \qquad (4.24)$$

where E_B^o is the binding energy per atom in the case of two-atom bonds.

For the specific case of a dielectric, therefore, it is sufficient to consider the bonding between two atoms only as E_B is equal to E_B^o. In more complicated cases, where the density of states is non-symmetric or where E_F may lie within the lower or upper band as in the case of metals, the knowledge of both n(E) and E_F becomes necessary for calculation of binding energy. Thus, in case of dielectric linear chain, the problem is reduced to finding the effect of an electrostatic field on the binding between two atoms. The analysis is carried out by employing LCAO (linear combination of atomic orbitals) method using atomic orbital basis [28].

In the case of a linear diatomic molecule, the potential energy U(x) for an electron is given by a pair of δ-functions of equal strength separated by an inter-atomic distance 2a. The Hamiltonian, H, in this case is given by

$$H = -\frac{\hbar^2}{2m}\frac{d^2}{dx^2} - A\delta(x-a) - A\delta(x+a)$$

The molecular orbital (MO) for the linear diatomic molecule is a linear combination of the atomic orbitals (LCAO) of the isolated ions

$$\psi(x) = c_1\varphi_1(x) + c_2\varphi_2(x)$$

where, $\varphi_1(x) = \alpha^{\frac{1}{2}} \exp(-\alpha|x-a|)$ and $\varphi_2 = \alpha^{\frac{1}{2}} \exp(-\alpha|x+a|)$ with $2\alpha = A$, are the eigenfunctions of H for the free atoms, centered on the respective atoms. The energy of the MO is obtained by a variational principle [29] and is written as

$$E = \frac{\sum_{ij} c_i^* c_j H_{ij}}{\sum_{ij} c_i^* c_j S_{ij}}$$

where, $H_{ij} = \int_{-\infty}^{\infty} \varphi_i^* H \varphi_j \, dx$ and $S_{ij} = \int_{-\infty}^{\infty} \varphi_i^* \varphi_j \, dx$.

The condition for E to be minimum with respect to variations of the c_i now leads to the linear equations

$$\sum_j (H_{ij} - E S_{ij})\, c_j = 0 \quad (i = 1, 2 \ldots)$$

For consistency, E must therefore satisfy the secular equation

$$\det(H_{ij} - E S_{ij}) = 0$$

Since φ_i are normalized, $S_{ii} = 1$, and

$$S_{ij} = S = (1 + \beta)\, e^{-\beta} \qquad (i \neq j)$$

$$H_{ii} = \zeta = E_{\infty}(1 + 2\, e^{-2\beta})$$

$$H_{ij} = \eta = E_{\infty}(3 + \beta)\, e^{-\beta} \qquad (i \neq j)$$

where, $E_{\infty} = -\dfrac{mA^2}{2\hbar^2}$ = energy of the electron in a single δ-function potential

$$\beta = \frac{2mAa}{\hbar^2}$$

Thus, the secular equation reduces to

$$\begin{vmatrix} \zeta - E & \eta - ES \\ \eta - ES & \zeta - E \end{vmatrix} = 0$$

or,

$$E = \frac{\zeta \pm \eta}{1 \pm S} \qquad \text{and} \qquad \frac{c_1}{c_2} = -\frac{\zeta - E}{\eta - ES}$$

Thus, the bonding wave function, ψ_b for the linear molecule is given by

$$\psi_b = \frac{\varphi_1 + \varphi_2}{\sqrt{2}(1+S)}$$

which corresponds to the energy state $E_b = \frac{\zeta + \eta}{1 + S}$ and the binding energy, $E_B = E_b - E_{Co}$ per atom.

Now, to study the effect of an external electrostatic field on bonding, a linear chain of charges Q is introduced at a distance R from the linear chain of solid dielectric, at positions

$$x_n = 2 n a, \quad n = 0, \pm 1, \pm 2, \ldots \text{ as shown in Fig. 4.6.}$$

It is to be noted that these external charges only polarize the bonding electron cloud but do not capture the electrons themselves or bond covalently with the solid. This restricts the magnitude of both Q and R.

First, the effect of positive charges ($Q > 0$) on bonding is examined. The dominant effect of polarization comes from the charge lying in between the two atoms, i.e. nearest to the bond. The other charges introduce only small

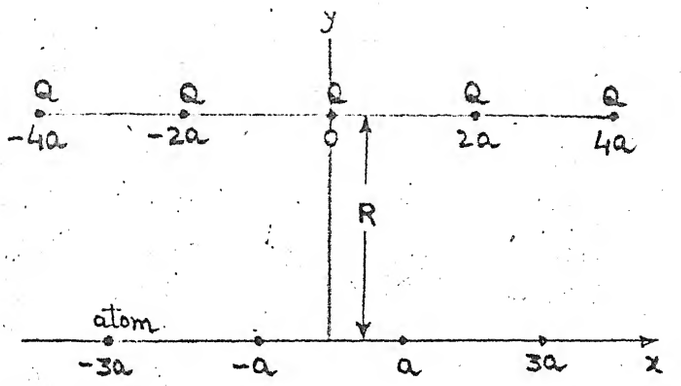

FIG. 4.6 A LINEAR CHAIN OF CHARGES Q AT A DISTANCE R FROM THE LINEAR CHAIN OF ATOMS.

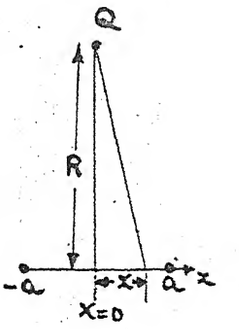

FIG. 4.7 BINARY ATOM SYSTEM WITH AN EXTERNAL CHARGE.

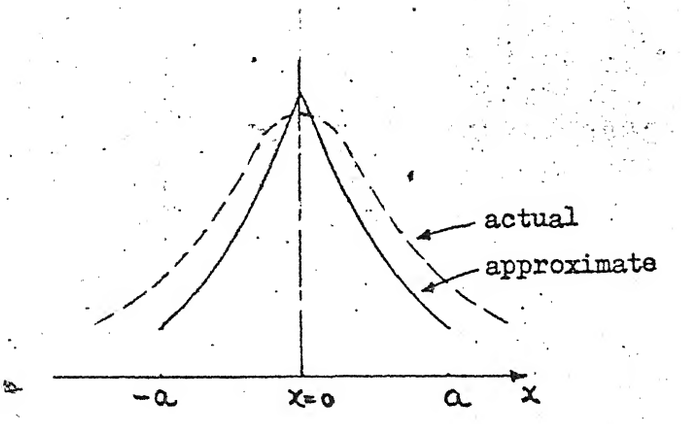

FIG. 4.8 THE WAVE FUNCTION $\psi(x)$

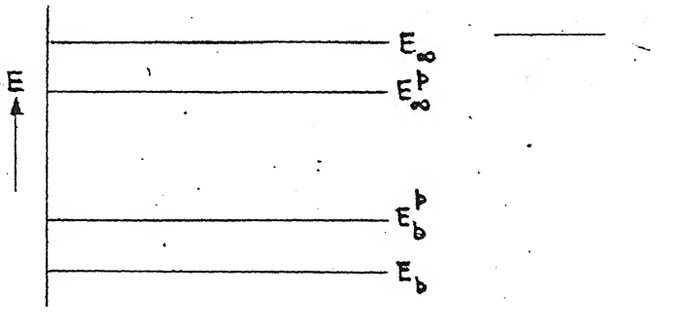

FIG. 4.9 ENERGY LEVELS

corrections to this. Thus the problem is reduced to determination of the effect of a charge Q placed at a distance R from the mid-point of the bond of a binary atom system as shown in Fig. 4.7

For the system shown in Fig.4.7 the Hamiltonian, H' is given by

$$H' = -\frac{\hbar^2}{2m}\frac{d^2}{dx^2} - A\delta(x+a) - A\delta(x-a) + v(x) \qquad (4.25)$$

where v(x) is the potential due to external charge and is given by

$$v(x) = -\frac{Q\,e}{\sqrt{(x^2 + R^2)}} \qquad (4.26)$$

Again, the LCAO method is adopted as before, with the modified basis Ψ_1 and Ψ_2, given by

$$\Psi_1(x) = \frac{\varphi_1(x) + r\,\xi(x)}{\sqrt{(r^2 + 2r\sigma + 1)}}$$

and $$\Psi_2(x) = \frac{\varphi_2(x) + r\,\xi(x)}{\sqrt{(r^2 + 2r\sigma + 1)}}$$

where, $\xi(x)$ is the eigenfunction of

$$\left[-\frac{\hbar^2}{2m}\frac{d^2}{dx^2} - v(x)\right]\xi(x) = \varepsilon\,\xi(x)$$

$$\text{and} \quad \sigma = \int_{-\infty}^{\infty} \varphi_1(x)\, \xi(x)\, dx$$

A rough picture of $\xi(x)$ may be obtained by approximating $v(x)$ as follows :

$$v(x) \simeq -B\,\delta(x) \qquad \text{where } B \propto \frac{Q}{R},$$

So that,

$$\xi(x) = \gamma^{\frac{1}{2}} \exp(-\gamma |x|) \quad \text{with } 2\gamma = B \qquad (4.27)$$

The actual shape of $\xi(x)$ is similar to that given by Eq. (4.27) but decaying less than exponentially as $x \to \pm\infty$ and with a rounded peak instead of a cusp at the origin as shown in Fig. 4.8. Qualitatively, the shapes are very similar with a suitable choice of B.

The admixture of $\xi(x)$ with the wave functions φ_1 and φ_2 reflects the polarization effect of the charge Q on the wave functions. The positive charge pulls some of the electron cloud towards it, increasing the probability density around x=o. The admixture coefficient, r can be determined by energy minimization.

Now the energy of a polarized atom E_{∞}^{p} is always less than the energy of an unpolarized atom (atom in the ground state). This can be easily deduced from the consideration of the binding energy of a binary atom system.

At the equilibrium separation, the energy per atom for the bonding state is always lower than the energy of a free atom. Thus $E^{p}_{\infty} < E_{\infty}$ as shown in Fig. 4.9. The change $\Delta E_0 = E^{p}_{\infty} - E_{\infty}$ is small unless the polarisation is very strong, a situation beyond our interest.

Using LCAO method with ψ_1 and ψ_2 as basis, since

$$H'_{ij} = \int_{-\infty}^{\infty} \psi_i^{*} H' \psi_j \, dx$$

Therefore,

$$H'_{ii} = \int_{-\infty}^{\infty} \psi_i^{*} H' \psi_i \, dx$$

$$= \int_{-\infty}^{\infty} \frac{(\phi_1(x)+r\,\xi(x))}{\sqrt{r^2 + 2r\sigma + 1}} \left(-\frac{\hbar^2}{2m}\frac{d^2}{dx^2} - A\delta(x+a) - A\delta(x-a) + v(x)\right)$$

$$\frac{(\varphi_1(x) + r\,\xi(x)}{\sqrt{r^2 + 2r\sigma + 1}} \, dx$$

$$= \frac{1}{r^2+2r\sigma+1} \int_{-\infty}^{\infty} \Big\{ \varphi_1(x) \left(-\frac{\hbar^2}{2m}\frac{d^2}{dx^2} - A\delta(x+a) - A\delta(x-a)\varphi_1(x)\right.$$

$$\left. + \varphi_1(x) v(x) \varphi_1(x) + 2r\varphi_1(x) H' \xi(x) + r^2 \xi(x) H' \xi(x) \Big\} \, dx \right.$$

$$= \frac{\zeta + v_o + 2rh_2 + r^2 h_1}{r^2 + 2\,r\,\sigma + 1}$$

Similarly,

$$H'_{ij} = \frac{\eta + v_1 + 2 r h_2 + r^2 h_1}{r^2 + 2 r \sigma + 1} \qquad (i \neq j)$$

where $$v_o = \int_{-\infty}^{\infty} \varphi_1(x)\, v(x)\, \varphi_1(x)\, dx$$

$$v_1 = \int_{-\infty}^{\infty} \varphi_1(x)\, v(x)\, \varphi_2(x)\, dx$$

$$h_1 = \int_{-\infty}^{\infty} \xi(x)\, H'\xi(x)\, dx$$

$$h_2 = \int_{-\infty}^{\infty} \varphi_1(x)\, H'\xi(x)\, dx\ .$$

Also, $$S_{ij} = \int_{-\infty}^{\infty} \Psi_1(x)\, \Psi_2(x)\, dx \qquad (i \neq j)$$

$$= \frac{S + r^2 + 2 r \sigma}{r^2 + 2 r \sigma + 1}$$

The energy for the bonding state is given by

$$E_b^p = \frac{H'_{11} + H'_{12}}{1 + S_{12}}$$

$$= \frac{\zeta + \eta + v_o + v_1 + 2r(2 h_2 + r h_1)}{1 + S + 2(r^2 + 2 r \sigma)}$$

Thus, the binding energy per atom of the molecule in the presence of a positive charge, E_B^p, is given by

$$E_B^p = |E_b^p - E_{\infty}^p| < |E_b^p - E_{\infty}| = \tilde{E}_B^p \qquad (4.28)$$

Now $\tilde{E}_B^p < E_B^o$ provided $E_b^p < E_b$ or $E_b^p - E_b < 0$

or, $$\frac{\zeta + \eta + v_o + v_1 + 2r(2h_2 + r h_1)}{1 + S + 2(r^2 + 2r\sigma)} - \frac{\zeta + \eta}{1 + S} < 0$$

or, $$(v_o + v_1 + 4rh_2 + 2r^2h_1)(1+S) - (\zeta + \eta)(2r^2 + 4r\sigma) < 0$$

or, $$r^2\left(2h_1 - \frac{2(\zeta+\eta)}{1+S}\right) + 4r\left(h_2 - \frac{\sigma(\zeta+\eta)}{1+S}\right) + (v_o + v_1) < 0 \qquad (4.29)$$

Since $(v_o + v_1) < 0$ as $v(x) < 0$, there is certainly a range of values of r, the values being small in magnitude, for which Eq. (4.29) is satisfied. The restriction on the magnitude of r is a consequence of the condition that the external charges can have only a polarizing effect on the electron cloud. Thus, in a range of small r values, the binding energy decreases due to polarisation. However, Eq. (4.29) may also give large values of r which means that the external field causes large distortions in the wave function resulting in a different chemical system. This situation is beyond the scope of present study.

Now, the effect of negative charges ($Q < 0$) on bonding is examined. In this case, the external charges repel the bonding electron cloud. The preceding method fails, since $\xi(x)$ for a repulsive state is a runaway solution, i.e. $\xi(x) \longrightarrow \pm\infty$ as $x \longrightarrow \pm\infty$. However, in a solid, the lattice of cores prevents such runaway solutions. Though, the simple two body LCAO method fails, one can proceed as follows :

The external negative charge near the center of the bond repels the electron charge cloud, creating a hole around $x = 0$ as shown in Fig. 4.10. The charge cloud piles up at the core sites, so that approximately,

$$\psi_1(x) = \hat{\alpha}^{\frac{1}{2}} \exp(-\hat{\alpha}\,|x-a|)$$

$$\psi_2(x) = \hat{\alpha}^{\frac{1}{2}} \exp(-\hat{\alpha}\,|x+a|)$$

where, $\hat{\alpha} = \frac{\hat{A}}{2}$ and $\hat{A} > A$.

In the absence of large constrictions (i.e. decrease of a), the situation resembles exactly the case of a linear chain without charge but with deeper core-potentials. In this case, therefore, the binding energy always decreases.

The above qualitative arguments can actually be demonstrated with a simple Kronig-Penney model with alternating wells of depth A at $x = \pm(a, 3a, 5a, \ldots)$ and barriers

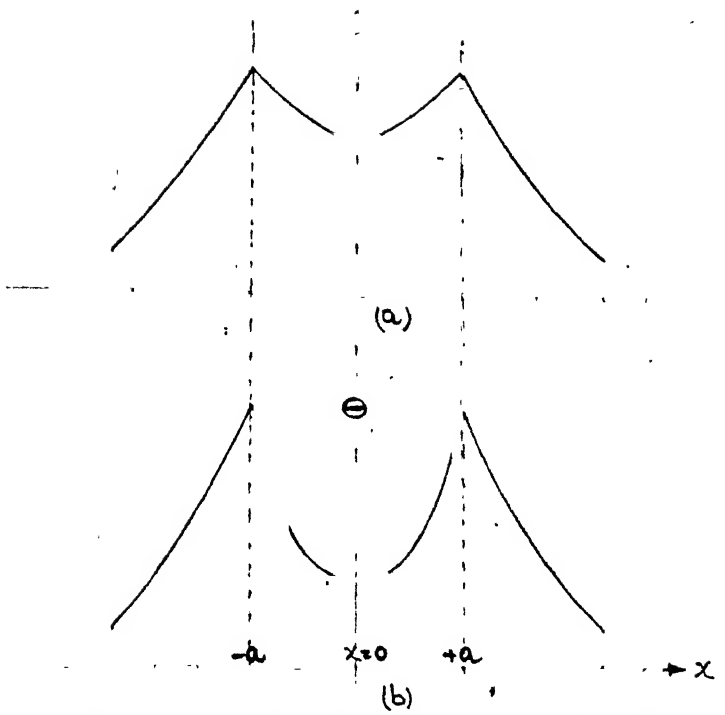

FIG. 4.10 ELECTRON CHARGE DENSITY IN A BINARY ATOM SYSTEM (a) WITHOUT ANY CHARGE (b) WITH A NEGATIVE CHARGE AT THE CENTRE AS SHOWN.

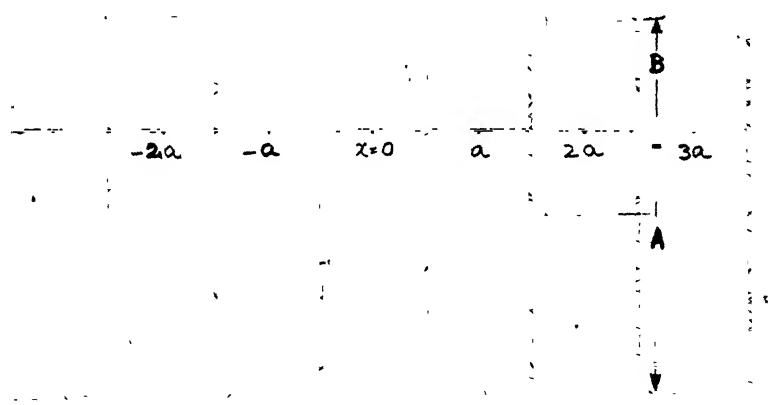

FIG. 4.11 SQUARE-WELL PERIODIC POTENTIAL OF KRONIG-PENNEY MODEL.

of height B at $x = \pm(0, 2a, 4a, \ldots)$ as shown in Fig. 4.11. The model is exactly equivalent to a Krönig-Penney model with well-depths of (A+B) at $x = \pm(a, 3a, 5a, \ldots)$. Such a model has bound solutions, and the binding energy decreases with increasing well-depths at the same separation.

4.4 A Linear Chain Model for a Metal

In order to examine the nature of the effect of local, external charge distributions on metallic binding forces, the linear chain model is studied. Again, it must be emphasized that the model is not physical but mathematically tractable and, therefore, illustrative. The analysis of a physically valid model is a heavy task beyond the scope of the present work. The aim here is to understand, at least, qualitatively the phenomenon.

If the total cohesive energy of a metal, i.e. the energy required to take the atoms apart, is expanded to second order in (valence) electron-ion interaction potential, V^{e-i}, then the resulting expansion of energy explicitly contains a term that represents a pair-wise interaction between atoms [30]. The pair-wise interaction consists of two parts, viz., the direct or "bare" Coulomb part, V_o^{e-i}, and an indirect ion-electron-ion interaction that depends on V_o^{e-i} and the dielectric constant of the electron gas. The effective pair-wise interaction between ions is important in accounting for the nature of binding forces in metals.

The bare interactions derived from ordinary Coulomb's law between a point-ion and an electron or two point-ions are respectively,

$$v_o^{e-i}(\vec{r}-\vec{R}_j) \simeq \frac{-Ze^2}{|\vec{r}-\vec{R}_j|}, \quad v_o^{i-i}(\vec{R}_i-\vec{R}_j) \simeq \frac{(Ze)^2}{|\vec{R}_i-\vec{R}_j|} \tag{4.30}$$

where Z is the chemical valence of the ion. The mobile Bloch electron gas effectively screens these bare interactions, with the result that if ε is the dielectric constant of the electron gas, then the screened potentials are [28]

$$v^{e-i}(\vec{r}-\vec{R}_j) \simeq \frac{-Ze^2}{\varepsilon|\vec{r}-\vec{R}_j|}, \quad v^{i-i}(\vec{R}_i-\vec{R}_j) \simeq \frac{(Ze)^2}{\varepsilon|\vec{R}_i-\vec{R}_j|} \tag{4.31}$$

and the total potential is given by

$$V(\vec{r}) = \sum_j v^{e-i}(\vec{r}-\vec{R}_j) + \frac{1}{2}\sum_i \sum_j v^{i-i}(\vec{R}_i-\vec{R}_j) \tag{4.32}$$

4.4.1 Effect of Screening on the Bare Electron-Ion Potential ($V_o^{e-i}(\vec{r})$)

Let the effective (screened) potential may be written in the form

$$V^{e-i}(\vec{r}) = V_o^{e-i}(\vec{r}) + V_{sc}(\vec{r}) \qquad (4.33)$$

where, the screening potential V_{sc} is related to the density $\rho(\vec{r})$ of the Bloch electrons by Poisson's equation

$$\nabla^2 V_{sc}(\vec{r}) = -4\pi e^2 \delta\rho(\vec{r}) \qquad (4.34)$$

$\delta\rho$ represents the fluctuations in the local electron density about its mean value due to electron-electron interactions among the Bloch electrons. $\rho(\vec{r})$ may be expressed in terms of the wave function $\psi_k(\vec{r})$ as

$$\rho(\vec{r}) = 2 \sum_{k \leq k_F} \psi_k^*(\vec{r}) \cdot \psi_k(\vec{r}) \qquad (4.35)$$

where ψ_k is determined from the solution of the Schrödinger equation

$$\left[-\frac{\hbar^2}{2m}\nabla^2 + V^{e-i}(\vec{r})\right]\psi_k(\vec{r}) = E_k \psi_k(\vec{r}) \qquad (4.36)$$

Here k = wave number and k_F = wave number corresponding to Fermi-energy.

The Eqs. (4.33) to (4.36) suggest that in order to calculate V^{e-i} in Eq. (4.33), the Eq. (4.36) must be solved which itself involves V^{e-i}. Thus a self-consistent solution is required. Using the fact that the screened potential V^{e-i}

is a weak potential, the wave equation can be solved by perturbation theory, to obtain

$$\psi_k(\vec{r}) = \frac{1}{\sqrt{\Omega}} \exp(i\vec{k}\cdot\vec{r}) + \frac{1}{\sqrt{\Omega}} \sum_{q\neq 0} \frac{V^{e-i}(q)\exp[i(\vec{k}+\vec{q})\cdot\vec{r}]}{T_k - T_{k+q}} \tag{4.37}$$

where, $V^{e-i}(q)$ is the Fourier transform of the potential $V^{e-i}(r)$,

$T_k \equiv \frac{\hbar^2 k^2}{2m}$ is the unperturbed (free electron) energy, and

Ω = volume of the crystal.

Knowing ψ_k, it is easy to evaluate $\rho(\vec{r})$ and then its Fourier transform. Using $V^{e-i}(q) = V^{*e-i}(-q)$, the Fourier transform of $\rho(\vec{r})$ is found to be

$$\begin{aligned}
\rho(q) &= \frac{1}{\Omega} \int \rho(\vec{r}) \exp(-i\vec{q}\cdot\vec{r})\, d^3r \\
&= \frac{2}{\Omega} \sum_{k\leq k_F} \int \psi_k^*(\vec{r})\psi_k(\vec{r}) \exp(-i\vec{q}\cdot\vec{r})\, d^3r \\
&= \frac{2}{\Omega} \sum_{k\leq k_F} \left[\frac{V^{e-i}(q)}{T_k - T_{k+q}} - \frac{V^{*e-i}(-q)}{T_k - T_{k-q}} \right] \\
&= V^{e-i}(q) \frac{4}{\Omega} \sum_{k\leq k_F} \frac{1}{T_k - T_{k+q}}
\end{aligned} \tag{4.38}$$

Now, the Poisson's Eq. (4.34) leads us to an equation connecting $V_{sc}(q)$ and $\rho(q)$; viz.,

$$V_{sc}(q) = \frac{4\pi e^2}{q^2} \rho(q) \tag{4.39}$$

Substituting the value of $V_{sc}(q)$ from Eq. (4.39) in Eq. (4.33), we get

$$V^{e-i}(q) = \frac{V_o^{e-i}(q)}{1 - \frac{4\pi e^2}{q^2} \frac{4}{\Omega} \sum_{k \leqslant k_F} \frac{1}{T_k^2 - T_{k+q}^2}}$$

$$= \frac{V_o^{e-i}(q)}{\varepsilon_H(q)} \tag{4.40}$$

where $\varepsilon_H(q)$ (called the Hartree dielectric constant of the free electron gas) is given by

$$\varepsilon_H(q) = 1 - \frac{4\pi e^2}{q^2} \frac{4}{\Omega} \sum_{k \leqslant k_F} \frac{1}{T_k^2 - T_{k+q}^2} \tag{4.41}$$

Taking atomic units $\frac{\hbar^2}{2m} = 1$ and $e^2 = 2$, then for a linear chain

$$\varepsilon_H(q) = 1 - \frac{8\pi}{q^2}\cdot\frac{4}{L} \sum_{k \leqslant k_F} \frac{1}{k^2-(k+q)^2}$$

$$= 1 + \frac{8\pi}{q^2}\cdot\frac{4}{2\pi} \int_0^{k_F} \frac{dk}{2kq+q^2}$$

$$= 1 + \frac{8}{q^3} \ln\left(1 + \frac{2k_F}{q}\right) \qquad (4.42)$$

The response function $r(q)$ is defined as

$$r(q) = \frac{\varepsilon_H(q) - 1}{\varepsilon_H(q)} \qquad (4.43)$$

Now, wave number, k_F can be expressed in terms of atomic radius, r_s, as follows :

For a free electron sea in a box of length L, the solution of one-dimensional Schrödinger equation $H\Psi = E\Psi$ gives the wave function ψ and eigenvalue E as

$$\psi_k(x) = \sqrt{\frac{2}{L}} \sin\frac{n\pi x}{L} \qquad n = 1,2,3,\ldots$$

$$E(k) = \frac{n^2\pi^2}{L^2} = k^2 \quad \text{remembering that } \frac{\hbar^2}{2m} = 1$$

The energy E represents the kinetic energy. Thus, the number

of states lying between energies o and E = $n(E) = \frac{L}{\pi}\sqrt{E}$.
Therefore, the number of states between E and E+dE = $\frac{d[n(E)]}{dE}$

$$= \frac{L}{2\pi} E^{-\frac{1}{2}}\, dE$$

or, the density of states, $D(E) = \frac{L}{2\pi} E^{-\frac{1}{2}}$

Now, each energy state can occupy upto a maximum of two electrons because of Pauli exclusion principle. Let n_F denotes the topmost filled energy level when N electrons are accomodated, then $2\, n_F = N$. The Fermi energy, E_F, is defined as the energy of the topmost filled level in the ground state (at 0^oK) and is given by

$$E_F = k_F^2 = \left(\frac{n_F \pi}{L}\right)^2 = \left(\frac{N \cdot \pi}{2L}\right) = \frac{\pi^2}{4 r_s^2}$$

So that

$$k_F = \frac{\pi}{2 r_s} \qquad (4.44)$$

where, $r_s = L/N$ is the atomic radius, and

$2r_s$ is the interatomic distance.

The total kinetic energy, E_T, of all the N electrons between 0 and E_F is given by

$$E_T = 2 \int_0^{E_F} E \cdot D(E) \cdot dE$$

$$= \frac{L}{\pi} \int_0^{E_F} E^{\frac{1}{2}} \cdot dE = \frac{2}{3} \frac{L}{\pi} E_F^{3/2}$$

Therefore, average kinetic energy per electron is

$$E_T/N = \frac{2}{3\pi} \cdot \frac{L}{N} \cdot \left(\frac{\pi}{2r_s}\right)^3 = \frac{\pi^2}{12} \cdot \frac{1}{r_s^2} \qquad (4.45)$$

Now, substituting Eq. (4.44) in Eq. (4.42), we get

$$\epsilon_H(q) = 1 + \frac{8}{q^3} \ln\left(1 + \frac{\pi}{qr_s}\right) \qquad (4.46)$$

and

$$r(q) = \frac{8}{q^3} \ln\left(1 + \frac{\pi}{qr_s}\right) \Big/ \left[1 + \frac{8}{q^3} \ln\left(1 + \frac{\pi}{qr_s}\right)\right] \qquad (4.47)$$

4.4.2 The Screened Ion-Ion Potential

The sea of Bloch electrons screens the ions from one another. As a result, the interaction between ions is modified. The 'indirect' part of the ion-ion interaction mediated by the electrons involves the bare-electron-ion interaction twice as shown in Fig. 4.12. To calculate the influence of this indirect interaction on the ''bare'' ion-ion interaction V_o^{i-i}, let the total interaction energy of the ions be written in the form

$$V^{i-i} = \frac{1}{2} \sum_{i \neq j} V_o^{i-i}(\vec{R}_i - \vec{R}_j) + V_{sc}^{i-i} \qquad (4.48)$$

where the contribution V_{sc}^{i-i} represents the indirect ion-electron-ion interaction and is given by

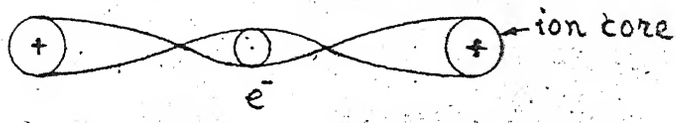

FIG. 4.12 INDIRECT ION-ION INTERACTION VIA THE POLARIZATION FIELD OF THE VALENCE ELECTRONS.

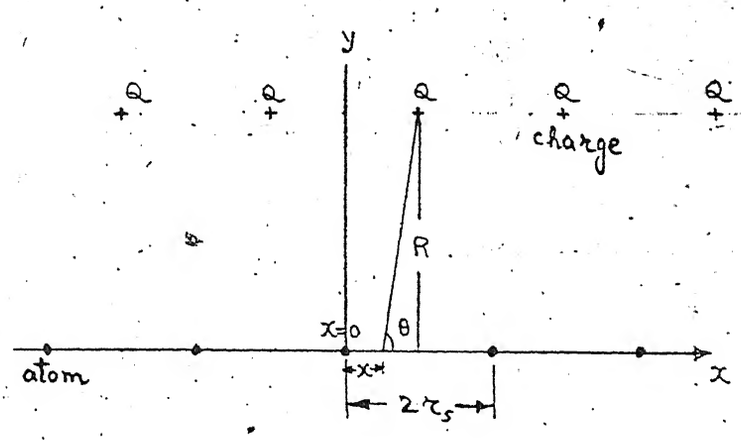

FIG. 4.13 A LINEAR CHAIN OF METALLIC ATOMS IN THE PRESENCE OF A CHAIN OF CHARGES Q AT A DISTANCE R.

$$V_{sc}^{i-i} = \int V_o^{e-i}(\vec{r})\, \rho(\vec{r})\, d\vec{r} \qquad (4.49)$$

i.e. by the product of the electronic charge density at $\vec{r}$ and the bare electron-ion interaction potential V_o^{e-i} at $\vec{r}$, integrated over the volume of the metal. Using the diffraction model, Fourier expansion of both, V_o^{e-i} and ρ are obtained as follows :

$$V_o^{e-i}(q) = S(q)\, v_o^{e-i}(q)$$

$$V^{e-i}(q) = S(q)\, v^{e-i}(q)$$

$$\rho(q') = S(q')\, \rho_a(q')$$

where, $\rho_a(q')$ is the Fourier transform of the screening charge associated with a single ion (at the origin),

S is the structure factor and

v^{e-i} and v_o^{e-i} refers to a single ion-electron screened and bare potentials respectively, and

$$v^{e-i}(q) = \frac{v_o^{e-i}(q)}{\epsilon_H(q)}$$

Substituting these values in Eq. (4.49), we get

$$V_{sc}^{i-i} = \sum_q \sum_{q'} \int S(q) v_o^{e-i}(q)\, S(q')\, \rho_a(q') \exp[i(\vec{q}+\vec{q}')\cdot\vec{r}]\, d\vec{r}$$

$$= \sum_{q} \sum_{q'} S(q)\, S(q')\, v_o^{e-i}(q)\, \rho_a(q')\, \delta_{q,-q'}$$

$$\equiv \sum_{q} S(q)\, S^{*}(q)\, v_o^{e-i}(q)\, \rho_a(q) \qquad (4.50)$$

Now, from Eq. (4.39)

$$\rho_a(q) = \frac{q^2}{4\pi e^2}\, v_{sc}(q)$$

where, $v_{sc}(q)$ is the screening potential for a single ion-electron pair and is given as

$$v_{sc}(q) = v^{e-i}(q) - v_o^{e-i}(q)$$

$$= - v_o^{e-i}(q)\, \Gamma(q)$$

Therefore,

$$\rho_a(q) = - \frac{q^2}{8\pi}\, v_o^{e-i}(q)\, \Gamma(q) \qquad (4.51)$$

For a linear chain with one atom per unit cell, the structure factor, S(q) is given by

$$S(q) = \delta_{q g_n} \quad \text{but } g_n = \frac{2\pi n}{2 r_s} = \frac{\pi n}{r_s} \qquad n = 1,2,3,\ldots$$

Thus

$$q = \frac{\pi n}{r_s} \quad \text{and} \quad S(q)\, S^{*}(q) = 1 \tag{4.52}$$

Substituting Eq. (4.51) and (4.52) in Eq. (4.50)

$$V_{sc}^{i-i} = -\sum_{n\neq o} [v_o^{e-i}(\tfrac{\pi n}{r_s})]^2 (\tfrac{\pi n}{r_s})^2 \cdot \frac{1}{8\pi} \frac{8\cdot(\frac{r_s}{\pi n})^3 \ln(1+\frac{1}{n})}{1+8(\frac{r_s}{\pi n})^3 \ln(1+\frac{1}{n})}$$

$$= -\sum_{n\neq o} \frac{r_s}{\pi^2} [v_o^{e-i}(\tfrac{\pi n}{r_s})]^2 \frac{\frac{1}{n}\ln(1+\frac{1}{n})}{1+(\frac{2r_s}{\pi n})^3 \ln(1+\frac{1}{n})} \tag{4.53}$$

Now, let the bare potential, v_o^{e-i}, be represented by a chain of δ-functions placed on the linear chain as shown in Fig. 4.4. The strength of the δ-wells is a characteristic of particular atoms which constitute the solid. It contains a Coulomb contribution from the nucleus, screened both by the core electrons and the other electrons in the Bloch sea.

Thus,

$$v_o^{e-i}(x) = -A\,\delta(x)$$

where A is the strength of each δ-function.

Therefore,

$$v_o^{e-i}(q) = -\frac{1}{2\pi}\int e^{-iqx} A\delta(x)dx$$

$$= -\frac{A}{2\pi} = -A' \text{ (say)} = \text{a constant} \qquad (4.54)$$

Substituting Eq. (4.54) in Eq. (4.53)

$$V_{sc}^{i-i} = -\frac{A'^2 r_s}{\pi^2} \sum_{n\neq o} \frac{\frac{1}{n}\ln(1+\frac{1}{n})}{1+(\frac{2r_s}{\pi n})^3 \ln(1+\frac{1}{n})} \qquad (4.55)$$

The total cohesive energy per atom, E, then, consists of three parts : the kinetic energy of the electrons, E_T, the Madelung energy, $-\frac{Z\gamma}{2r_s}$ (due to the bare ionic Coulomb potentials) and the self-consistent screened potential V_{sc}^{i-i}. Therefore,

$$E = \frac{\pi^2}{12r_s^2} - \frac{Z\gamma}{2r_s} - \frac{A'^2 r_s}{\pi^2} \sum_{n\neq o} \frac{\frac{1}{n}\ln(1+\frac{1}{n})}{1+(\frac{2r_s}{\pi n})^3 \ln(1+\frac{1}{n})} \qquad (4.56)$$

Now, to analyse the effect of an electrostatic field on the cohesive energy of the linear chain of atoms given by Eq. (4.56), let a chain of charges Q be considered at a distance R normal to the linear chain as shown in Fig. 4.13.

In this case, there is one charge per unit cell and

$$v_o^{e-i}(x) = -A\delta(x) - \frac{Q\,e}{\sqrt{\{R^2+(r_s-x)^2\}}} \quad \text{for } Q > 0 \tag{4.57}$$

Therefore,

$$v_o^{e-i}(q) = -A' - Qe \int_{-\infty}^{\infty} \frac{e^{-iqx}\,dx}{\sqrt{\{R^2(r_s-x)^2\}}}$$

Now,

$$\int_{-\infty}^{\infty} \frac{e^{-iqx}\,dx}{\sqrt{\{R^2+(r_s-x)^2\}}} = e^{-iqr_s} \int_{-\infty}^{\infty} \frac{e^{iq(r_s-x)}\,dx}{\sqrt{\{R^2+(r_s-x)^2\}}}$$

$$= e^{-iqr_s} \int_{-\infty}^{\infty} \left[\frac{\cos q(r_s-x)+i\sin q(r_s-x)}{\sqrt{\{R^2+(r_s-x)^2\}}}\right] dx$$

$$= -e^{-iqr_s} \int_{\infty}^{\infty} \frac{\cos qt + i\sin qt}{\sqrt{\{R^2+t^2\}}}\,dt$$

by putting $r_s - x = t$

$$= 2\,e^{-iqr_s} \int_{0}^{\infty} \frac{\cos qt\,dt}{\sqrt{\{R^2+t^2\}}}$$

$$= 2\,e^{-iqr_s} K_o(qR)$$

where K_o is the modified Bessel's function. Therefore,

$$v_o^{e-i}(q) = -A' - Qe\cdot 2\, e^{-iqr_s} K_o(qR)$$

but from Eq. (4.52), $qr_s = \pi n$, therefore,

$$e^{-iqr_s} = e^{-i\cdot\pi n} = (-1)^n$$

Therefore,

$$v_o^{e-i}(q) = -A' \left[1+\frac{2\sqrt{2}}{A'} Q(-1)^n K_o\left(\frac{\pi n}{r_s}R\right)\right] \tag{4.58}$$

Substituting Eq. (4.58) in Eq. (4.53), the modified expression for the total cohesive energy in the presence of positive charges is given by

$$E_m = \frac{\pi^2}{12r_s^2} - \frac{Z\gamma}{2r_s} - \frac{A'^2 r_s}{\pi^2} \sum_{n\neq o} \left[1+\frac{2\sqrt{2}}{A'} Q(-1)^n K_o\left(\frac{n\pi R}{r_s}\right)\right]^2 \cdot \frac{\frac{1}{n}\ln\left(1+\frac{1}{n}\right)}{1+\left(\frac{2r_s}{\pi n}\right)^3 \ln\left(1+\frac{1}{n}\right)} \tag{4.59}$$

Therefore,

$$\Delta E = E - E_m = \sum_{n\neq o} \left[\frac{8Q^2 r_s}{\pi^2} K_o^2\left(\frac{\pi n R}{r_s}\right) \pm \frac{4\sqrt{2}\, QA' r_s}{\pi^2} (-1)^n K_o\left(\frac{\pi n R}{r_s}\right)\right] \cdot \frac{\frac{1}{n}\ln\left(1+\frac{1}{n}\right)}{1+\left(\frac{2r_s}{\pi n}\right)^3 \ln\left(1+\frac{1}{n}\right)} \tag{4.60}$$

where, (+) sign is taken for $Q > 0$ and (-) sign for $Q < 0$, and the percentage change in the cohesive energy in the presence of charges

$$= \frac{\Delta E}{E} \times 100\% \qquad (4.61)$$

Equations (4.56) and (4.60) are solved on a digital computer. To simplify the calculation, the Madelung energy term in these equations is neglected which will affect the percentage change in cohesive energy. (Eq. (4.61)) by overestimating it to some extent. Thus, by taking a suitable value of the constant A', the energy, E is calculated from Eq. (4.56) by varying r_s and shown in Table 4.1. The value of r_s for which E is minimum, gives the equilibrium inter-atomic distance, $(r_s)_{eq}$. Keeping A' the same, Eq. (4.60) is solved for ΔE by assuming

$$R = p \cdot (r_s)_{eq} \quad \text{and} \quad Q = \pm Ne$$

where, p is a constant, say $\frac{1}{4}$, $\frac{1}{2}$, 1, 2, ... etc. and

N is an integer, say 1, 10, 100 etc.

Then, the percentage change in the cohesive energy due to the presence of charges is found from Eq. (4.61). The Tables 4.2 and 4.3 show the results at A' = 0.1 and 0.5 for different values of R and Q. It is clear that no significant decrease in cohesive energy is found in the region near $r_s = (r_s)_{eq}$

for the values of R and Q. shown in the table. It is concluded, therefore, that the presence of charges has a quite small effect on the bond strengths of a metallic linear chain. Truly speaking, in a linear chain all atoms are near the ''surface'' as seen by the external field. Therefore, the effect of an electrostatic field on atomic bonds of a bulk solid will be even more insignificant, since the bulk atoms are effectively screened from the external field by the conduction electrons. The external field penetrates only a few atomic layers below the surface (determined by the skin depth). The results of tensile rupture tests on Al-foils in the presence of a field (described in the previous chapter) support the theoretical findings in the case of a metallic chain.

Table 4.1

S.No.	r_s (in Bohr radius)	E in Rydbergs	
		A' = 0.1	A' = 0.5
		x10^{-2}	
1	30	- 0.681	- 0.19217
2	40	- 0.882	- 0.23276
3	50	- 1.034	- 0.26637
4	60	- 1.131	- 0.28835
5	70	- 1.174	- 0.29762
6	71	-	- 0.29788
7	72	- 1.17690	- 0.29803
8	73	- 1.17748	- 0.29807
9	74	- 1.17762	- 0.29800
10	75	- 1.17732	- 0.29784
11	80	- 1.169	- 0.29552
12	90	- 1.129	- 0.28481
13	100	- 1.066	- 0.26853
14	120	- 0.911	- 0.22917
$(r_s)_{eq}$ at minimum E		74.0	73.0

Table 4.2

A'=0.1

S.No.		1	2	3	4	5	6
r_s in Bohr radius		50	60	70	80	90	100
	E in Rydbergs	$\times 10^{-2}$ -1.034	-1.131	-1.174	-1.169	-1.129	-1.066
Q=100e at R=148.0	ΔE	$\times 10^{-6}$ -0.864	-2.06	1.98	30.7	123.0	337.0
	$\Delta E/E$ %	$\times 10^{-2}$ 0.835	1.820	-1.68	-26.3	-109.0	-316.0
Q=e at R=74.0	ΔE	$\times 10^{-5}$ -0.118	-0.153	-0.130	-0.010	0.147	0.390
	$\Delta E/E$ %	$\times 10^{-2}$ 1.14	1.35	1.11	0.256	-1.3	-3.65
Q = e at R=37.0	ΔE	$\times 10^{-4}$ 0.156	0.409	0.709	1.030	1.35	1.68
	$\Delta E/E$ %	-0.151	-0.361	-0.604	-0.882	-1.20	-1.57
Q = e at R=18.5	ΔE	$\times 10^{-3}$ 0.670	0.922	1.166	1.396	1.623	1.843
	$\Delta E/E$ %	-6.49	-8.15	-9.92	-11.93	-14.40	-17.30
Q= -e at R=74.0	ΔE	$\times 10^{-5}$ 0.147	0.268	0.427	0.623	0.864	1.126
	$\Delta E/E$ %	$\times 10^{-2}$ 1.42	2.37	3.64	5.32	7.65	10.56
Q= -e at R=37.0	ΔE	$\times 10^{-4}$ 0.450	0.699	0.976	1.267	1.561	1.862
	$\Delta E/E$ %	-0.435	-0.617	-0.831	-1.082	-1.385	-1.750

Table 4.3

$A' = 0.5$

$R = 73.0$

S.No.	r_s (in Bohr radius)	E (in Rydbergs)	Q = 100e		Q = e		Q = -e	
			ΔE $\times 10^{-2}$	$\Delta E/E$ %	ΔE $\times 10^{-5}$	$\Delta E/E$ % $\times 10^{-3}$	ΔE $\times 10^{-5}$	$\Delta E/E$ % $\times 10^{-3}$
1	50	-0.26637	0.09924	-0.372	-0.6929	2.6	0.7269	2.73
2	60	-0.28835	0.5383	-1.86	-1.050	3.64	1.180	4.10
3	70	-0.29762	1.503	-5.05	-1.294	4.35	1.624	5.47
4	80	-0.29552	3.090	-10.45	-1.375	4.65	2.027	6.87
5	90	-0.28481	5.394	-18.90	-1.313	4.62	2.429	8.54
6	100	-0.26853	7.989	-29.70	-1.074	4.00	2.709	10.00

CHAPTER 5

EFFECT OF ELECTROSTATIC FIELD ON ULTRASONIC MACHINING OF GLASS

5.1 Introduction

Broadly, there are two distinct classes of solid state manufacturing processes. Deformation processes produce the required shape with the necessary mechanical properties by plastic deformation. Machining processes produce the required shape by removal of selected areas of workpiece in the form of small chips. Conventional machining is accomplished by straining a local region of the workpiece due to the relative motion between the tool and the workpiece.

The recent increase in the use of hard, high-strength, and temperature - resistant materials in engineering has necessitated the development of new machining techniques (generally called the unconventional machining processes), as the conventional machining methods except grinding, are not readily applicable to these new materials. Even when such machining is possible, it is usually slow, highly inefficient and the degree of accuracy and surface finish attainable are poor.

Ultrasonic machining (USM) is one of the important unconventional machining processes and is suitable for machining both conducting and non-conducting materials. In

USM process shown in Fig. 5.1, the material is removed due to the mechanical action of abrasive grains. These are driven into the work-surface by a tool oscillating normal to the work-surface at frequencies of the order of 20 to 30 Kc/s with an amplitude of about 0.02 mm. The tool is pressed against the workpiece by a load of the order of a few kilograms and moves downwards as the machining progresses due to the gravitational force.

Not all the materials are suitable for machining by this process. A classification of materials which shows the degree of suitability of USM for machining them is shown in Table 5.1 [31]. The materials are classified into three main groups based on the analysis of the deformation and fragmentation (shear-failure of a brittle material) of various materials during ultrasonic machining. Materials in group I undergo practically no plastic deformation in ultrasonic machining so that most of the energy applied produces elastic strains only. USM is particularly effective for machining materials of this group. The group II includes heat-resistant alloys, hardened steels and hard-alloys. When these materials are ultrasonically machined, the abrasive grains set-up microplastic, as well as elastic deformations, and the greater the part played by these plastic deformations, the less suitable is the material for ultrasonic machining. In the ultrasonic machining of group III materials, almost

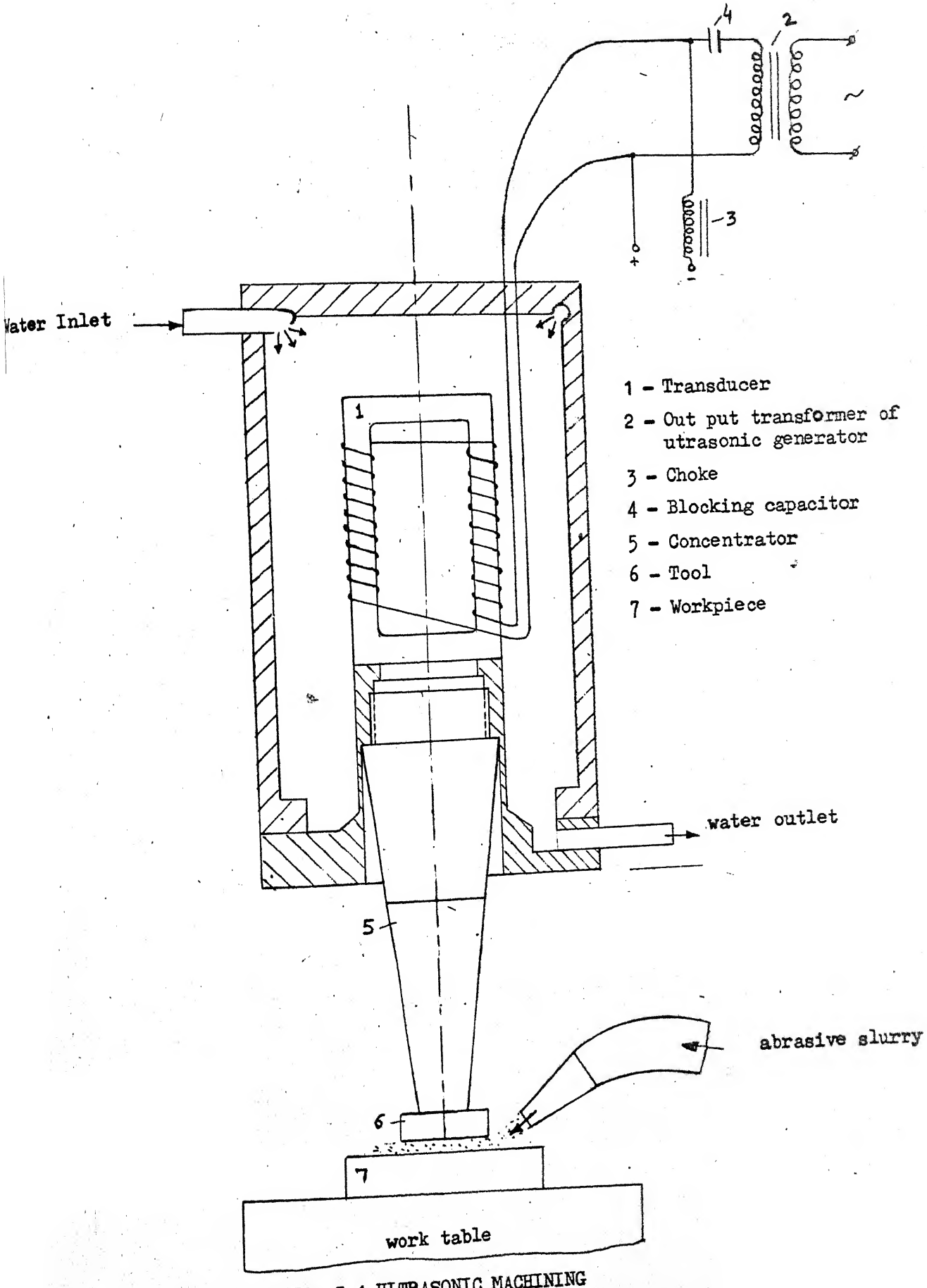

FIG. 5.1 ULTRASONIC MACHINING

Table 5.1

Classification of materials and fields of applications of USM

Group	Material	Criterion of brittleness (t) = $\frac{\text{shear strength}}{\text{tensile strength}}$	Predominant type of deformation	Type of failure	Field of applications of USM
I	Glass, quartz, ceramic, diamond, germanium, silicon, ferrite, Alsifier and others	> 2	Elastic	Brittle	1. Making parts of semiconducting materials 2. Cutting industrial diamonds 3. Cutting special ceramics 4. Making parts of glass, quartz and minerals in the optical and jewelry industries. 5. Machining ferrite, Alsifer, and other materials of high coercivity.
II	Alloys tempered to high hardness, carburised and nitrided steels, titanium alloys	1-2	Elastic-plastic	Brittle after work-hardening by plastic deformation	1. Making and repairing hard alloy dies, press tools and punches. 2. Shaping and sharpening hard-alloy tools.
III	Lead, Copper, soft steel	< 1	Plastic	Practically no failure	Unsuitable for USM

all the energy of the abrasive grains is expended on micro-plastic deformation of the surface layers of a material with practically no work-hardening. The material hardly fragments at all and, accordingly, ultrasonic machining is not recommended for materials of this group.

The major limitation of the process is its comparatively low material removal rate even when machining materials of group I. Any attempt to improve the material removal rate associated with this process is, therefore, highly desirable and promising from technological view-point.

One of the possibilities of increasing the material removal rate or cutting speed and reducing the tool wear in USM is by changing the properties of work material in the working zone. Based on this, a combination of USM and anodic etching has been tried when cutting conducting materials, and gives a much higher cutting speed and lower tool wear than USM alone [31]. However, this approach of changing the properties of work materials has not been tried in the machining of dielectric materials. It is thought that when machining these materials, the presence of an external electrostatic field might improve the material removal rate. The experimental investigations reported here are aimed at finding the effect of presence of such a field on ultrasonic machining of glass.

5.2 Physics of Material Removal in USM

In ultrasonic machining, the vibrating tool acts on the abrasive grains in two ways as follows :

(i) Abrasive grains are accelerated by the vibrating tool and impact against the work-surface.

(ii) The tool impacts directly on the abrasive grains lying on the work surface, forcing or hammering the grains into the surface.

Investigations [32,33] show that the first of these processes is relatively unimportant in removing material from the work surface and its contribution to material removal is insignificant. It is the second process which is responsible for material removal by chipping small particles off the surface. When a brittle material is machined ultrasonically, the hammering of abrasive particles into its surface produces cracks on its surface which cause degradation of the strength characteristics and ultimately result in fragmentation of surface material. Neglecting dynamic effects associated with an impact, the hammering of an abrasive particle into worksurface may be considered simply as an indentation process. The relationship between the depth of an indentation and the force with which an indentor is pressed into the surface of a brittle material is shown in Fig. 5.2. The curve is a broken line consisting of nearly

straight segments which shows that the process of fragmentation of a brittle material is discontinuous [31].

Indentations can be separated into essentially two classes - those caused by "blunt" indentors and those caused by "sharp" indentors depending on whether the contact is governed by elastic or plastic conditions. One of the earliest studies of indentations by blunt indentors is that of a spherical indentor pressed against a flat surface. It was analysed first by Hertz in 1881 and the elastic stress field produced in the material is illustrated by the trajectories in the vertical section through the axis of symmetry shown in Fig. 5.3(a) [34]. The principal stresses near the surface are a tensile radial stress σ_1, a hoop stress σ_2 (not shown in Fig.5.3(a)) which is tensile except immediately beneath the indentor where it is compressive, and a compressive axial stress σ_3. Further below the surface, the directions of σ_1 and σ_3 change as shown in Fig. 5.3(a). In general, $\sigma_1 > \sigma_2 > \sigma_3$ and the maximum tensile stress acts across the circle of contact, dropping off rapidly outside the circle. A tensile "skin" layer" consequently exists beyond the immediate indentation site, thereby creating highly favourable conditions for crack initiation. At some critical loading, the elastic limit of the material being indented is exceeded marked by the sudden development of Hertzian cone crack. The sequence of events leading to the initiation of Hertzian cone

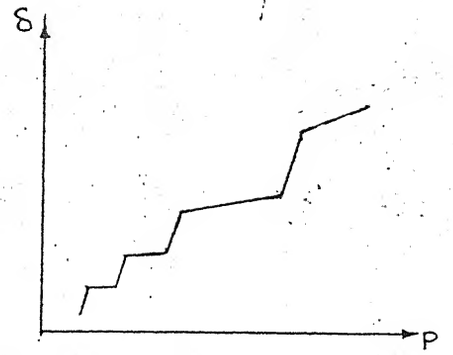

FIG. 5.2 DEPTH OF INDENTATION (δ) VS. INDENTOR LOAD (P)

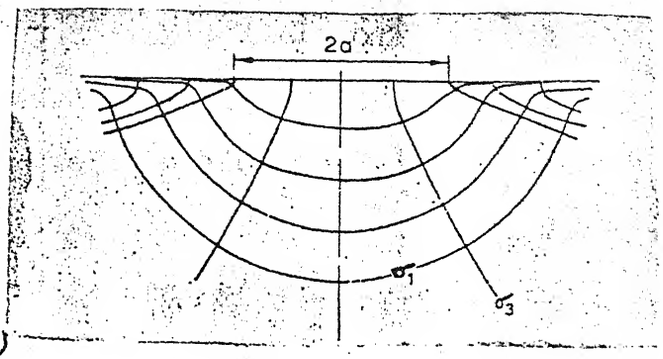

(a) Stress trajectories in the Hertzian stress field.

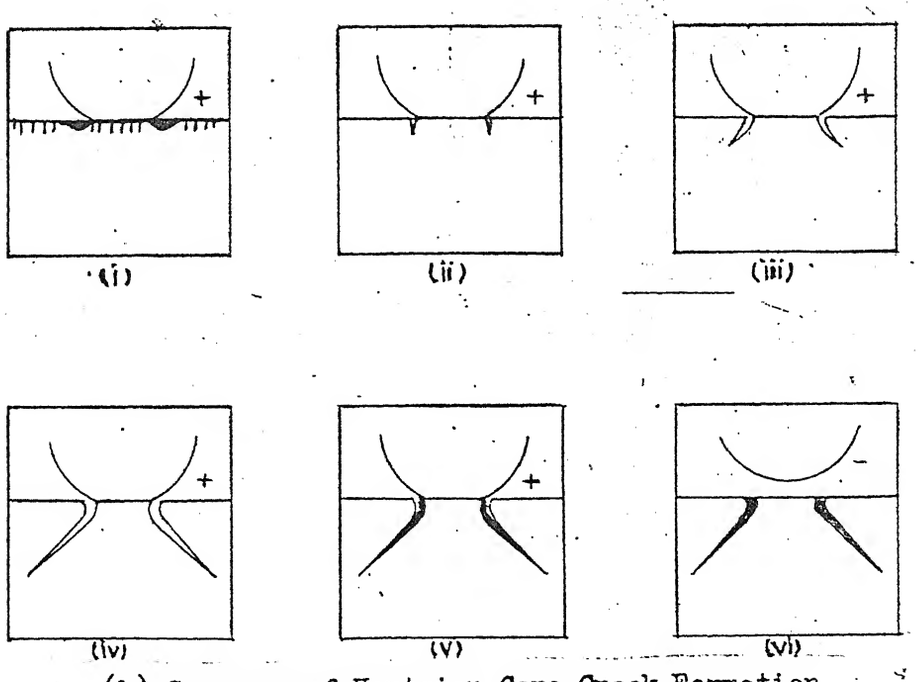

(b) Sequence of Hertzian Cone Crack Formation

FIG. 5.3 INDENTATION BY A SPHERICAL INDENTOR

crack in glass surface is shown in Fig. 5.3(b) where a spherical indentor is pressed against a brittle surface subjecting the surface flaws to tensile stresses (i), a ring crack forms (ii) and grows (iii), (iv) until a cone is formed (v); on unloading, the cone crack tries to close but cannot do so because of the debris present in the crack (vi) [35]. The problem of indenting a brittle surface by a sphere and the subsequent patterns of crack formation, are also of wide interest in the field of fracture mechanics and have been extensively studied in the recent years [36].

In case of indentation of a brittle material by a sharp indentor, non-elastic processes (e.g. plastic flow, densification) at the indentor site become important. Fig. 5.4(a) shows an indentation scar when a conical indentor (with an included angle of 60°-90° to avoid cracking) is pressed into a brittle surface. In this case, the edges of the scar are flat, the angle α at the base of the scar is equal to the cone tip angle, and the much greater angle β is the natural shear angle which is independent of the depth of indentation or the cone tip angle. Further, there is no accumulation of plastically deforming material around the edges of the indentation as in the case of indentation of a ductile metal as shown in Fig. 5.4(b). The sequence of events leading to cracking under a sharp indentor is shown

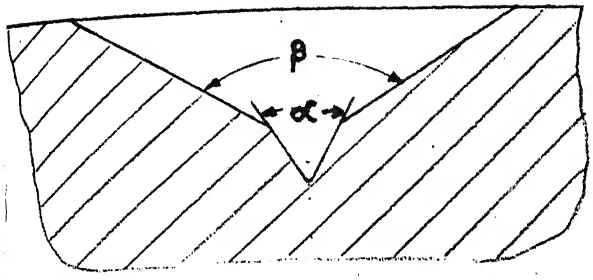

(a) Indentation of a brittle body by a conical indentor

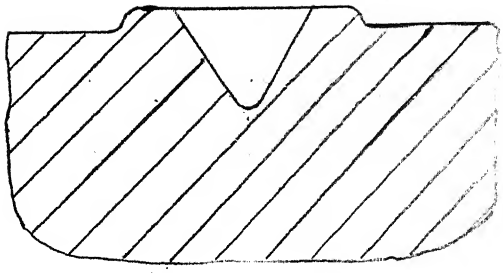

(b) Indentation of a ductile body by a conical indentor

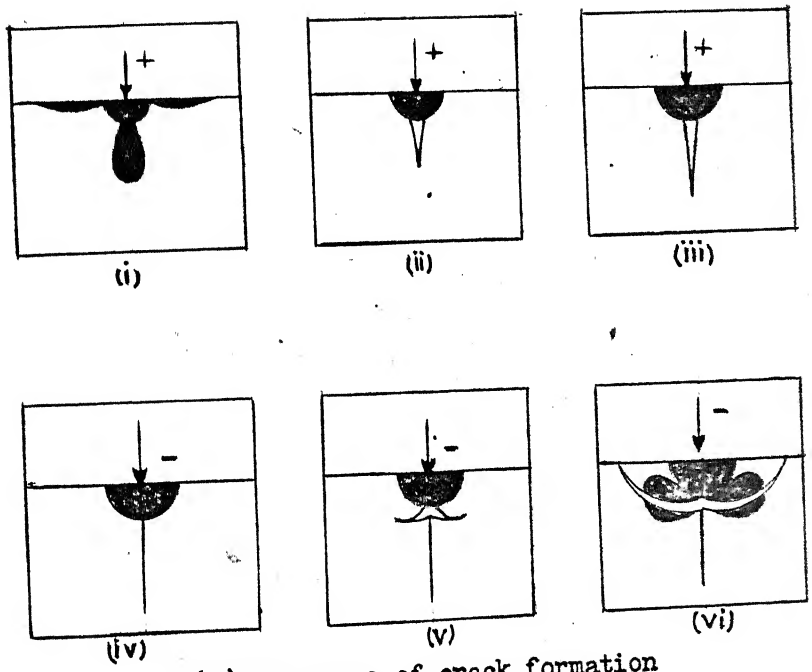

(c) Sequence of crack formation in conical indentation

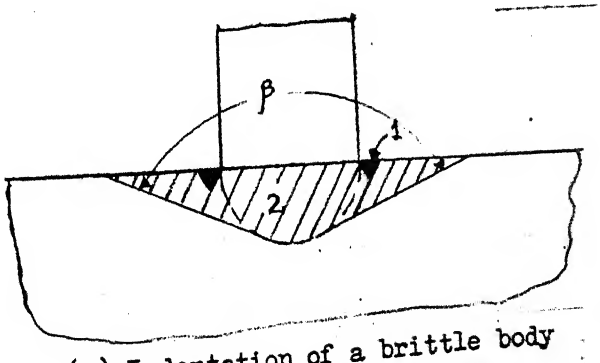

(d) Indentation of a brittle body by a cylindrical indentor

FIG. 5.4 INDENTATION BY CONICAL AND CYLINDRICAL INDENTORS

schematically in Fig. 5.4(c). Two sets of cracks are formed in this case. ''Median'' or ''radial'' cracks form as semi-circles perpendicular to the surface and ''lateral'' cracks initiate below the deformation zone, then grow in the outward and upward directions, until they reach the surface. Referring to Fig. 5.4(c), (i) the material under the indentor is stressed (dark area), (ii), (iii) sub-surface flaws grow to form median cracks, (iv) during unloading lateral cracks form and (v),(vi) expand and grow to the surface. The radial cracks cause strength degradation while the lateral cracks are responsible for the loss of material (fragmentation) [35,37].

The abrasive grains used in USM process are mainly crystals of irregular shape and size and have both sharp tips and flat faces. In practice, the sharp tips of an abrasive grain are blunted on impact by the tool. The blunted tips impart the grains the necessary mechanical strength required for causing deformation of work-surface material. To a first approximation, the blunting of abrasive grains may be considered spherical and the sharpness of grain characterised by the radius of curvature of the sphere. The smaller the radius of curvature of a grain pressed into the workpiece, the greater the stress concentration around it and, therefore, the greater its effectiveness.

The studies of USM process by using high speed cinematographic techniques show that not only the sharp tips but the flat faces of the abrasive grains also act on the work surface leading to its fragmentation. The mode of fragmentation may be approximated to that in case of a cylinder pressed against a flat surface as shown in Fig. 5.4(d) [31]. As the load on the cylinder is increased, the stresses in the material under the base of the cylinder increase but the compressive stress (pressure) around the periphery is much higher than under the remainder of the plane of indentation. Therefore, shear failure occurs first around the periphery of the cylinder as soon as the stress in this region equals the fracture stress. This pattern of failure is similar to that of a wedge-shaped indentation around the periphery of the cylinder. This region of failure is designated as the zone I of initial shear as shown in Fig. 5.4(d). As the load is further increased, the stresses in the material under the base of the cylinder increase. As soon as the stresses on the axis of the cylinder attain the ultimate value, failure occurs at the natural shear angle β. This is designated as zone II of general shear as shown in the figure.

Since the abrasive grains have both conical tips and flat faces, the mode of fragmentation of a brittle work-material in USM follows the patterns shown in Fig. 5.4(a) and (d).

However, it is still not clear which of these two models is more accurate. Their relative importance may depend on the properties and size of the abrasive, the amplitude of tool vibration and the properties of workpiece material.

Further, since the abrasive grains are irregular in shape and non-uniform in size, the force due to the impact of the tool is not distributed uniformly between all the grains but acts only on individual grains whose tips are at the maximum height (from the work-surface). The force on the grains, in general, may be resolved into components normal and tangential to the worksurface. The normal force causes the grain to indent the work material and the tangential component scratches the surface. Therefore, a better model of the mechanism of fragmentation of surface material in ultrasonic machining, can be obtained by super imposing a tangential force component on the indentors of the models considered above in Figs. 5.4(a) and (d).

5.3 Mechanics of USM Process

In USM, the material is removed due to the mechanical action of abrasive grains on the worksurface. The impact of tool on abrasive grains produces local high instantaneous stresses in the surface of the material which cause fragmentation of surface material. The rate of material removal,

in general, depends on the physical and mechanical properties of the workpiece, the abrasive used, the amplitude and frequency of tool vibration, the concentration of abrasive slurry and the static force applied to the tool. Many research workers have studied the mechanics of material removal in USM. Based on certain assumptions, theoretical relations have been developed for estimating the rate of material removal.

Shaw [38] considered the process of material removal in ultrasonic machining to take place mainly by two mechanisms :

(i) The abrasive grains are accelerated by the vibrating tool and thrown onto the workpiece.

(ii) The abrasive grains are hammered into the worksurface in a chisel-like action.

All the abrasive grains are considered to be spheres of diameter 'd' which hit or indent the work surface and generate a crater or indentation as shown in Fig. 5.5(a). When the depth of penetration is sufficient to cause rupture, it is assumed that a particle having a volume approximately proportional to the size of the indentation is chipped off. The volume rate of material removal is calculated on the basis of two mechanisms outlined above and it is shown that the thrown-abrasive mechanism accounts for (as already

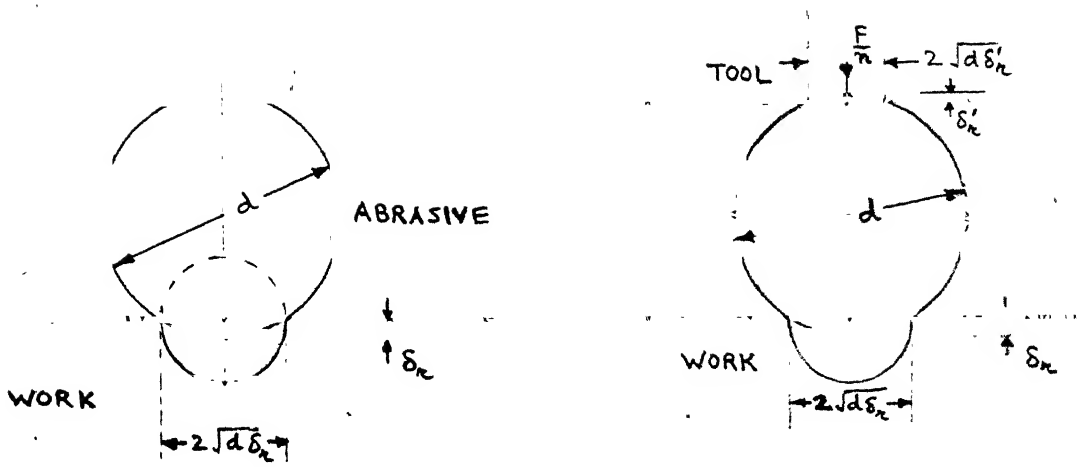

(a) Shaw's Model

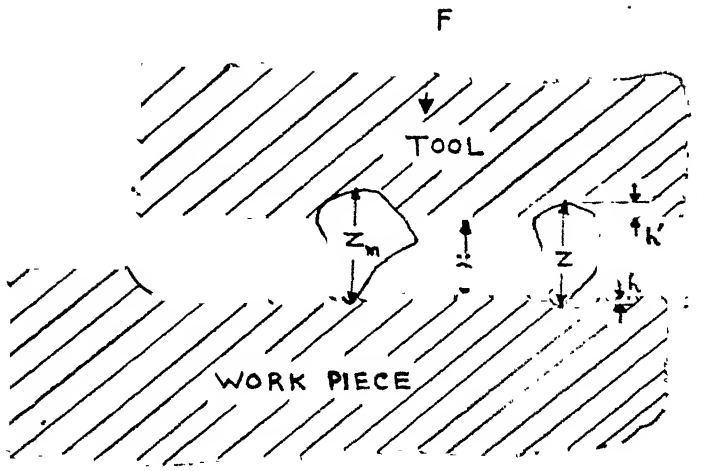

(b) Kazantsev's Model

FIG. 5.5 MODELS FOR THE ANALYSIS OF MATERIAL REMOVAL RATES IN USM.

mentioned) only an insignificant percentage of the total material removed. Thus, the major portion of the material removed is contributed by the hammering mechanism.

Miller [39] proposed that during machining of a ductile material, the abrasive particles imbedded in the work-surface cause plastic deformation and work-hardening. The work-hardened material is subsequently removed by chipping. In case of brittle materials, the chipping without plastic deformation causes material removal and the rate of removal depends on the size of the chips. An expression for material removal rate is obtained on the assumption that the abrasive particles are cubic in shape.

Shaw's and Miller's analyses are approximate as they are based on certain simplified assumption. Both are simple to use for estimating the rate of material removal.

The analysis proposed by Kazantsev [40] also assumes that material is removed by brittle fracture. The abrasive grits are assumed to be of irregular shape and their size distribution is taken into account in the expression for material removal rate. The model on which the analysis is based is shown in Fig. 5.5(b). When the tool comes down to its lowest point, it causes some grains to penetrate both the tool and the work surface. The volume of material taken away by an abrasive particle is a function of penetration (z-x). The analysis is more realistic in comparison to other analyses but very cumbersome to use.

5.4 Experimental Investigations

The objective of the experimental investigations, as already pointed out, is to determine the effect of an electrostatic field, if any, on the rate of machining of a dielectric material. Glass, because of its brittleness is found to be a very suitable material for machining ultrasonically. At the same time, it is cheap, easily available and possesses good dielectric properties. Therefore, glass is machined ultrasonically to conduct tests to determine the effect of an applied electrostatic field on the rate of material removal. As pointed out earlier, the hammering of abrasive particles into the work-surface causes formation of cracks. The cracks grow and propagate in the sub-surface region and ultimately cause fragmentation (chipping) of surface material. It is expected that the application of a suitable electrostatic field might either cause an increase in the depth of indentation due to a reduction in the hardness of the surface layer or a decrease in the stress required to chip a particle off the surface. It is also possible that both these effects appear simultaneously. Each of these effects is likely to enhance the rate of material removal.

5.4.1 Experimental Details

The ultrasonic machining tests are performed on microglass slides purchased from the local market. These slides

are normally, used for pathological examinations of blood, stool etc. in hospitals and clinics. Each slide is roughly 75 mm long, 25 mm wide and approximately 1.3 mm thick. The slides are cut into three pieces of approximately equal length and these pieces are used as test specimens. For applying the field during machining, the specimen is prepared as follows :

A rectangular Al-foil strip of size 20 mm x 20 mm x 0.04 mm is pasted on one face of the glass specimen by quick-fix adhesive. A suitable wire is provided for connecting the strip to a high voltage terminal as shown in Fig. 5.6(a). The exposed surface of the Al-strip is now covered with araldite to give a thick layer of insulation over it. The araldite is allowed to dry and set for 24 hours. The insula- obtained thus, gives a resistance of about 100-300 mega-ohms. About forty specimens are prepared in this fashion for performing tests on them in the presence of a field. When machining without a field, specimens cut from the slides are used directly.

For machining a specimen, it is held in a box-type fixture made of perspex as shown in Fig. 5.6(b). The fixture has a shallow rectangular cavity into which the specimen is placed and then, covered by a closely fitting lid having a hole in the centre. The fixture is fixed to the table of the ultrasonic machine by bolts and levers so that the tool

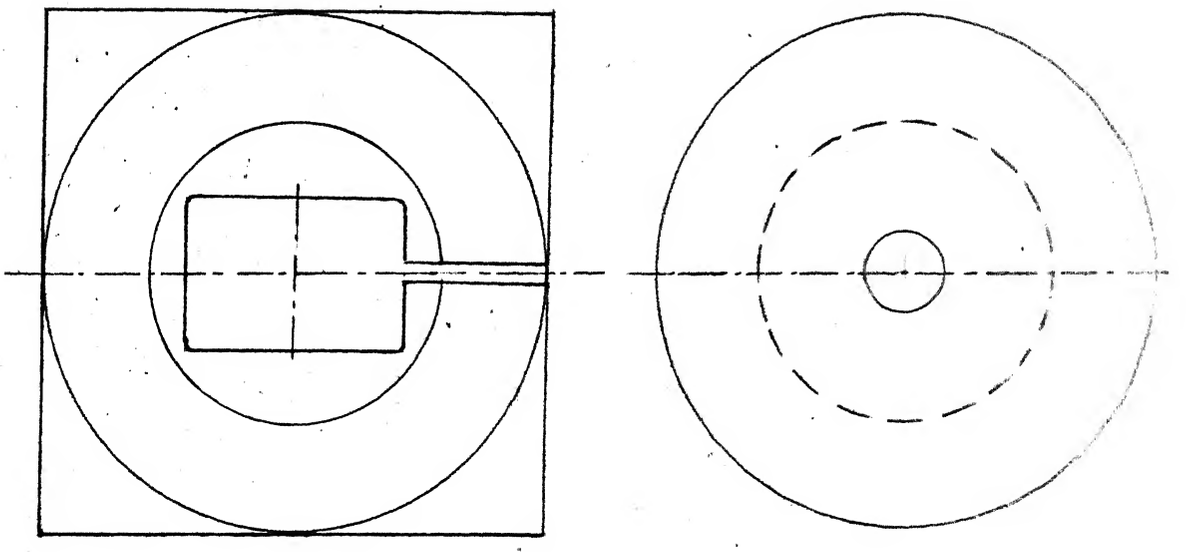

Top View

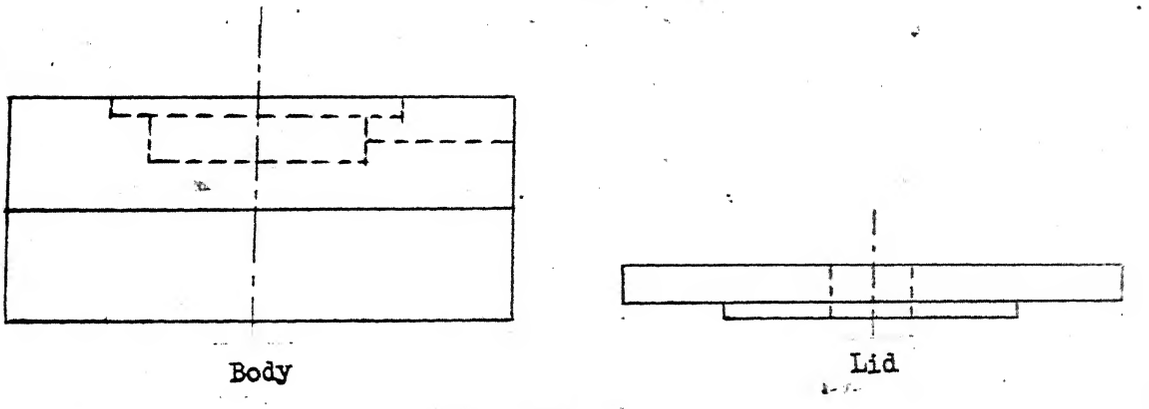

Front View

(b) Fixture for holding test specimen

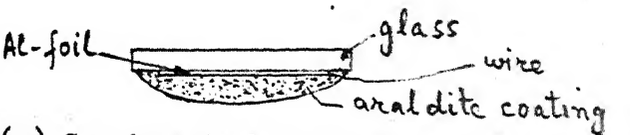

(a) Specimen to be machined in the presence of an electric field

FIG. 5.6 GLASS SPECIMEN AND FIXTURE FOR HOLDING IT

can pass through the central hole in the lid without any interference. The tool, a solid circular cylinder of 5.0 mm diameter, is then brought down to touch the work-surface by suitably adjusting the counter-weights. The reading of the gage, indicating travel of the tool during machining, is set to zero. The gage is divided into 100 divisions, each division representing 0.001 inch of travel.

The araldite coated specimen, after it has been mounted in the fixture, is connected to the positive terminal of a high voltage d.c. supply (0-5 KV) through a microammeter and a resistance of 0.3 mega-ohm as shown in Fig. 5.7(a). The other terminal of the supply is connected to the tool.

The abrasive used for cutting is silicon carbide (SiC) of mesh size 220. Four hundred grams of this abrasive powder are mixed in two litres of tap water, resulting in an abrasive-water ratio of 1:5 by weight.

To take a cut, the machine is started by first switching on the circulation of slurry and then exciting the tool at a frequency of 25 KHz. A load of 0.5 lb. is removed from the counter-weight pan to give a static load of the same amount. As the cutting starts, the movement of the tool into the work surface is indicated on the dial gage fixed on the machine head. Two stop-watches are used for recording the durations of time required for cuts I and II as shown in Fig. 5.7(b). The watches are started when the gage-pointer

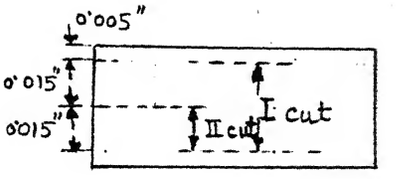

(b) The two depths of cut

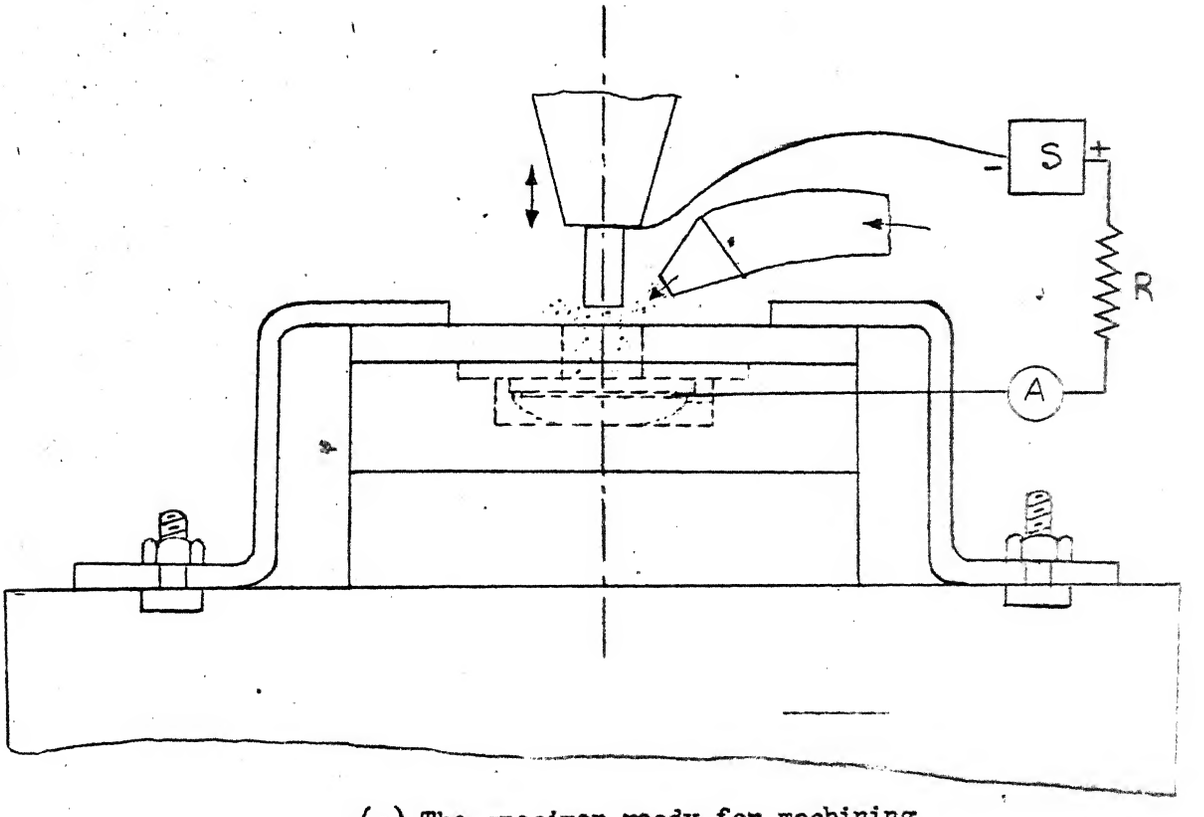

(a) The specimen ready for machining

FIG. 5.7 DIAGRAM ILLUSTRATING THE MACHINING IN THE PRESENCE OF THE FIELD.

reads 5th and 20th divisions (marked on the dial gage) respectively and stopped simultaneously when the pointer shows 35th division. Thus, the time required for cuts I and II is recorded. The observations are taken both without and in the presence of an electrostatic field. Generally, three to four cuts are made on a single specimen and the specimens without and with field (V = 5.0 KV) are machined alternately to minimize the influence of any chance variation in the process on the observations taken. Later, the observations are taken by applying voltages of 3.5 and 2.0 KV across the terminals. The observations are recorded in Table 5.2.

5.4.2 Results and Discussion

From the data in Table 5.2, average values of the time required for the two cuts I and II are calculated at various intensities of the field applied during investigations. From these average values, the percent changes in the cutting times due to the presence of various fields are calculated and shown in Table 5.3. It is obvious that the time of cut is reduced significantly in the presence of a field. Generally, the reduction in cutting time in the presence of electric fields (corresponding to impressed voltages of 2.0 to 5.0 KV) is between 10 to 20 percent. However, the effect is always more in the case of cut II

Table 5.2

The time of cut measured in seconds for the cuts I and II

D.C. voltage applied	0.0 V		5.0 KV		3.5 KV		2.0 KV	
S.No.	Cut I	Cut II	Cut I	Cut II	Cut I	Cut II	Cut I	Cut II
(1)	(2)	(3)	(4)	(5)	(6)	(7)	(8)	(9)
1	67.3	35.8	75.4	34.0	61.1	32.9	64.9	28.7
2	73.4	28.4	64.7	28.6	58.2	32.5	63.2	24.0
3	66.1	31.8	65.9	29.2	63.1	30.1	62.5	25.9
4	72.0	37.2	69.5	31.0	70.2	30.8	65.2	28.0
5	71.9	37.0	67.1	27.3	70.8	25.4	64.5	29.5
6	76.0	28.7	74.2	27.2	64.9	33.3	63.6	27.5
7	72.4	34.0	72.8	27.2	71.1	30.8	72.3	29.1
8	75.8	46.7	73.5	33.7	65.7	34.6	63.3	23.8
9	58.0	28.9	64.1	27.3	72.2	31.6	65.0	28.7
10	74.0	35.2	78.1	27.9	67.4	25.0	65.0	25.5
11	70.5	32.5	65.2	27.5	66.5	26.7	67.0	28.1
12	71.1	36.0	85.4	35.5	81.0	39.8	60.7	21.8
13	68.8	36.6	79.4	32.1	80.6	34.9	69.7	36.8
14	67.7	32.8	78.2	30.0	75.6	31.6	69.6	33.5
15	90.8	38.5	75.9	29.0	83.4	37.0	57.9	29.9
16	77.5	34.0	81.5	28.4	62.7	31.6	-	-
17	83.5	37.6	75.5	32.9	74.3	36.6	-	-
18	74.0	25.3	77.7	26.5	81.6	26.6	-	-
19	97.2	43.3	78.3	26.5	-	-	-	-
20	87.9	32.1	78.0	26.5	-	-	-	-
21	75.9	31.5	76.3	31.9	-	-	-	-
22	78.5	34.9	82.5	29.2	-	-	-	-
23	83.6	36.8	75.4	29.2	-	-	-	-
24	77.2	33.5	84.7	29.5	-	-	-	-
25	73.8	27.6	-	-	-	-	-	-
26	83.8	38.1	-	-	-	-	-	-
27	77.4	30.4	-	-	-	-	-	-
28	87.2	37.1	-	-	-	-	-	-
29	81.6	44.9	-	-	-	-	-	-
30	77.7	45.4	-	-	-	-	-	-
31	78.6	40.7	-	-	-	-	-	-
32	73.3	33.5	-	-	-	-	-	-
Total	2444.5	1126.8	1799.3	708.1	1260.4	571.8	974.4	420.8
Average	76.4	35.21	74.97	29.50	70.03	31.76	64.96	28.05

Table 5.3

Precent reduction in the time of cut in the presence of a field.

	Cut I				Cut II			
D.C. Voltage applied	0.0 V	5.0 KV	3.5 KV	2.0 KV	0.0 V	5.0 KV	3.5 KV	2.0 KV
Average time of cut	76.4	74.97	70.03	64.96	35.21	29.50	31.76	28.05
Reduction in percent	-	1.87	8.35	15.0	-	16.2	9.79	20.3

Table 5.5

A summary analysis of variance table

Sources of Variation	d.f.	SS	MS
Between machining with and without field	1	305.02	305.02
Within machining with or without field	46	653.87	14.21
Total	47	958.91	

which is taken at a depth of 0.02 inch below the work surface. This shows that as the tool penetrates deeper into the work-material, the rate of tool penetration is enhanced due to the presence of a field. This enhancement of the rate of tool penetration is considered to be very important by the author because of the fact that the tool penetration rate is known to decrease with the increase in the depth of cut when machining without a field. The increase in the tool penetration rate may occur due to the effect of increasing field intensity caused by the decreasing thickness of the dielectric in the gap between the two electrodes, tool (negative) and Al-foil at the base of the glass specimen (positive), as the cut progresses. The percent reductions in the cutting time do not show a linear variation with the impressed voltages. But it is felt that a sufficiently large number of observations are to be taken at every applied voltage to show convincingly how the effect of field on cutting time varies with the applied voltage. The author could not do so because of the shortage of time.

The relative frequency distributions of the time required for the two cuts are calculated and shown in Table 5.4 and plotted in Fig. 5.8. Under the influence of the applied fields, the frequency distribution curves show a shift towards the left in case of both the cuts. However, the effect on frequency distribution curves is more clear and well-defined in the case of cut II as shown in Fig. 5.8.

Table 5.4

Frequency distributions of the time of cut

	D.C.Voltage applied	0.0 V		5.0 KV		3.5 KV		2.0 KV	
	time-range seconds	no.of obs.(n)	rel. freq.(f)	(n)	(f)	(n)	(f)	(n)	(f)
Cut I	55.1-60.0	1	0.031	0	0.0	1	0.055	1	0.067
	60.1-65.0	0	0.0	2	0.083	4	0.222	9	0.600
	65.1-70.0	4	0.125	4	0.167	3	0.167	4	0.267
	70.1-75.0	10	0.312	3	0.125	6	0.333	1	0.067
	75.1-80.0	9	0.282	11	0.458	1	0.055	0	0.0
	80.1-85.0	4	0.125	3	0.125	3	0.167	0	0.0
	85.1-90.0	2	0.062	1	0.042	0	0.0	0	0.0
	90.1-95.0	1	0.031	0	0.0	0	0.0	0	0.0
	95.1-100.0	1	0.031	0	0.0	0	0.0	0	0.0
	Total No. of obs.	32		24		18		15	
Cut II	20.1-23.0	0	0.0	0	0.0	0	0.0	1	0.067
	23.1-26.0	1	0.031	0	0.0	2	0.111	4	0.267
	26.1-29.0	4	0.725	12	0.50	2	0.111	5	0.333
	29.1-32.0	3	0.094	7	0.292	6	0.333	3	0.200
	32.1-35.0	8	0.250	4	0.167	5	0.278	1	0.067
	35.1-38.0	9	0.282	1	0.042	2	0.111	1	0.067
	38.1-41.0	3	0.094	0	0.0	1	0.055	0	0.0
	41.1-44.0	1	0.031	0	0.0	0	0.0	0	0.0
	44.1-47.0	3	0.094	0	0.0	0	0.0	0	0.0
	Total No. of obs.	32		24		18		15	

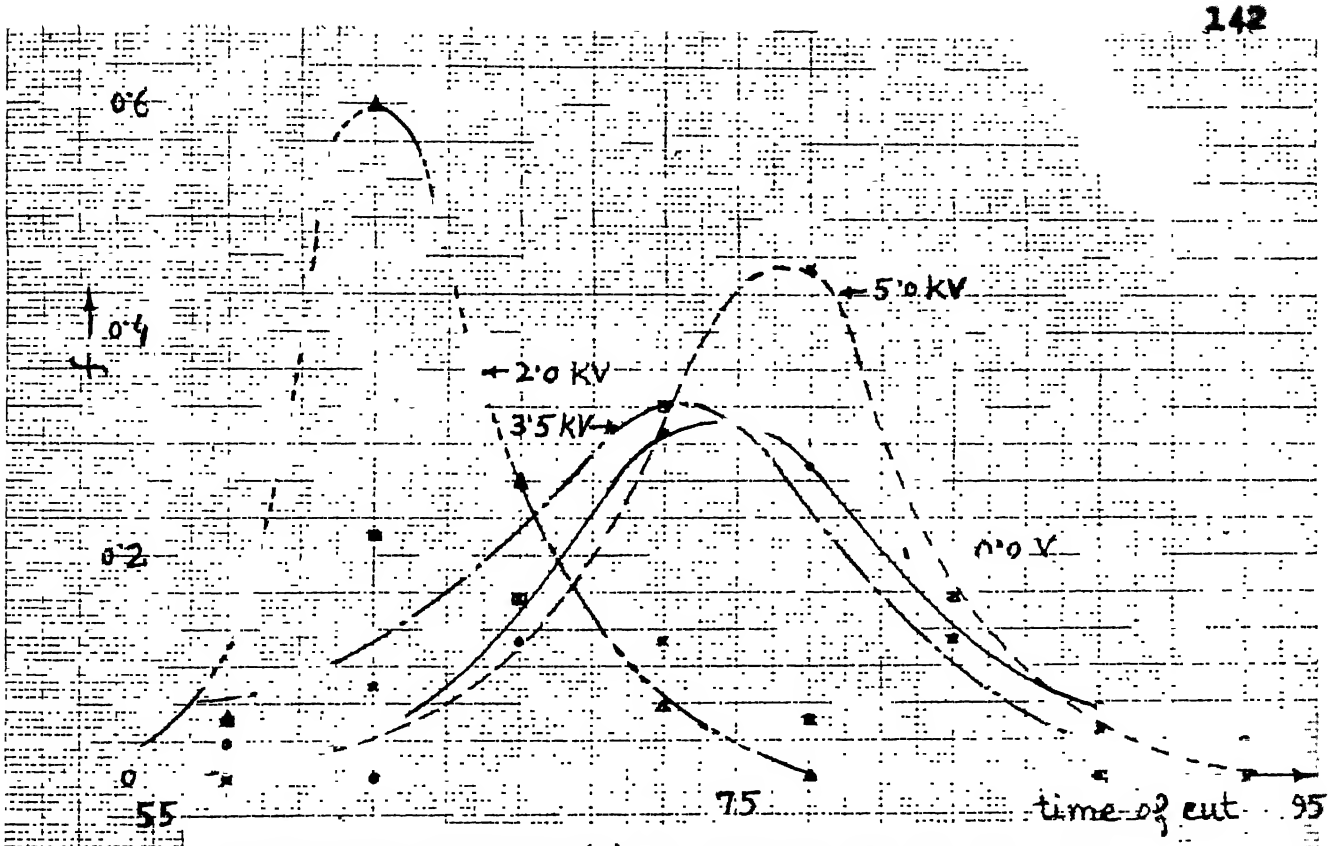

(a) Relative frequency (f) VS. Cutting time for the I cut.

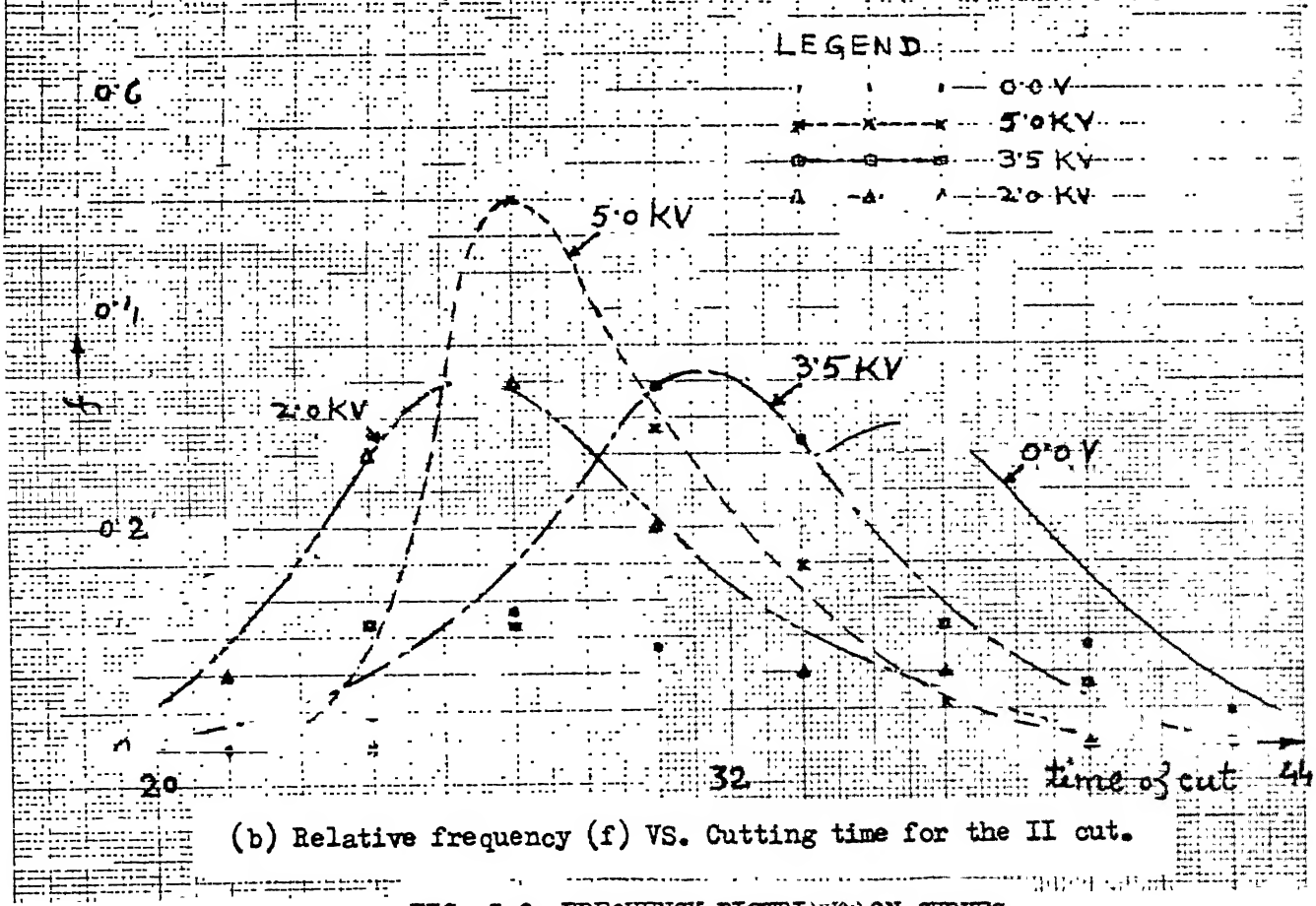

(b) Relative frequency (f) VS. Cutting time for the II cut.

FIG. 5.8 FREQUENCY DISTRIBUTION CURVES

The improvement in the rate of cutting when machining glass in the presence of an electrostatic field, is considered to be the consequence of polarization of the work material which affects its mechanical properties. However, the field may also have an affect on the concentration of abrasive particles (silicon carbide) in the working zone. It is to be noted that the field in the gap between the tool and the workpiece is uniform in the central region but non-uniform near the edges of the tool. A body carrying a charge when placed in an electric field experiences a force which causes its motion and this phenomenon is known as electrophoresis. On the other hand, if a neutral (carrying no charge), polarizable body is placed in a non-uniform electric field, it also experiences a force and undergoes translational motion and this effect is known as dielectrophoresis. In Fig. 5.9, a charged and a neutral body are shown in a non-uniform electric field. The charged body is pulled towards the electrode of opposite charge as in case of a uniform electric field. On the other hand, the neutral body acquires, in effect, a negative charge on the side nearest the positive electrode and a positive charge on that side nearer the negative electrode. Since the body is overall neutral, the two effective charges are, in fact, equal. The externally applied electric field being non-uniform, diverges across the particle and produces unequal forces on

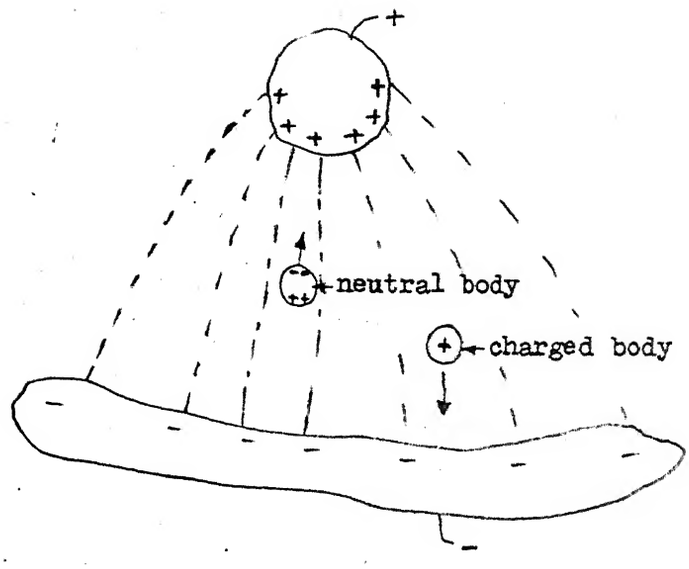

FIG. 5.9 DIELECTROPHORETIC EFFECT

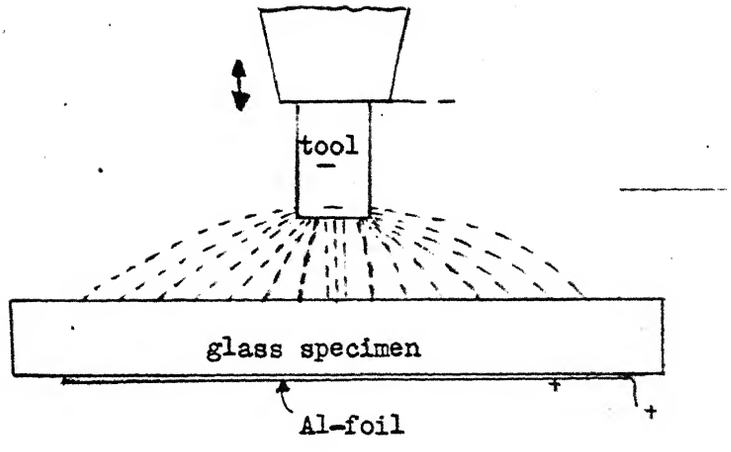

FIG. 5.10 FIELD IN THE GAP BETWEEN THE TOOL AND THE WORKPIECE.

the two effective charges. The net effect is an overall force on the neutral body which impels it into the region of stronger field (i.e. toward the ''sharper'' electrode where the field is more intense). It is to be noted that force on the neutral, polarizable body due to the non-uniform electric field is in the same direction no matter which electrode is positive or negative [18].

In case of ultrasonic machining of glass, the electric field existing in the gap between the tool and workpiece is shown in Fig. 5.10. The silicon carbide abrasive particles (suspended in water) on entering the field zone may get polarized and thus subjected to forces due to dielectrophoretic effects. The force on an abrasive particle will depend directly on its volume (v), its polarizability (α) and the square of the electric field intensity (ε_e) and is given by

$$F = \tfrac{1}{2} v \alpha \nabla |\varepsilon_e|^2$$

However, since the abrasive particles are continuously in motion due to a continuous supply of the slurry, their inertia forces are considered to be large in comparison with the forces due to the field. Therefore, it is assumed that the field does not have any significant influence on the concentration of abrasive particles in the working zone.

Thus, the improvement in the rate of cutting is solely due to the polarization of the work material.

5.4.3 Analysis of Variance of Test Data

The observations in Table 5.2 can be analysed statistically to show that the variation exhibited by the observations is not due to chance alone but because of the presence of an electrostatic field. For this purpose, the analysis of variance technique is applied to the data in columns (3)* and (5) of Table 5.2 on the assumption of a completely randomized one-variable design. The results of the analysis of variance [41] are shown in Table 5.5 (p.139).

The null hypotheses to be tested is

H_o : average cutting time for cut II without field

= average cutting time for cut II with field

and the test is at an $\alpha = 0.025$ significance level.

The mean square (MS) represent two independent, chi-square distributed, unbiased estimates of the population (observations) variance σ_x^2 when H_o is true. Their ratio is F-distributed with 1 and 46 degrees of freedom (d.f.). If H_o is true, by chance alone this F-ratio is expected to exceed $F_{0.025,1,46} = 5.37$ only 2.5% of the time.

* only first 24 values are considered from column (3).

Since,

$$\frac{305.02}{14.21} = 21.45 > 5.37$$

the hypotheses H_o is rejected.

The conclusion is that the presence of a field does affect the process of ultrasonic machining of a dielectric material.

CHAPTER 6

CONCLUSIONS AND SCOPE FOR FUTURE WORK

From the theoretical analyses and the experimental results, the following major conclusions can be drawn :

1. In molecular systems, the presence of an external electrostatic field leads to a redistribution of the bonding electron charges. The net overlap charge which is a measure of the bonding is always found to decrease in the presence of a field. The maximum fractional decrease in the overlap charge is 0.28 in case of H_2^+-ion.

2. Since in case of dielectric materials, the electrostatic field penetrates into the bulk, the overlap charge is reduced leading to a weakening of the atomic bonds. The results of tensile rupture tests on aluminised mylar and macrofol specimens show a decrease in the rupture strength of the order of 5 to 15% .

3. In metals, the field is screened by the conduction electrons and therefore, the effect of field on bonding is negligible except perhaps on the surface. The results of tensile rupture tests on Al-foil specimens are in agreement with the theoretical predictions.

4. The manufacturing processes predominantly dependent on brittle fracture, like ultrasonic machining, are enhanced

when cutting dielectric materials in the presence of suitable electrostatic fields. Thus, the rate of material removal during ultrasonic machining can be increased by applying an electrostatic field of sufficient intensity.

5. The results of the wear experiments on macrofol specimens do not indicate any significant change in the wear rate due to the field. This is, perhaps, due to the fact that direct rupture does not play a significant role in the process of wear of such materials.

The experiments conducted on ultrasonic machining with electrostatic fields appear to be quite encouraging although higher intensities of field could not be applied because of limitations of high voltage d.c. supply. An extensive experimental work could be taken up by the future research workers to make an elaborate study of ultrasonic machining in the presence of electrostatic fields. Apart from this, the effect of field on other manufacturing processes could also be taken up.

The techniques for generating intense localised electrostatic fields should also be developed for easy application. In case such techniques are already existing, their adaptability to this kind of experiments has to be developed.

Over and above, the theory of the effect of electrostatic fields on the bonding of realistic models of materials and surfaces needs to be developed.

REFERENCES

1. G. Barrow, 'Machining of high strength materials at elevated temperatures using electric current heating', Annals C.I.R.P., Vol. 14 (1966), p. 145-51.
2. G. Barrow, 'The effect of hot machining by electric current on the mechanics of orthogonal cutting', Proc. 8th IMTDR Conf. (1967), p. 795-819.
3. M.E. Merchant and E.J. Krabacher, 'Basic factors in hot machining of metals', Trans. ASME, Vol. 73 (1951), p. 761-76.
4. P.K. Bagchi and A. Ghosh, 'Effect of magnetisation on the wear characteristics of cutting tools', J. Inst. Engrs. (India), 50 (1970), p. 264.
5. P.K. Bagchi and A. Ghosh, 'Mechanism of cutting tool wear in presence of a magnetic field', Ind. J. Technol., 9 (1971).
6. M.K. Muju, 'Effect of magnetic field on wear', Ph.D. Thesis, I.I.T., Kanpur (India), 1975.
7. D.S. Kamenetskaya et al., 'Influence of steady magnetic field on the plastic deformation of high-purity iron,' Fiz. metal. metalloved., 35 (1973), p. 318-22.
8. O.A. Troitskii, 'Effect of the electronic state of a metal on its mechanical properties and the electro-plasticity effect', Strength of Materials (english translation of the Soviet Journal Probl. Prochn.), Vol. 9 (1977), p. 35-45.

9. O.A. Troitskii and A.G. Rozno, 'Electroplastic effect in metals', Fiz. Tverd. Tela., Vol. 12 (1970), p. 203-10.

10. K. Okazaki et al., 'A study of the electroplastic effect in metals', Scripta Metallurgica, Vol. 12 (1978), p. 1063-68.

11. S.K. Varma and L.R. Cornwell, 'The electroplastic effect in Aluminium', Scripta Metallurgica, Vol. 13 (1979), p. 733-38.

12. O.A. Troitskii et al., 'Application of high-density current in plastic working of metals,' Phys. Stat. Sol. (a), Vol. 52 (1979), p. 85-93.

13. K.M. Klimov et al., 'Electroplasticity of metals,' Sov. Phys. Dokl., Vol. 19 (1975), p. 787-88.

14. Y. Wada, H. Kokado et al., 'Charge Storage, charge transport and Electrostatics with their applications', Elsevier (1979), p. 89-93.

15. F.L. Sayakhov et al., 'Study of the effect of a high frequency electric field on the surface tension of liquids', Electron Obrab. Mater., Vol. 90 (1979), p.34-35.

16. S.M. Korobeinikov, 'Bubble deformation in an electric field,' J. Eng. Phys., Vol. 36 (1979), p. 588-89.

17. M. Mutoh et al., 'Convergence and disintegration of liquid jets induced by an electrostatic field', J. Appl. Phys., Vol. 50 (1979), p. 3174-79.

18. A.D. Moore (Ed.), 'Electrostatics and its applications', John Wiley and Sons, N.Y. (1973).

19. J.J. Gilman, 'Micro mechanics of flow in solids', McGraw-Hill (1969), Ch. 1 and 3.

20. D. McLean, 'Mechanical properties of metals', Robert E. Krieger Pub. Co., Huntington, N.Y. (1977), Ch. 7.

21. M.F. Ashby and R.H.J. David, 'Engineering materials - An introduction to their properties and applications', Oxford, Pergamon (1980), Ch. 13.

22. M.O.A. Mokhtar, 'Friction - Is it an intrinsic property of metals?', Wear, Vol. 72 (1981), p. 287-93.

23. N.P. Bogoroditsky et al., 'Electrical engineering materials', Mir Pub., Moscow (1979), Ch. 1.

24. D. Rosenthal and R.M. Asimov, 'Introduction to properties of materials', East-West Press, New Delhi (1974), Ch. 13.

25. L.I. Schiff, 'Quantum Mechanics (II ed.), McGraw Hill Book Co. (1955), Ch. 6,7,10.

26. J.C. Slater, 'Quantum Theory of Matter (II ed.), McGraw Hill Book Co. (1968), Ch. 20.

27. M. Luban et al., 'Exact Solution for the Linear Response of a Hydrogenic atom to an external Electromagnetic field', J. Math. Phys., Vol. 18 (1977), p. 1871-81.

28. A.O.E. Animalu, 'Intermediate Quantum Theory of Crystalline Solids', Prentice-Hall (1977), Ch. 3.

29. H. Margenau and G.M. Murphy, 'The Mathematics of Physics and Chemistry, D. Van Nostrand Co. (1966), Ch. 11.

30. Cohen, J. Phys. Radium, Vol. 23 (1962), p. 643.

31. A.I. Markov, 'Ultrasonic Machining of Intractable Materials', London Iliffe Books Ltd. (1966), Ch.2,7,10.

32. L.D. Rozenberg and V.F. Kazantsev, 'The Physics of Ultrasonic Machining of Hard Materials', Sov. Phys. Doklady, Vol. 4 (1959), p. 182-85.

33. L.D. Rozenberg and V.F. Kazantsev, 'An Investigation of the Mechanism of Ultrasonic Cutting by means of High-Speed Cinematography, Stanki i instrument, n. 5 (1959), p. 20-22.

34. K.H.G. Ashbee, 'The Mechanics and Physics of Fracture', Metals Society/Inst. of Phys., Cambridge (1975), p.140-47.

35. B.R. Lawn and D.B. Marshall, 'Fracture Mechanics of Ceramics', Vol. 3, Plenum Press, N.Y. (1978), p. 205-29.

36. D.R. Uhlmann and N.J. Kreidl (Eds.), 'Glass Science and Technology,' Vol. 5, Academic Press (1980), Ch. 2.

37. B.R. Lawn and M.V. Swain, 'Microfracture beneath point indentations in brittle solids', J. Mater. Sci., 10 (1975), p. 113-22.

38. M.C. Shaw, 'Ultrasonic Grinding', Microtecnic, Vol. 10 (1956), p. 257-65.

39. G.E. Miller, 'Special Theory of Ultrasonic Machining', J. Appl. Phys., Vol. 28 (1957), p. 149-55.

40. V.F. Kazantsev and L.D. Rozenberg, 'The Mechanism of Ultrasonic Cutting,' Ultrasonics, Vol. 3 (1965), p. 166.

41. E.G.Kirkpatrick, 'Introductory Statistics and Probability for Engineering,Science and Technology,' Prentice-Hall Inc. (1974), Ch. 11.

42. O.A. Troitskii et al., 'Electroplastic Drawing of Stainless Steel, Sov.Phys. Dokl., Vol. 22 (1977), p. 769-70.

ME-1993- D- KHA- EFF